

# Investigations on Environmental Stress Cracking Resistance of LDPE/EVA Blends



## Dissertation

zur Erlangung des akademischen Grades

Doktor-Ingenieurin (Dr.-Ing.)

vorgelegt der

Mathematisch-Naturwissenschaftlich-Technischen Fakultät

(Ingenieurwissenschaftlicher Bereich)

der Martin-Luther-Universität Halle-Wittenberg

von Frau Dipl.-Ing. Bistra Andersen

geb. am 09.01.1973 in Ruse, Bulgaria

Gutachter:

1. Prof. Dr. J. Kreßler
2. Prof. Dr. G. H. Michler
3. Prof. Dr. J. Piglowski

verteidigt am 28.06.2004

**urn:nbn:de:gbv:3-000006970**

[<http://nbn-resolving.de/urn/resolver.pl?urn=nbn%3Ade%3Agbv%3A3-000006970>]

## Contents

<b>List of Publications</b>	4
<b>Acknowledgements</b>	5
<b>Abbreviations and Symbols</b>	6
<b>1. Introduction</b>	9
1.1 Significance of Environmental Stress Cracking for the Long-Term Service of Plastic Products	9
1.2 Research Tasks	10
<b>2. Definition of Environmental Stress Cracking (ESC)</b>	11
2.1 The Occurrence of ESC	11
2.2 The Stress Factor	12
2.3 Stress Cracking Agents	12
2.4 A Graphic Model for Failure	14
2.5 Factors Influencing the ESC-Behavior	17
<b>3. Test Methods for Evaluation of ESCR of Plastics</b>	18
3.1 Tests at Constant Strain	18
3.1.1 Three-Point Bending Test	18
3.1.2 Bell Telephone Test (BTT)	19
3.2 Tests at Constant Load (Stress)	20
3.2.1 Constant Tensile Load Test	20
3.2.2 Monotonic Creep Test	22
3.2.3 Test Method for Determining ESCR of Polyethylene Based Plastics	23
3.3 Bottle ESCR Test	24
<b>4. Thermodynamics of Polymer Blends</b>	25
<b>5. Polyethylene and Poly(ethylene-co-vinyl acetate)</b>	30
5.1 Polyethylene (PE)	30
5.2 Poly(ethylene-co-vinyl acetate) (EVA)	31
5.3 PE/EVA Blends	32
5.4 Polyethylene and ESC	33
<b>6. Experimental Part</b>	37
6.1 Materials and Preparation	37
6.2 Environmental Stress Cracking Resistance Test	38
6.3 Thermal Analysis	38

6.4 X-ray Analysis	39
6.5 Microscopic Techniques	39
6.6 Tensile Testing and Mechanical Properties	40
6.7 Image Processing System analySIS 3.1	40
<b>7. Results and Discussion</b>	<b>42</b>
7.1 ESC Experiments	42
7.2 DSC and WAXS Investigations	47
7.3 SAXS Investigations	58
7.4 Morphology Analysis	62
7.4.1 AFM and TEM Investigations	62
7.4.2 SEM Investigations	75
7.4.3 HVEM Investigations	77
7.5 Mechanical Properties	81
<b>8. Summary and Conclusions</b>	<b>85</b>
<b>9. Outlook</b>	<b>88</b>
<b>10. Zusammenfassung</b>	<b>89</b>
<b>11. References</b>	<b>93</b>
<b>Appendices</b>	<b>98</b>

## List of Publications

Bistra Borisova, Jörg Kressler, “Environmental Stress-Cracking Resistance of LDPE/EVA Blends” in *Macromol. Mater. Eng.* **2003**, 288, 509-515.

Bistra Borisova, Jörg Kressler, H.-W. Kammer, “Relation between Environmental Stress Cracking Resistance of LDPE/EVA Blends and Their Morphology and Micromechanical Deformation Behavior” in *Polymer*. Submitted.

Bistra Borisova, Jörg Kressler, “Environmental Stress Cracking of Polyethylene Compounds”. Poster presented at the Polymerwerkstoffe 2002, Halle (Saale), 25-27 September 2002.

Bistra Borisova, Jörg Kressler, “Nanostructures Responsible for the Environmental Stress Cracking Behavior of PE/EVA Compounds”. Poster presented at the Innovation Forum Nanostructured Materials, Halle (Saale), 24-25 November 2003.

## **Acknowledgements**

I would like to thank my supervisor Prof. Dr. rer. nat. habil. Jörg Kreßler for providing the topic of this work, for his support and encouraging discussions we have had throughout the period of this work.

Many sincere thanks go to Dr. J. Vogel for his support and discussions concerning the DSC investigations and helps during the clarification of several bureaucratic problems. Thanks are due to Dr. H. Kausche for his help in many aspects like software, computer problems, WAXS experiments, etc.

I also would like to thank Prof. Dr. G. Michler for providing the electron microscopy investigations. I would like to thank S. Goerlitz (TEM), Dr. R. Adhikari (AFM), Dr. E. Ivankova and Dr. G.-M. Kim (HVEM) for the beautiful electron micrographs.

Special thanks goes to Dr. R. Androsch for many scientific discussions and help in DSC and WAXS investigations.

Furthermore, I would like to express thanks to the following persons for their help and cooperation during my research work: Prof. Dr. H.-W. Kammer, Dr. Z. Funke, Dr. K. Busse, Dr. R. Godehardt, Dr. Bierögel, Dr. A. Wutzler, Maria Pogert, Siegfried Kunze, Ursula Mittag, Daniela Kantcheva, Hazrat Hussain, Nasir Mahmood.

I would like to acknowledge the DOW-BSL Olefinverbund GmbH, Schkopau for providing the samples and financial support of this project.

Finally, my deepest thanks goes to my parents and sister for their moral and financial support. In addition, I sincerely thank my husband Torsten Andersen for his unlimited moral support and encouragement.

## Abbreviations and Symbols

$A_0$	cross-sectional area
ABS	poly(acrylonitrile-co-butadiene-co-styrene)
AFM	atomic force microscopy
BTT	Bell telephone test
COD	crack opening displacement
d	diameter of EVA particle
DSC	differential scanning calorimetry
$\delta$	deflection
$\Delta G_m$	Gibb's free energy of mixing
$\Delta H_m$	enthalpy of mixing
$\Delta S_m$	entropy of mixing
$\Delta V_m$	change of volume during mixing
ESC	environmental stress cracking
ESCR	environmental stress cracking resistance
EVA	ethylene vinyl acetate copolymer
$\varepsilon$	strain
F	applied force
$F_y$	applied force at yield
FWHM	full width at the half maximum of the diffraction peak
$\phi_i$	volume fraction
G	crack driving force
HDPE	high density polyethylene
HIPS	high-impact polystyrene
HMWPE	high molecular weight polyethylene
HVEM	high voltage electron microscopy
kN	kilo Newton
kV	kilovolt
$L_a$	thickness of amorphous layer
$L_c$	lamella thickness
$L_0$	initial length of a sample
$\Delta L$	change in the length
$\lambda$	wavelength
LCST	lower critical solution temperature

LDPE	low density polyethylene
LLDPE	linear low density polyethylene
MDPE	middle density polyethylene
mg	milligramm
min	minute
mm	millimeter
$\mu\text{m}$	micrometer
mol.-%	molar percent
MPa	mega Pascal
$M_w$	molar mass
n	total number of measured EVA particles
nm	nanometer
$N_i$	degree of polymerization
ORL	Oita Research Laboratory, Japan
P	pressure
PA	polyamide
PB	polybutylene
PC	polycarbonate
PE	polyethylene
PMMA	poly(methylmethacrylate)
PP	polypropylene
PS	polystyrene
PVC	poly(vinylchloride)
q	scattering vector
$\theta$	diffraction angle
r	radius of a spherical particle
$r_i$	number of polymer segments
R	universal gas constant
$\rho_i$	density of component i
S	surface area of EVA particle
SAN	poly(styrene-co-acrylonitrile)
SAXS	small angle X-ray scattering
SCG	slow crack growth
SEM	scanning electron microscopy
$\sigma$	stress

$\sigma_y$	stress at yield (tensile strength at yield)
t	thickness of the sample for the BTT
$t_f$	time to failure
TEM	transmission electron microscopy
T	absolute temperature
$T_a$	annealing temperature
$T_g$	glass transition temperature
UCST	upper critical solution temperature
UHMWPE	ultra high molecular weight polyethylene
VA	vinyl acetate
vol.-%	volume percent
w	width of the sample for the BTT
wt.-%	weight percent
WAXS	wide-angle X-ray scattering
$\chi$	Flory-Huggins binary interaction parameter



# 1. Introduction

## 1.1 Significance of Environmental Stress Cracking for the Long-Term Service of Plastic Products

Failure has been a serious problem in the use of materials since the beginning of recorded history. These sometimes catastrophic failures were a driving force for the development of material science and engineering. Failure can be described as any change of properties which make the material or component functionally, structurally or aesthetically unacceptable. In the last few decades, engineering polymers have succeeded in replacing metals in many demanding applications and such failures will become even more important. It is often necessary to understand why polymer failure has occurred, so that measures can be taken to prevent its reoccurrence. Polymeric materials are sensitive to processing and affected by the environment, time and temperature during storage, transportation and service. Especially the long-term properties are frequently “unpredictable”.<sup>[1]</sup> Failure in polymer components can occur at relatively low stress levels (far below the tensile strength in many cases) due to long-term stress (creep rupture), cyclic stresses (fatigue failure) or liquid agents (environmental stress cracking). When a polymer is stressed in air to just below its yield point, stress cracking can occur after period of time. However, when simultaneously exposed to both stress and a chemical medium this will result in a dramatic reduction of the time to failure. This type of failure has been named environmental stress cracking (ESC). ESC has been a subject of extensive investigations for almost 50 years. It has deserved much attention because approximately 15-20 % of all failures of plastic components in service are due to ESC.<sup>[2]</sup> In addition the phenomenon of ESC is very interesting to both chemists and physicists as it involves, stress enhanced absorption, permeation, the thermodynamics of mixtures, local yielding, cavitation, fibrillation and fracture.<sup>[3]</sup>

In the early days of its commercial development, polyethylene was widely considered to be inert to all liquids. The supposed stability of this new material lead immediately to new applications, e.g. one of the first polyethylene bottle applications was the packaging of concentrated hydrofluoric acid.<sup>[4]</sup> At this point, the industry was confronted with numerous reports of polyethylene failure. Polyethylene was reported to be unsatisfying for cable usage, and it was found to crack violently on contact with methanol at room temperature.<sup>[5]</sup> The term ESC was officially defined by J. B. Howard who had pioneered research in this phenomenon. Polyethylene offers a good property profile and through corresponding treatment and/or additives the range of possibilities of application becomes more diverse. Therefore, the

problem of ESC is very important for many applications including packaging industry (bottles, containers, foils, films, etc.), electric industry and electronics (wire and cable insulation), medicine (labware, caps, implant components, etc.), automobile industry (tanks, pipes, coatings, etc.) and many more.

## **1.2 Research Tasks**

Within the framework of the Ph.D. thesis, investigations on environmental stress cracking resistance (ESCR) were carried out on polyethylene compounds comprising low density polyethylene (LDPE) and different amounts of ethylene-vinyl acetate random copolymer (EVA). Furthermore, the system contains carbon black as filler. These blends are used mainly as cable insulation. It is well known that neat LDPE is susceptible to ESC. It has been known that the addition of an elastomeric material to polyethylene can improve its resistance to ESC. EVA is a rubber-like material that may retard the process of ESC in polyethylene.

The primary aim of this work is to investigate the ESCR of LDPE/EVA blends. Bell-telephone test is carried out in order to investigate the influence of the EVA content and the test temperature on the failure time. As a result of the long thermal treatment of the samples during the Bell telephone test, different reorganization processes can occur. Therefore, any changes in the thermal properties are detected by differential scanning calorimetry. Wide- and small angle X-ray scattering investigations are carried out for determination of any changes in the crystal structure and lamellae arrangement as a result of the long thermal treatment in the Igepal surfactant during the Bell telephone test. Relevant microscopic techniques (atomic force microscopy, transmission electron microscopy, scanning electron microscopy, high voltage electron microscopy) are applied for morphology characterization, monitoring the process of brittle failure and micromechanical deformation mechanism. The morphological data should be then correlated with the results of the ESCR test and the mechanical tests in order to create a correlation model for morphology and ESCR behavior of polyethylene compounds.

## 2. Definition of Environmental Stress Cracking (ESC)

Environmental stress cracking (ESC) in plastics means the failure at about room temperature due to continuously acting external and/or internal stresses in the presence of surface active substances (known as stress cracking agents) such as alcohols, soaps, dyes, agents containing moisture.<sup>[1, 2, 6, 7]</sup> Although ESC results from the interaction of the polymer with certain chemicals, it is not a chemical reaction between the polymer and the active environment. The stress cracking agents do not cause any chemical degradation of the polymer but they accelerate the process of macroscopic brittle-crack formation.

ESC is a major problem in the long-term service behavior of plastic products. ESC can produce quite expensive failures when these occur after manufacturing, for example, during warehouse storage, shipping, at point of sale, or during long time applications.

ESC of polymers is analogous to the stress corrosion problem in metals.<sup>[8, 9]</sup> A similar process was observed in metals under stress and in the presence of surfactants. Macroscopically ESC is characterized by the slow brittle failure of polymers by organic substances. ESC takes place after a certain period of time: the lower the stress, the longer the durability.<sup>[10]</sup> The time factor arises from two sources. First, plastic deformation takes place over a period of time and, second, it will take some time for the stress cracking agent to penetrate the micro-cracks from which the ultimate fracture is initiated. The tendency for stress cracking to occur increases with increasing temperature and occurs at loads significantly below the yield point.<sup>[11]</sup>

### 2.1 The Occurrence of ESC

In principle, ESC occurs in amorphous polymers as ABS, PC, PMMA, PS, PVC and SAN as well as in semi-crystalline thermoplastics like PE, PP, PA, PB.<sup>[2, 12]</sup> Amorphous polymers (glassy polymers) exhibit a higher tendency for this type of failure because their loose structure facilitates fluid permeation into the polymer. Amorphous polymers show enhanced sensitivity to ESC at temperatures close to their  $T_g$  values due to the increased free volume as  $T_g$  is approached, which facilitates fluid permeation into the polymer. The solvent then becomes locally dissolved and promotes crazing, cracking or plasticization. In amorphous polymers, crack formation due to ESC is often preceded by craze formation. Crazes are expanded regions held together by highly drawn fibrils which bridge the micro-cracks and prevent their propagation and coalescence. Semi-crystalline polymers such as PE show brittle fracture under stress if exposed to stress cracking agents. In such polymers, the crystallites are connected by the tie molecules through the amorphous phase. The tie molecules play a

decisive role in the mechanical properties of the polymer, through the transmission of load. Stress cracking agents act to lower the cohesive forces which maintain the tie molecules in the crystallites, thus facilitating their “pull-out” and disentanglement from the lamellae. Consequently, cracking is initiated at stress values lower than the critical stress level of the material.

In general, the failure process begins with the embrittlement of the polymer. Then the crack initiation takes place, which is favored by the acting load. ESC type of failure is characterized by the presence of macroscopic cracks and a fibrillar structure of the craze, formed ahead of the crack.<sup>[6]</sup>

Several molecular mechanisms for ESC have been proposed over the past few years.<sup>[11, 13-16]</sup> Lustiger et al.<sup>[11, 17]</sup> have proposed “interlamellar failure” as the controlling mechanism of ESC, with the concentration of the tie molecules as a factor in ESCR. Brown et al.<sup>[14, 18]</sup> concluded that the mechanism of slow crack growth involves the disentanglement of the tie molecules from the crystals. The number of tie molecules and the strength of the crystals that anchor them are considered the controlling factors.

## **2.2 The Stress Factor**

As the name suggests, stress cracking requires the polymer to have exposure to an intrinsic residual stress or an externally applied stress. If the plastic moulding is completely free of stress, then no stress cracking will occur.<sup>[1]</sup> Even polymers exposed to liquids or vapours that have a swelling or wetting effect will not undergo ESC unless there is an externally applied or moulded-in stress present. External stress may be the result of component assembly, improper packing or storage, incorrect use, etc.

## **2.3 Stress Cracking Agents**

All liquids that are significantly absorbed by a plastic in a short period under simple immersion conditions have a high probability of being severe stress cracking agents for that particular plastic. Such liquid/plastic pairs can be easily assessed via simple chemical compatibility tests. These pairs should be avoided in service by good design and polymer selection. Most liquids with weak hydrogen bonding are usually strong or moderate stress cracking agents. These include organic liquids as aromatic hydrocarbons, halogenated hydrocarbons, ethers, ketones, aldehydes, esters, and nitrogen and sulphur containing compounds.<sup>[2]</sup> Aliphatic hydrocarbons and liquids with strong hydrogen bonds, for example

water and alcohols, are less aggressive agents in this respect. Many liquids are more aggressive at temperatures near to their boiling point. Liquids with a high molar volume are less likely to be aggressive stress cracking agents. Such liquids tend to have high viscosity and high boiling temperatures.

Typical solvents that cause stress cracking in most amorphous polymers include petroleum ether, carbon tetrachloride, toluene, acetone, ethanol and chloroform. Plastic medical device components can often suffer ESC due to the exposure to compounds as isopropanol and lipid solutions.<sup>[1]</sup>

In general, surface-active environment is a liquid, which is able to lower the polymer surface energy, but does not swell or dissolve polymer. The higher the ability of the liquid environment to lower the polymer surface energy, the lower the yield point and shrinkage, and *vice versa*.<sup>[19]</sup>

The potential of a stress cracking agent to promote stress cracking of the polymer is governed by the driving force by which the stress cracking liquid transports through the craze fibril structure. Once the liquid penetrates to the craze tip, it then begins to plasticize the polymer and allows the craze to grow. The degree of absorption of a solvent into a polymer is a function of the solubility parameters of the liquid and the polymer. The solubility parameter as defined by Hansen comprises three types of cohesive forces: dispersive, polar and hydrogen bonding.<sup>[1, 20]</sup> The solubility parameter of a stress cracking agent is a measure of the total cohesive attraction between the fluid molecules. If the solubility parameter of the polymer matches that of the fluid, then diffusion of the agent will occur and ESC is likely. Kambour et.al.<sup>[21]</sup> were the first to show that the critical strain for solvent-induced craze initiation and stress cracking is related to the solubility parameter of the solvent. In cases where the stress cracking agent is an organic solvent, the severity of the stress cracking can be predicted by examining the solubility parameters of both the polymer and the stress cracking agent.<sup>[22]</sup>

ESC is due to the selective absorption of the stress cracking agent into a micro-yielded or stress-dilated zone. This process locally reduces yield strength of the polymer and leads to fracture. The fracture may be either ductile or brittle depending on stress and time considerations. Diffusion of detergent molecules into the polymer due to stress might result in increased chain mobility and therefore in a reduction of the activation energy (plasticizing effect) of the deformation process.<sup>[7]</sup> Stress-cracking agents act to lower the cohesive forces which maintain the tie molecules in the crystallites, thus facilitating their “pull-out” and disentanglement from the lamellae.<sup>[1]</sup>

## 2.4 A Graphic Model for Failure

In order to describe ESC on a molecular level it is useful to review the deformation process in semi-crystalline polymers through a graphic presentation. This model then can be used to contrast ductile behavior with the brittle behavior. When describing the failure mechanism, it is important to consider the intercrystalline or amorphous polymer chains. Three types of intercrystalline material are shown in Figure 2.1a:

- 1) Cilia – chains suspended from the end of a crystalline chain,
- 2) Loose loops – chains that begin and end in the same lamella,
- 3) Tie molecules – chains that begin and end in adjacent lamellae.

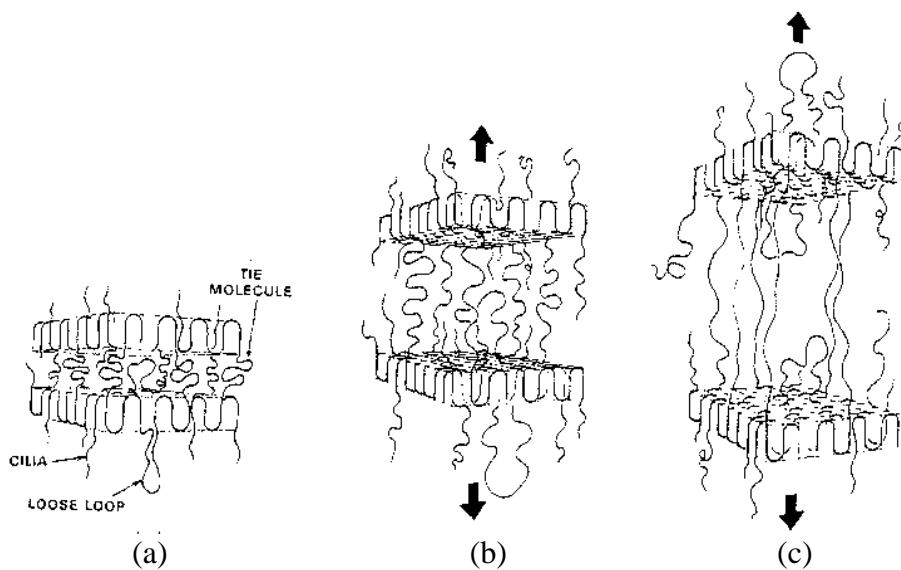


Figure 2.1 Initial steps in the deformation of polyethylene.<sup>[4]</sup>

The failure may be either ductile or brittle depending on stress level and time considerations. When a tensile load is applied normal to the face of lamellae, the tie molecules stretch as shown in Figure 2.1b. At a certain point, the tie molecules can be pulled out no further (Figure 2.1c). At this time the lamellae break up into small units (Figure 2.2a). According to this model<sup>[23]</sup>, these so-called “mosaic blocks” are directly incorporated into a new fiber morphology (Figure 2.2b). Because the tie molecules hold the lamellae “bricks” together, their integrity is critical for ductile-type behavior to occur.<sup>[4]</sup>

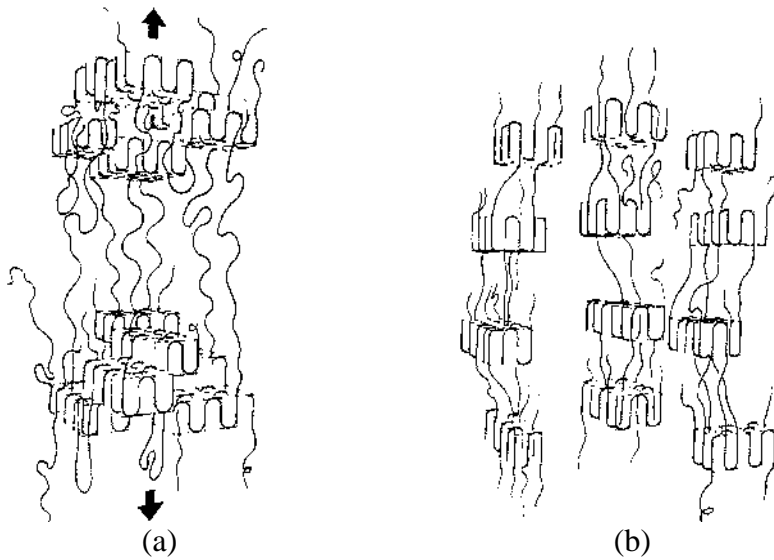


Figure 2.2 Steps in the ductile deformation of polyethylene.<sup>[4]</sup>

Brittle-type failure of plastics takes place over long periods of time at lower stress levels than the ductile mechanism discussed above.<sup>[24]</sup> The stress necessary to achieve large-scale fiber pullout is not attained because the material is under a low stress level. Therefore, the loading situation can be expected to remain as shown in Figure 2.1 for a relatively long time. After a finite period of time, most of the tie molecules disentangle and the load cannot be supported by a few tie molecules remaining, and, as a result the material fails in brittle manner (Figure 2.3).

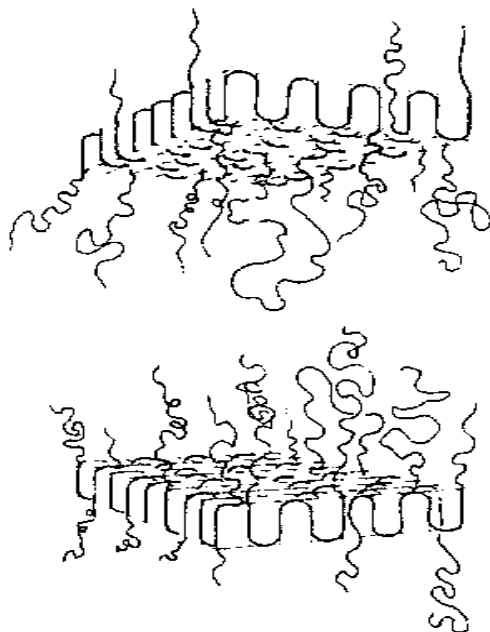


Figure 2.3 Final step in the brittle failure of polyethylene.<sup>[4]</sup>

As mentioned already, the stress cracking agents accelerate the brittle-failure process. Any stress cracking agent will lubricate the tie molecules and that will facilitate their pull-out from the lamellae.

The deformation behavior of each semicrystalline polymer depends on several factors as morphology, molecular orientation, degree of crystallinity, molar mass, and drawing conditions in a rather complex manner. When polyethylene is deformed in the solid state, until fracture, it passes through a series of different structural states. Strobl et. al.<sup>[25-27]</sup> studied the deformation behavior of various polyethylenes under an applied tensile load based upon measurements of true stress-strain curves, elastic-recovery properties, and texture changes at different stages of the deformation process. Their results showed that there exists a common general scheme for the deformation behavior which can be associated with: (1) the onset of isolated slip processes, (2) a change into a collective activity of the slips, (3) the beginning of fibril formation after a fragmentation of the lamellar crystals, and (4) chain disentanglement resulting in a finite truly irreversible deformation. The strains at which these points take place remain constant over various drawing temperatures and crystallization temperatures. In contrast to this, the corresponding stresses vary considerably.

Raman spectroscopy and polarized vibrational spectroscopy can be used to characterize the changes in bulk orientation of both crystalline and amorphous chain segments.<sup>[28-30]</sup> In general, when a polymer is stretched, chain backbones align in the direction of the stretch. Especially, for polyethylene, Pezolet<sup>[31]</sup> reported that at draw ratios of 7 the amorphous chains show stronger alignment in the strain direction than the crystalline chains because of the high mobility of the flexible amorphous regions. At higher draw ratios, as the original crystalline lamellae begin to break down, the crystalline chains also orient in the stress direction.

For high density polyethylene X-ray scattering data indicate that the predominant deformation mechanism involves the rotation of blocks of lamellae facilitated by the flexible amorphous regions.<sup>[32]</sup> Beyond the yield point, the deformation mechanism is chain-slip process within the lamellae. Kip et al.<sup>[33]</sup> carried out a detailed morphological study of cold-drawn polyethylene materials by Raman spectroscopy and wide-angle X-ray scattering. Their results suggest that the crystalline structure with dislocations and ruptured crystals formed by cold-drawing is probably a result of molecules being pulled through the crystals.

Somorjai et.al.<sup>[34]</sup> characterized the surface of low and high density polyethylene by atomic force microscopy as the polymers were stretched. The surfaces roughen when the polymers are stretched. The nodular domains on the surface expand in the direction of the stretch as the strain is increased and contract when strain is decreased.



The degree of crystallinity has a profound effect on the yielding and fracture of polyethylenes. However, the influence of degree of crystallinity depends on the temperature of deformation. In the temperature range where yielding is the failure mode, the yield point increases with degree of crystallinity.<sup>[35]</sup> In the low-temperature regime, where the brittle fracture is the failure mode, the fracture toughness generally increases with decreasing the degree of crystallinity for linear polyethylenes.

## **2.5 Factors Influencing the ESC-Behavior**

The ESC behavior of a polymer is strongly dependent on the concentration of the stress-cracking agent, exposure temperature, exposure time, and most of all, the level of strain on/in the polymer.

The transition to brittle behavior is accelerated to shorter times by increasing temperature, cyclic loading, dilational stress, stress concentrations.<sup>[2]</sup> The effect of temperature is complex. Physical aging is a manifestation of small scale relaxation processes that take place in the amorphous regions of a glassy polymer, causing volume contraction and densification of the sample.<sup>[36]</sup> The polymer structure remains unchanged but the local packing of the chain alters. This leads to dimensional changes and alteration of physical properties such as brittleness, tensile strength, and the glass transition temperature. As the extent of physical aging increases there are corresponding decreases in the enthalpy, the specific volume and the fracture toughness, while increases in glass transition temperature, the yield stress and tensile modulus of the material may also be observed.

Localized concentration of the stress due to local geometrical features as notches, voids, and inclusions will increase the stress and modify the nature of the stress field. Craze initiation is accelerated by stress fields with high dilational stress and retarded under hydrostatic pressure.<sup>[2]</sup>

There are critical polymer properties and variables which affect ESCR. The higher the molar mass the longer the polymer chains, which results in more tie molecules and increased ESCR.<sup>[37]</sup> ESCR decreases with increasing the degree of crystallinity.<sup>[6, 37]</sup> Higher comonomer content and longer comonomer short chain branches (higher  $\alpha$ -olefins) provide better ESCR of LLDPE.<sup>[4, 38]</sup> Increased pigment content usually decreases the ESCR.<sup>[39, 40]</sup> The thermal history of the material and the processing conditions are also important factors for the ESCR behavior of the polymers.<sup>[41-44]</sup>

### **3. Test Methods for Evaluation of ESCR of Plastics**

A common laboratory request for ESC-prone polymers is to check ESCR performance for quality control, competitive product evaluations, and research and development work. There is a variety of test methods available for assessing the ESCR of thermoplastics and they can be divided into two groups: tests at constant strain and tests at constant load (stress). It should be remembered, that any test that involves the application of a constant strain is less severe than the apparently equivalent test involving the application of a constant load because the strain is not maintained constant during the test.<sup>[2]</sup> The stress in the sample induced by constant strain will decay with time due to stress relaxation, which makes the ESC conditions less severe.

#### **3.1. Tests at Constant Strain**

Constant strain methods are most commonly used because they are cheap to perform and the investment in equipment is small. The main limitation of using constant strain tests with plastics is that the stress will decay with time due to stress relaxation. It is important for the accuracy of the ESC tests to select the most appropriate strain applied on the sample, because high strain will result in cracking too quick to observe, and lower strain will cause long-term experiments. Wang et. al.<sup>[45]</sup> carried out investigations to determine the appropriate values of strain to be exerted in the ESC test of different kinds of plastics. They found that for the brittle plastics the strain should be selected in the elastic region of the stress-strain curve, while for toughened plastics the plastic region is the best selection.

##### **3.1.1 Three-Point Bending Test**

This normally involves the application of a mid-point deflection  $\delta$  which generates a maximum surface strain. There are two major variants of the test which are shown in Figure 3.1.<sup>[2, 46]</sup> Samples are placed in the test device and the desired strain is attained by adjusting the screw. Deformed samples (strips) are immersed in the stress cracking agent. After a predetermined test period the samples are removed, rinsed with distilled water and allowed to dry at room temperature for 24 hours. Following this, the samples are inspected for crazing and their tensile properties are investigated.

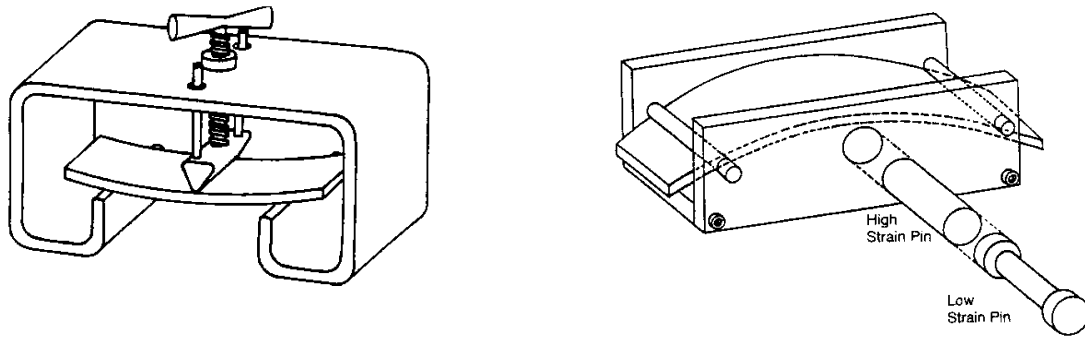


Figure 3.1 Three-point bending apparatus for testing the ESCR under constant strain.

### 3.1.2 Bell Telephone Test (BTT)

This test was developed by Bell Laboratories in the USA for testing the ESCR performance of polyethylene cable insulation.<sup>[1, 2, 47]</sup> The test specimens (38 x 13 x 3 mm) are notched and bent (at about 180°C) with the notch pointing upwards in a metal U-shaped specimen holder (Figure 3.2).

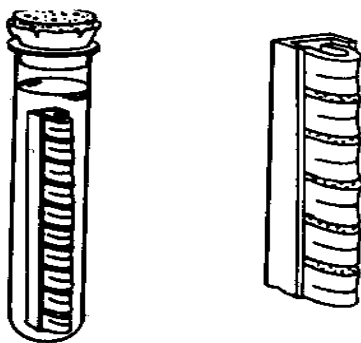


Figure 3.2 Bent-strip test for flexible materials (Bell telephone test).

The maximum surface strain is calculated by using the following equation:

$$\varepsilon_{\max} = \frac{t}{w - t} \times 100, [\%] \quad (3.1)$$

where  $t$  is the thickness of the sample and  $w$  is the width of the holder.

The holder is placed in a glass tube containing a 10 vol.-% Igepal CO-630 water solution. The tubes are sealed and placed in a water bath at 50°C. The number of samples that exhibit cracking is recorded as a function of time. Failure is determined as the appearance of any crack visible by the naked eye. Duration of the test should be at least 48 h. All samples have to pass the test. If one test specimen has failed, the test is to be considered as not passed.

BTT method has been widely adopted as the standard method. This method, however, cannot be easily automated. The occurrence of cracks or fracture in the test pieces is detected solely by visual evaluation conducted at fixed intervals. Thus, the method may give rise to an error. Saeda and Suzaka<sup>[48]</sup> proposed a method to measure the ESC at constant strain which is almost completely free from the influence of human error. This method is denoted as ORL method because the method was developed in Oita Research Laboratory, Showa Denko, Japan. The longitudinally sectioned view of the device is shown in Figure 3.3.

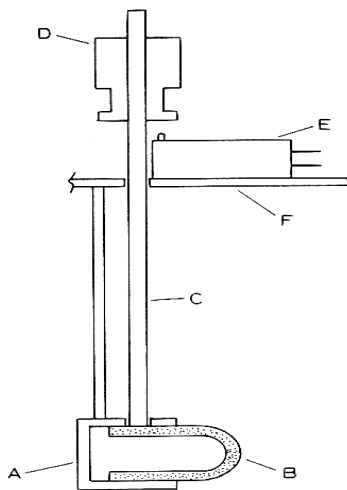


Figure 3.3 Oita Research Laboratory (ORL) ESCR test device.<sup>[48]</sup>

A – sample holder, B – bent strips, C – shaft, D – load, E – electric switch, F – supporting plate.

The sample holder is made the same size as the sample holder of ASTM-D1693 (Bell telephone test) which can hold ten bent strips in position for testing. While the BTT measures the time when a small crack appears in the specimen by visual means, the ORL method can detect the time to failure correctly by automated means (by using an electric device) without a human error.

## 3.2 Tests at Constant Load (Stress)

### 3.2.1 Constant Tensile Load Test

The test was developed by Lu and Brown<sup>[49, 50]</sup> for measuring the slow crack growth behavior of polyethylenes. The method involves a constant load test on a single edge notched specimen under plain strain conditions in air or stress cracking agent at various temperatures. Figure 3.4

shows a scheme of the device used for the test at constant load. A simple timer is used to record the failure time. The timer switches off when the specimen cracks. The rate of slow crack growth can be monitored with a microscope by measuring the crack opening displacement versus time.

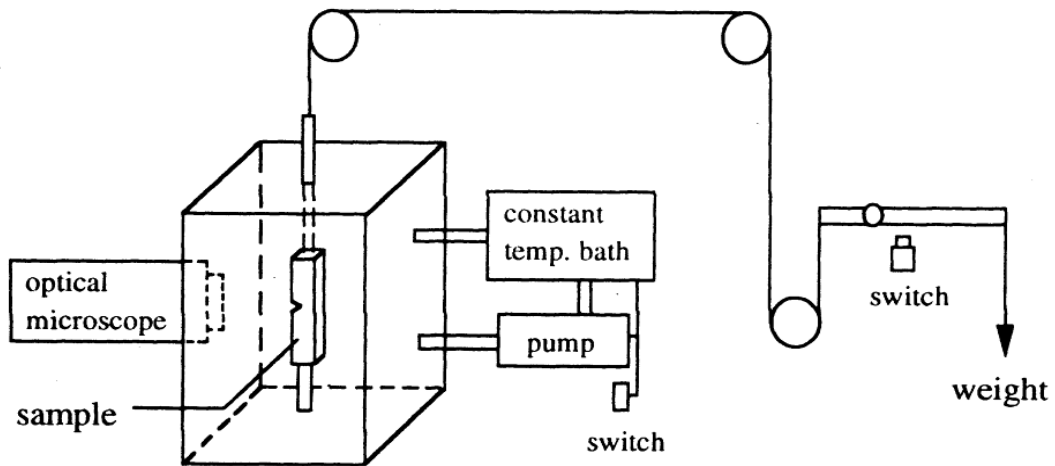


Figure 3.4 Apparatus for the test at constant load.<sup>[51]</sup>

The value of the applied stress depends on the testing temperature. The recommended value is that which produces brittle failure as fast as possible. Based on extensive investigations by Lu and Brown<sup>[24, 52, 53]</sup> on many different polyethylenes, the constant load test is usually carried out in 10 vol.-% Igepal solution at load of 4.2 MPa , and temperature of 50°C.

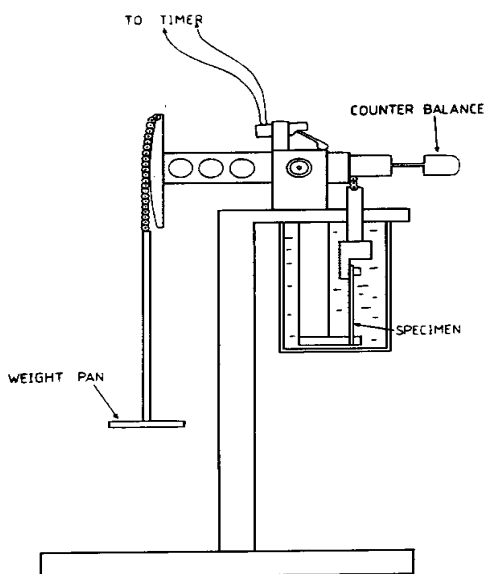


Figure 3.5 Rapra high temperature tensile creep rupture set-up.<sup>[2]</sup>

Figure 3.5 shows Rapra high temperature tensile creep rupture testing device which is quite similar to the common test at constant load. It involves application of a tensile stress and the recording of the time to rupture.

### 3.2.2 Monotonic Creep Test

Hough and Wright<sup>[3]</sup> developed a monotonic creep testing machine for assessing the ESC of amorphous thermoplastics. This is similar to the slow strain rate testing technique used for many years by the metal industry to assess the stress corrosion cracking and the hydrogen embrittlement.<sup>[54]</sup> However, here the strain response to a constant stressing rate is monitored. The method as shown in Figure 3.6 employs a tensile creep machine with the weight pan replaced by a blow moulded vessel. Specimen strain is monitored via a Moirè fringe extensometer which is shown in Figure 3.7.

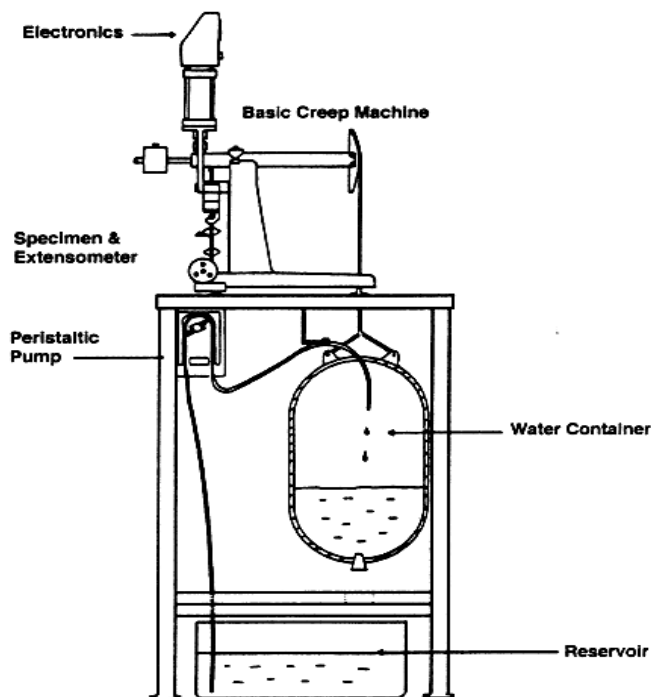


Figure 3.6 Monotonic creep testing machine.<sup>[3]</sup>

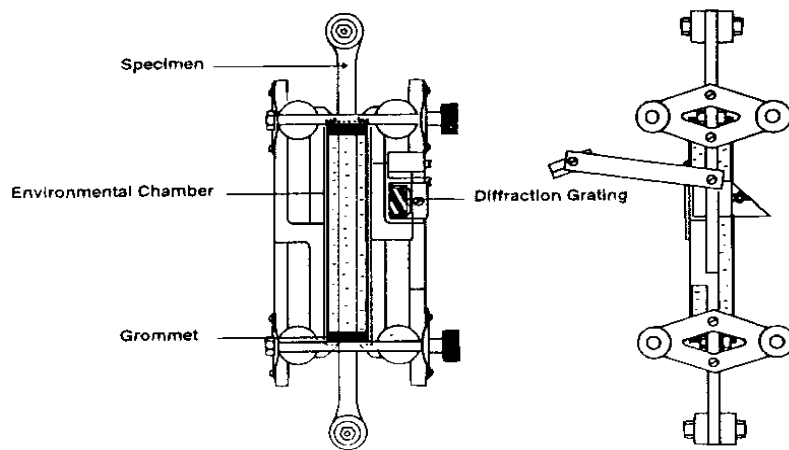


Figure 3.7 Rapra Moirè fringe extensometer with environmental chamber attached to the specimen.<sup>[3]</sup>

The monotonic creep method is capable of high resolution and discrimination. The fact that the method generates critical time, critical stress and critical strain proposes the use of the method for investigating the criterion for initiation of the ESC phenomenon.<sup>[2]</sup>

### 3.2.3 Test Method for Determining ESCR of Ethylene Based Plastics

BTT has been the method most commonly accepted by industry as a measure of the ESCR of ethylene based plastics. While BTT is attractive from the point of view of simplicity, it has been criticized on several counts. There are a few variables that can affect reproducibility of the test results: the curvature of the bent specimen depends on the stiffness of the polymer material; the strain is not maintained constant during the test; it is difficult to assure a sharp notch that is reproducible from specimen to specimen. Crissman<sup>[55]</sup> developed a new method for determining the ESCR of ethylene plastics under different stresses and temperatures (Figure 3.8). A strip specimen is bent around a metal cylindrical form having a specified radius of curvature. This ensures that all the specimens conform to the same geometry during the test. Typically the specimens are unnotched strips. The stress cracking agent is a 10 vol.-% Igepal solution in water. The stress-cracking behavior of different polyethylenes is investigated in the temperature range from 23 to 90°C and constant applied stress. A set of conditions was determined that can be applied to polyethylenes having widely different densities and molar masses. The optimum test conditions are as follows: a nominal specimen thickness from 1 to 1.25 mm, a bend radius of 5.5 mm, applied stress of 5 MPa, and a temperature of 75°C.

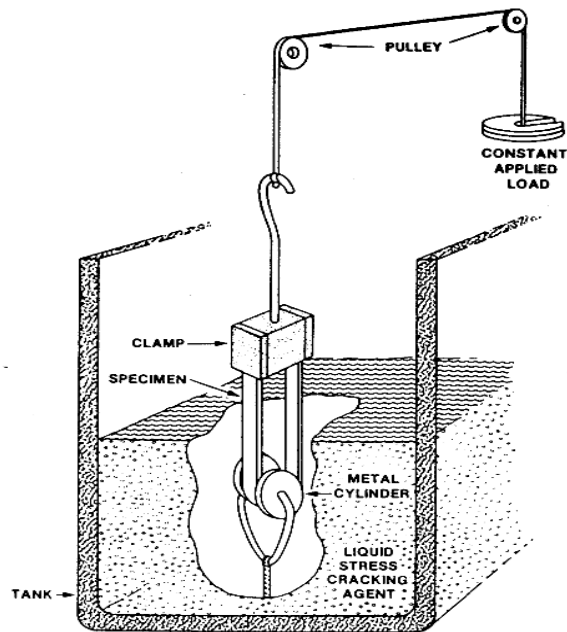


Figure 3.8 View of the device for testing ESCR of ethylene based plastics.<sup>[55]</sup>

### 3.3 Bottle ESCR Test

Unfortunately, the data obtained by bent strip methods do not necessarily correlate with those results obtained for bottles made from the same polymer. A bottle ESCR test has been developed for assessing the ESCR of plastic bottles. In this technique, the bottles are filled with a stress cracking solution which fills 10 vol.-% of the bottle. The capped bottles are then placed in an oven at 60°C and a stress is generated by the increased internal pressure.<sup>[1]</sup> Bottles that do not fail after 7 days are considered adequate.

It can be concluded that the constant strain methods are widely used for examination of the ESCR of plastics due to their simplicity and cheap equipment necessary for the tests. But the reproducibility of the results is not so good because of human error (failure is detected visually), the curvature of the test specimen depends on the stiffness of the polymer material and strain is not maintained constant during the test. The stress will decay with time due to stress relaxation. Tests at constant load are more accurate because an optical microscope is usually used for detecting of the notch opening and crack opening displacement. The time to complete failure is directly proportional to the time for crack initiation<sup>[15, 55]</sup> and that makes it possible to predict time to failure in the initial stage of the slow crack growth process. And therefore, the test procedure is shorter than the one at constant strain.



## 4. Thermodynamics of Polymer Blends

Polymeric materials find growing applications in various fields of everyday life because they offer a wide range of application relevant properties. Blending of polymers is a technological way for providing materials with full set of desired specific properties at the lowest price, e.g. a combination of strength and toughness, strength and solvent resistance, etc. Blending also benefits the manufacturer by offering improved processability, product uniformity, quick formulation changes, plant flexibility and high productivity.<sup>[56]</sup>

If two polymers are mixed, the most frequent result is a system that exhibits a complete phase separation due to the repulsive interaction between the components (i.e. the chemical incompatibility between the polymers).<sup>[57, 58]</sup> Complete miscibility in a mixture of two polymers requires that the following condition is fulfilled:

$$\Delta G_m = \Delta H_m - T\Delta S_m < 0 \quad (4.1)$$

where  $\Delta G_m$ ,  $\Delta H_m$ , and  $\Delta S_m$  are the Gibb's free energy, the enthalpy and entropy of mixing at temperature T, respectively.

For a stable one-phase system, criteria for phase stability of binary mixtures of composition  $\phi$  at fixed temperature T and pressure p are:

$$\Delta G_m < 0 \quad , \quad \left( \frac{\partial^2 \Delta G_m}{\partial \phi^2} \right)_{p,T} > 0 \quad (4.2)$$

Miscible polymer blend is a polymer blend which is homogeneous down to the molecular level and associated with the negative value of the free energy of mixing and the domain size is comparable to the dimensions of the macromolecular statistical segment. The value of  $T\Delta S_m$  is always positive since there is an increase in the entropy on mixing. Therefore, the sign of  $\Delta G_m$  always depends on the value of the enthalpy of mixing  $\Delta H_m$ . The polymer pairs mix to form a single phase only if the entropic contribution to free energy exceeds the enthalpic contribution, i.e.,

$$\Delta H_m < T\Delta S_m \quad (4.3)$$

For most polymer blends the miscibility increases with increasing the pressure. The effect depends on the magnitude of the heat of mixing  $\Delta H_m$ . For  $\Delta H_m < 0$  the miscibility is enhanced by compression, whereas for those with  $\Delta H_m > 0$  it is reduced.

A schematic phase diagram is shown in Figure 4.1. There are three regions of different degree of miscibility: 1. The single-phase miscible region between the two binodals, 2. The four fragmented metastable regions between binodals and spinodals, and 3. The two-phase separated regions of immiscibility, bordered by the spinodals. The diagram also shows two critical solution temperatures, the lower, LCST (at higher temperature), and the upper, UCST (at lower temperature). The phase diagram with two critical points is a rule for mixtures of low molar mass components, whereas the polymer blends usually show either LCST (most) or UCST.

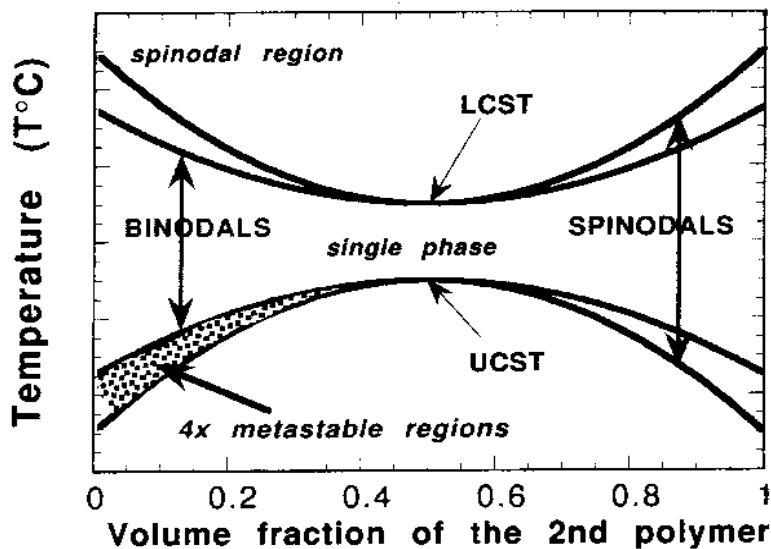


Figure 4.1 Phase diagram for liquid mixtures with the upper and the lower critical solution temperature, UCST and LCST, respectively.<sup>[59]</sup>

The binodals (Figure 4.1) separate miscible (one-phase) and metastable region, the spinodals separate metastable and two-phase region. The thermodynamic conditions for phase separations are given by<sup>[59]</sup>:

spinodal: 
$$\left( \frac{\partial^2 \Delta G_m}{\partial \phi^2} \right)_{p,T} = 0 \quad (4.4)$$

critical point: 
$$\left( \frac{\partial^2 \Delta G_m}{\partial \phi^2} \right)_{p,T} = \left( \frac{\partial^3 \Delta G_m}{\partial \phi^3} \right)_{p,T} = 0 \quad (4.5)$$

The phase separation takes place when a single-phase system suffers a change of either composition, temperature or pressure that forces it to enter either the metastable or the spinodal region. When the system enters from single-phase region into the metastable region, the phase separation occurs by the mechanism resembling crystallization – slow nucleation followed by growth of the phase separated domains.<sup>[59]</sup> By contrast, when the system is forced to jump from a single-phase into the spinodal region of immiscibility the phases separate spontaneously by a mechanism called spinodal decomposition.

Starting point for most of the theoretical interpretations of polymer solutions and blends is the Flory-Huggins lattice theory. It is basically an extension of the concept of regular solutions on polymer solutions. Thus the model restrictions are no change of volume during mixing (incompressible model), the entropy of mixing is entirely given by the number of rearrangements during mixing (combinatorial entropy) and the enthalpy of mixing is caused by interactions of different segments after the dissolution of interactions of the same type of segments. It is a mean-field model, i.e. only average interactions are taken into consideration. The main problem was to find an expression for the entropy of mixing because it was found experimentally that polymer solutions show significant deviations from values expected for ideal solutions. Assuming a rigid cubic lattice model, this problem was independently solved for polymer solutions by Huggins and Flory.

The lattice theory for the enthalpy of mixing in polymer solutions, developed by Flory and Huggins, can be formally applied to polymer mixtures, which provides a rough estimation of the miscibility of the polymers.<sup>[60, 61]</sup> Assuming random mixing of two polymers and  $\Delta V_m = 0$  yields the well-known expression for the combinatorial entropy of mixing  $\Delta S_m$  of the Flory-Huggins theory:

$$\Delta S_m = -R \left[ \frac{\phi_1}{r_1} \ln \phi_1 + \frac{\phi_2}{r_2} \ln \phi_2 \right] \quad (4.6)$$

where  $\phi_i$  is the volume fraction of the component  $i$  and  $r_i$  is the number of polymer segments,  $R$  is the gas constant. It can be seen that the entropy of mixing decreases with increasing molar mass ( $r_i$  is proportional to the degree of polymerization) and vanishes for infinite molar

masses. Applying the concept of regular solutions and assuming all pair interactions in the framework of a mean-field theory yields for the enthalpy of mixing  $\Delta H_m$ :

$$\Delta H_m = RT\chi\phi_1\phi_2 \quad (4.7)$$

For binary systems the Flory-Huggins equation can be expressed in the following form <sup>[62, 63]</sup>:

$$\Delta G_m = RT \left[ \frac{\phi_1}{r_1} \ln \phi_1 + \frac{\phi_2}{r_2} \ln \phi_2 + \chi\phi_1\phi_2 \right] \quad (4.8)$$

where  $\chi$  is the so called Flory-Huggins binary interaction parameter. R is the universal gas constant, and T is the absolute temperature. The first two terms of the right hand side in Equation 4.8 are related to the entropy of mixing and the third term is originally assigned to the enthalpy of mixing.

For polymers having infinite molar mass (i.e.  $r_i$  is infinite) the entropic contribution is very small and the miscibility or immiscibility of the system mainly depends on the value of the enthalpy of mixing (Equation 4.7). Miscibility can only be achieved when  $\chi$  is negative.

The term ‘parameter’ is widely used to describe  $\chi$  but it is definitively better characterized by the term ‘function’, because  $\chi$  depends on such quantities as temperature, concentration, pressure, molar mass, molar mass distribution and even on model parameters as the coordination number of the lattice and segment length.<sup>[56]</sup>

For polymers, the miscibility can only be achieved when  $\chi < \chi_{cr}$ . The  $\chi$  parameter at the critical point  $\chi_{cr}$  can be obtained from the definition of the critical point (Figure 4.1) and Equation 4.8 as follows:

$$\chi_{cr} = \frac{1}{2} \left( \frac{1}{\sqrt{r_1}} + \frac{1}{\sqrt{r_2}} \right)^2 \quad (4.9)$$

where  $r_i$  is the number of polymer segments (which is proportional to the degree of polymerization).

It should be mentioned that the Equations 4.8 and 4.9 are based on the assumption that  $\chi$  is not a function of composition,  $\chi_{cr}$  is only a function of the molar masses.

PE/EVA blends under investigations in this work are blends of a homopolymer and a copolymer (PE/E<sub>x</sub>VA<sub>1-x</sub>). The effective interaction parameter  $\chi$  between the homopolymer and the copolymer is given by:

$$\chi = x\chi_{EE} + (1-x)\chi_{EV} - x(1-x)\chi_{EV} \quad (4.10)$$

where  $\chi_{ij}$  are the segmental interaction parameters and  $x$  is the copolymer composition in mol.-%.  $\chi_{EE} = 0$  in the case of PE/EVA blends and therefore the effective interaction parameter  $\chi$  is equal to:

$$\chi = (1-x)\chi_{EV} - x(1-x)\chi_{EV} \quad (4.11)$$

And as already mentioned, the polymers are miscible when  $\chi < \chi_{cr}$ .

## 5. Polyethylene and Poly(ethylene-co-vinyl acetate)

### 5.1 Polyethylene (PE)

Polyethylenes are polymers produced by polymerization of ethylene. The well known structure of PE  $(-\text{CH}_2\text{CH}_2-)_n$  is simplified because practically all polyethylenes are branched. The basic properties of PE are determined by the molecular structure. Specifically they depend on degree of crystallinity, degree of polymerization, average molar mass  $M_w$  and molar mass distribution. PE is partially crystalline solid, somewhat flexible, whose properties are strongly influenced by the relative amounts of crystalline and amorphous phases. The smallest crystalline units, called lamellae, are planar in shape and consist of chains that are perpendicular to the plane and fold back and forth every 5-15 nm.<sup>[64]</sup> Lamellae are interconnected by a few chains, tie molecules, that pass from one lamella, through a small amorphous region, to another lamella. Staples of lamellae form fibrils. The lamellae form much larger spherically shaped units, called spherulites, which are connected through amorphous regions. The crystalline phase provides rigidity and a high softening temperature of about 120°C, whereas the amorphous phase provides flexibility and high impact strength.

Polyethylenes can be classified according to their density which is a result of their degree of crystallinity and type and content of branches. Commercially available grades are high density polyethylene (HDPE, PE-HD), medium density polyethylene (MDPE, PE-MD), low density polyethylene (LDPE, PE-LD), linear low density polyethylene (LLDPE, PE-LLD). HDPE is one of the highest-volume commodity plastics produced in the world. HDPE is manufactured by two methods distinguished by the catalyst system involved: the Ziegler method uses titanium halides, titanium esters and aluminum alkyls as catalysts, the Phillips method uses a chromium oxide catalyst and a co-catalyst.<sup>[65]</sup> In both methods the pressure is low (up to 50 MPa) and the ethylene molecules are coordinationally polymerized to predominantly linear macromolecules (i.e. non-branched). The low degree of branching of HDPE leads to a high degree of crystallinity (60 to 80 %) and corresponding high density of 0.942 to 0.965 g/cm<sup>3</sup>.

LDPE is produced by free-radical polymerization at high pressures of 100 to 300 MPa with oxygen or organic peroxide catalysts. Under such conditions PE macromolecules with long side-chain branches are produced. Typical commercial products have a degree of crystallinity of about 40 to 50 % and density between 0.915 and 0.935 g/cm<sup>3</sup>. These products contain 15-25 short-chain branches per 1000 carbon atoms.<sup>[64]</sup> For LLDPE products, ethylene is copolymerized with an  $\alpha$ -olefin, such as 1-butene, 1-hexene, or 1-octene, which gives LLDPE copolymers having density between 0.917 and 0.939 g/cm<sup>3</sup>. In polymerization catalyzed by

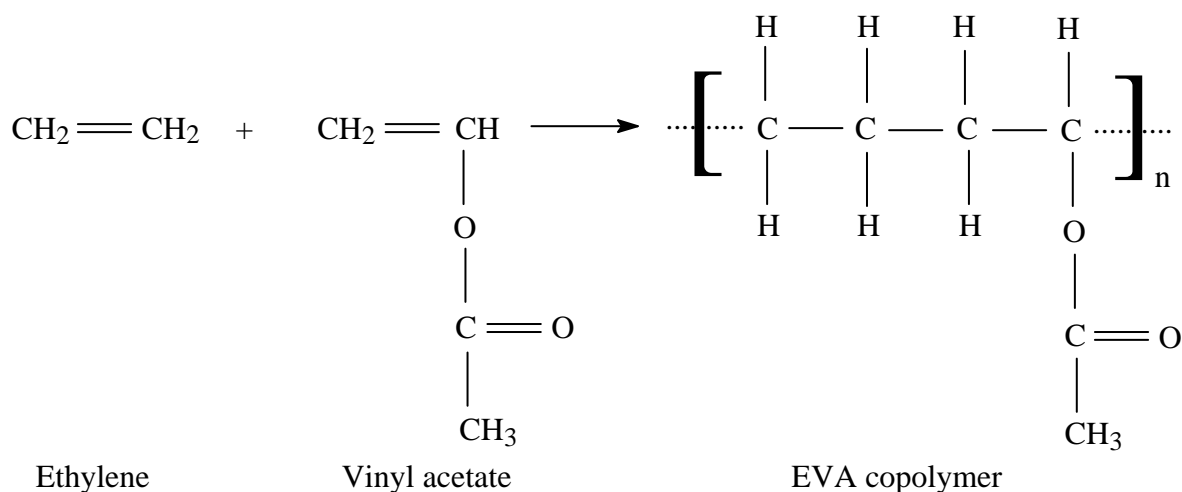
transition metals at low pressures (less than 2 MPa) and low temperatures (about 100°C) , polymerization occurs by a coordination polymerization mechanism. Propagation occurs by monomer coordination and integration into a transition metal-carbon bond. Titanium halides, aluminum alkyls and chromium oxides are used as catalysts.

For special applications there is high molar mass polyethylene (HMW-HDPE) with molar masses between 200.000 to 500.000 g/mol and ultra high molar weight polyethylenes (UHMWPE, HDPE-UHMW) which has a molar mass between  $3 \times 10^6$  and  $6 \times 10^6$  g/mol.<sup>[66]</sup> The high molar mass imparts outstanding abrasion resistance, high toughness (even at cryogenic temperatures), and excellent ESCR, but it does not generally allow the material to be processed conventionally. Because of its extremely high molar mass, UHMWPE cannot be processed by injection molding, blow molding, thermoforming or screw extrusion. Nevertheless, UHMWPE can be processed by compression sintering into sheet, block, and precision parts; and ram extrusion into rods, pipes, and profiles.

The characteristic properties of standard PE are: low density compared to other plastics, high toughness and elongation at break, very good electrical and dielectrical properties, very low water absorption, low water vapor permeability, high resistance to attack by chemicals, resistance to ESC increases with molar mass and the copolymers are more resistant to ESC than homopolymers.<sup>[67]</sup> Because of its non-polar, paraffinic hydrocarbon nature and high molar mass, PE shows unusually high resistance to chemical attack. PE is resistant to dilute acids, alkaline substances, solvents, alcohols, gasoline and water. PE is not resistant to oxidizing acids, ketones, aromatic hydrocarbons, chlorinated hydrocarbons and some detergents. These substances combined with internal or external stress lead to ESC. Resistance to ESC increases with decreasing density and increasing molar mass.

## **5.2 Poly(ethylene-co-vinyl acetate) (EVA)**

EVA is produced by copolymerization of ethylene and vinyl acetate (VA). With increasing proportion of the polar comonomer VA, the products change from modified PE to rubber-like products. EVA is mainly recognized for its flexibility and toughness (even at low temperatures), adhesion characteristics and stress-cracking resistance. Compared to LDPE, EVA is more polar and less crystalline due to the acetate groups.



Scheme 5.1 Chemical structure of monomers and EVA copolymer.

With increasing VA content, EVA copolymer becomes softer due to the decreased crystallinity. Up to a VA content of 10 wt.-%, the density decreases and the crystalline structure is not destroyed. While higher densities usually mean higher stiffness and a higher glass transition temperature, the opposite is true in the case of EVA copolymers.<sup>[67]</sup> Transparency increases with increasing VA content, the product becomes rubber elastic and the ultimate tensile strength passes through a maximum.

Products with up to 10 wt.-% VA are more transparent, flexible and tougher than LDPE. The high resistance to ESC is especially useful for cable isolation. Between 15 and 30 wt.-% VA the products are comparable with plasticized PVC. They are very soft and flexible. Compounds with 30 to 40 wt.-% VA are soft, elastic and highly fillable. Strength and adhesion are the desirable properties for coatings and adhesives. Between 40 and 50 wt.-% of VA rubber-like properties predominate and these products can be cross-linked as cable insulation by either peroxide or radiation. Copolymers with 70 to 95 wt.-% VA are used for manufacturing of emulsion paints, adhesives and film coatings.

EVA is resistant to dilute mineral acids, alkaline substances, alcohols, fats, oils and detergents but not to concentrated mineral acids, ketones, and aromatic or chlorinated hydrocarbons. The resistance to ESC increases with increasing VA content and decreasing melt index. It is significantly higher for EVA copolymers than for comparable LDPE.<sup>[67]</sup>

### 5.3 Polyethylene and Poly(ethylene-co-vinyl acetate) Blends

It is well known that EVA has been used in the modification of PE for better flexibility, toughness, and resistance to environmental stress cracking. The modifying effect of the EVA



copolymer on the mechanical properties of LDPE was studied recently. Serenko et al.<sup>[68]</sup> have found that the modification of LDPE with EVA copolymer results in an enhancement of the material toughness due to the increase of the adhesive strength at the matrix-rubber particle interface. Increasing the carbon black filler content in the LDPE matrix leads to an increase in the mechanical strength and a decrease in the elongation at break.<sup>[69]</sup> The brittleness of the carbon black filled LDPE can be balanced by adding flexible components such as EVA. Detailed studies on the relation between morphology of LDPE/EVA blends and their mechanical properties, dynamic mechanical properties and electrical resistance have been reported.<sup>[70-75]</sup> Ray and Khastgir<sup>[71]</sup> have found that an interpenetrating polymer network like structure was formed in LDPE/EVA blends with a minimum of 50 wt.-% EVA in the blend. The tensile strength and elongation at break of different LDPE/EVA blends improve with an increase in EVA content up to 50 wt.-%, after which the change is marginal.<sup>[72]</sup>

#### **5.4 Polyethylene and ESC**

The term ESC was used in the context of PE cable insulation.<sup>[4]</sup> This term was defined by J. B. Howard, who has pioneered research in this phenomenon. According to Howard, ESC is the “failure in surface initiated brittle fracture of a polyethylene specimen or part under polyaxial stress in contact with a medium in the absence of which fracture does not occur under the same conditions of stress”.<sup>[4]</sup> The stress-cracking resistance of PE is of considerable importance in such applications as cables, pipes, bottles, and geomembranes. Workers at the Bell Telephone Company in the USA in the 1960s observed frequent cracking of cable insulation after it had been cleaned with a soapy solution.<sup>[1]</sup> Following this, extensive work was then conducted on the ESC behavior of PE. This work also laid the foundation for the widespread use of HDPE in detergent bottles. In the case of an ESC failure of a PE detergent bottle, an important test is to check the density of the polymer, since the ESCR decreases as the density increases.

In the long term and under stress, PE exhibits slow crack growth (SCG) and brittle failure in non-aggressive environments such as air and water. Brown and co-workers have investigated the SCG in a wide variety of PEs.<sup>[76-80]</sup> They investigated the kinetics of SCG by using single edge notched specimens under a constant load. The crack opening displacement (COD) was measured by looking into the middle of the notch with an optical microscope. The COD was measured at the surface of the specimen and at the root of the notch. The mechanism of failure involves the formation of a craze at a point of stress concentration and the subsequent growth and fracture of the craze.

The SCG behavior of PE depends primarily on the molecular structure. The most important factors are molar mass, type of short branches, and density of the branches. PE is a semicrystalline polymer in which the lamella crystals are bonded by the tie molecules. The key to understanding the effect of molar mass is the tie molecules which join the crystalline blocks together.<sup>[37, 53]</sup> The number of tie molecules increases markedly with molar mass. The higher the molar mass the longer the polymer chains, which results in more tie molecules and more effective network of tie molecules.

Huang and Brown<sup>[37]</sup> investigated the effect of molar mass on SCG in linear HDPE with different molar masses by using single-edge notched tensile specimens. Sudden fracture was observed when the molar mass was below 18 000 g/mol, which is a critical molar mass below which tie molecules are not formed. The probability of forming a tie molecule depends on the end-to-end distance of the random coil in the melt relative to the long period.<sup>[77]</sup>  $L_c + L_a$  is the long period in which  $L_c$  is lamella thickness and  $L_a$  is the thickness of the amorphous layer. If the end-to-end distance of a random coil is greater than about twice the long period, tie molecules will be formed during crystallization.<sup>[37, 53]</sup> The rate of disentanglement of the tie molecules depends not only on the density of the tie molecules but also on the strength of the crystals. The stronger the crystals, the greater the resistance to the movement of the tie molecules. Annealing increases the crystal strength and the life time of PE when the annealing temperature is below 113°C, below which most thick crystals are not melted on annealing.<sup>[53]</sup> Generally, quenching reduces the degree of crystallinity and increases the density of tie molecules in PE. Density of tie molecules increases because quenching changes the kinetics of crystallization so that a given molecule has less time to gather together into the same crystal.<sup>[81]</sup> Crystallinity decreases with quenching since less time is available to form crystals and the crystals tend to be thinner.

Huang and Brown investigated the dependence of SCG on butyl branch density.<sup>[82, 83]</sup> Short chain branches increase the probability of forming tie molecules. As the branch density increases, the number of tie molecules increases, but, at the same time, the thickness of the lamella crystals decreases. The resistance to SCG of ethylene-hexene copolymers increases by a factor of  $10^4$  as branch density increases from 0 to 4.5/1000 C atoms.<sup>[82]</sup> Yeh et al.<sup>[51]</sup> investigated the influence of branch length on ESCR of PEs in Igepal solution. They found that the ESCR increased dramatically as the short-chain branch length increased from 2 to 4 and 6 carbon atoms in the side chain. This improvement in ESCR was attributed to the increased sliding resistance of the polymer chains through the crystal and through the entanglement in amorphous region.

Brown et al.<sup>[84]</sup> measured the resistance to SCG in binary blends of HDPE and model ethylene-butene copolymers (15, 61 and 117 branches/1000 C atoms) under a constant stress intensity. They found an increase in the time to failure with the addition of the copolymer if the copolymer could crystallize and the increase was the greater the higher the branch density. The copolymer with 117 branches/1000 C atoms could not crystallize and therefore its blends had time to failure that was less than that of the neat HDPE.

The effect of temperature on SCG was also measured. The resistance to SCG was investigated in binary blends of HDPE and ethylene-butene copolymers under constant stress and temperatures from 30 to 80°C.<sup>[85]</sup> There is a general exponential decrease in time to failure with increasing temperature because the process of chain sliding that occurs during disentanglement is a thermally activated process. The key to understanding the effect of test temperature on SCG in PE is based on the work of Lu, McGhie and Brown.<sup>[86, 87]</sup> SCG in linear polyethylene was investigated at constant load and temperatures from 30 to 80°C. Morphology of the samples was varied by annealing the quenched material at temperatures from 86 to 135°C. In the quenched state the crystals are relatively weak and imperfect. Annealing increases the crystal thickness and perfection. It was found that decreasing in resistance to SCG with increasing test temperature was greatest when the crystal thickness was least.

As shown by Lustiger and Corneliussen<sup>[11]</sup>, the same process of SCG occurs in the commonly used environmental stress cracking agent known as Igepal CO-630 (nonylphenoxypolyethylenoxide surfactant). Igepal not only enhances craze formation, but it also reduces the time for initiation of crack growth. The same authors investigated the effect of Igepal on the interlamellar links in PE.<sup>[88]</sup> It was found that the stress cracking agent breaks the interlamellar links when these links are subjected to thermally induced stresses arising from secondary crystallization. Ward et al.<sup>[52]</sup> measured the time to failure of 22 polyethylenes in air and Igepal at 50°C. It was observed that shortening of failure time by Igepal did not occur unless the time to failure was longer than 10<sup>3</sup> min. Igepal plays two roles in the process of SCG. It enhances craze growth by plasticizing amorphous regions, and it enhances fracture by interacting with the crystalline region of the fibrils at the base of the craze.<sup>[14]</sup> Igepal must diffuse into the crystal in order to accelerate fracture which is a relatively slow process. There is a delay time called “Igepal transition time”, which corresponds to the time required by the Igepal to diffuse into the crystalline region in order to accelerate the fracture process.<sup>[14]</sup>

Tonyali et al.<sup>[89]</sup> investigated the ESC of LDPE in various organic liquids and water. They found that the structure of the detergent solution played a large role in the cracking behavior and, furthermore, they attributed the increase in the crack speed with detergent concentration

as being due to the increase in the number of micelles in the water solution.<sup>[90]</sup> The effect of 10 vol.-% Igepal CO-630 in water, ethanol and ethylene glycol was investigated. The lowest constant crack speed (0.02 mm/h) was observed in the ethanol solution and the highest speed (0.55 mm/h) in the water solution. It has been known for many years that the detergent solutions in water have micellar structure.<sup>[91]</sup> Igepal CO-630 gives rise to micellar solution in ethylene glycol and water, but it does not form micelles in ethanol.<sup>[92]</sup> The higher crack speed in water solutions was supposed to be related to the micellar structure of the solutions, which may create more efficient plasticization at the crack tip. A linear relationship between crack speed and Igepal concentration up to 25 vol.-% was established.<sup>[93]</sup> Chang and Donovan<sup>[94]</sup> studied the effect of stress intensity on crack growth in LDPE in Igepal solutions having concentrations up to 10 vol.-%. Crack growth was measured as a function of time with an optical microscope. According to their results, there are three regions in the crack driving force /crack speed diagrams: Region I where the crack speed increases with crack driving force (G) in the specimen, Region II where the crack speed is independent of G, and Region III where the crack speed decreases. Brown et al.<sup>[95]</sup> measured the SCG in LLDPE by a notch tensile test at 50 °C in Igepal CO-630. The concentration of Igepal was varied from 0 to 100 vol.-%. A minimum in time to failure occurred at ~ 50 vol.-% Igepal solution. There is a significant increase in time to failure when the concentration is increased from 50 to 100 vol.-%, which was related to the observation that the higher concentration produces a greater blunting of the notch. Instead of forming a craze as it is in the case at lower concentration, a shear zone forms at the root of the notch. The basic mechanism of failure involves the disentanglement of the tie molecules from the crystals. Fracture is initiated in the fibrils of the craze that forms at the root of the notch when the specimen is first loaded. The time to fracture the fibrils at the base of the craze governs the subsequent time to failure.

## 6. Experimental Part

### 6.1 Materials and Preparation

Polyethylene blends were prepared using a commercially available low-density polyethylene (LDPE) with a melt flow index of 0.28 g/10 min (ASTM D1238) and a density of 0.920 g/cm<sup>3</sup> (ASTM D792) and an EVA random copolymer, having vinyl acetate content of 28 wt.-%. In the following, the LDPE used in the experiments presented here is referred to as PE. The EVA contained 2.5 wt.-% carbon black. PE was blended in an extruder with different contents of EVA (1.8, 3.6, 5.4, 7.1, and 8.9 wt.-% EVA). Blends were compression molded between two rigid metal plates (having an area of 200 mm x 230 mm) at a temperature of 165-170°C and with a maximum force of 200 kN. The details of the molding process are described in the international standard IEC 811-4-1.<sup>[47]</sup> Molded plates were conditioned in an oven at 145°C for 1 h, then cooled down to 30°C. Test specimens with a specific geometry were cut from the plates. The geometry of the test specimen is shown in Figure 6.1. Each specimen was notched to a depth of 0.50-0.65 mm lengthwise using a razor blade fixed in a notching device.

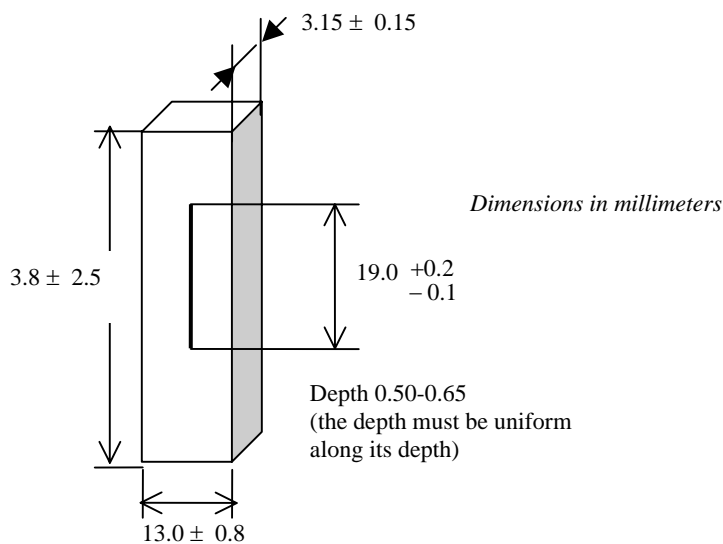
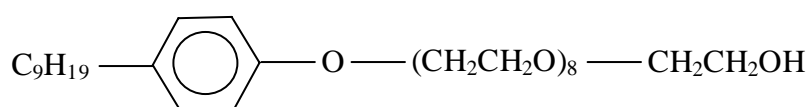


Figure 6.1 Geometry of the test specimen for the Bell-telephone ESCR test.

## 6.2 Environmental Stress Cracking Resistance Test

The Bell telephone test was performed in order to study the ESCR of LDPE/EVA blends. This is a constant-strain bent-strip test method with Igepal CO-630 as stress cracking agent.<sup>[1]</sup> The chemical structure of Igepal is shown in Scheme 6.1. Water solution of Igepal was prepared by paddle-stirring the mixture at 60°C to 70°C for at least 1 h.



Scheme 6.1 Chemical structure of Igepal CO-630.

Test specimens were bent with the notch pointing upwards in a metal U-shaped specimen holder (Figure 6.2). The holder was placed in a glass tube containing a 10 vol.-% Igepal solution. The tubes were sealed and put in a water bath at 50°C. Failure is defined as the appearance of any crack visible to the naked eye. Five specimens were used for each test.

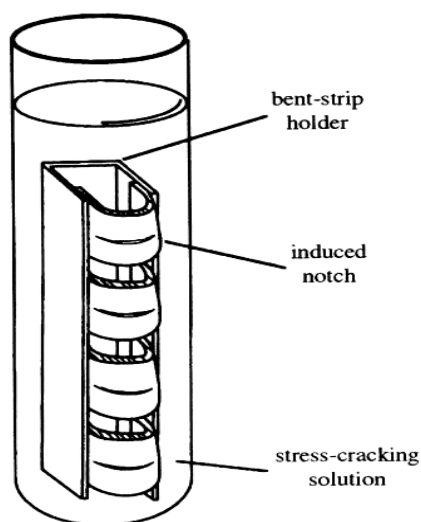


Figure 6.2 Bent strips in the U-shaped specimen holder.

## 6.3 Thermal Analysis

Thermal behavior of the blends was estimated from differential scanning calorimetry (DSC) traces. DSC measurements were carried out with a Perkin-Elmer DSC-2C. Samples (approximately 15 mg) were heated at a constant rate of 20°C/min and cooled at a rate of 10°C/min.

## 6.4 X-Ray Analysis

Wide angle X-ray scattering (WAXS) was performed using a URD 63 diffractometer (Seifert-FPM).  $\text{CuK}_\alpha$  radiation with a wavelength  $\lambda = 0.154$  nm was used. Investigations were carried out at room temperature in reflection mode.

Small angle X-ray scattering (SAXS) investigations were performed in an evacuated Kratky compact camera (Anton Paar KG, Graz, Austria) with  $\text{CuK}_\alpha$  radiation ( $\lambda = 0.154$  nm, Ni-filter). The scattered intensity was recorded by a scintillation counter in a step-scanning mode at room temperature or at  $140^\circ\text{C}$ . The scattering profiles were corrected for background scattering and desmeared.<sup>[96]</sup> Thin samples (thickness about 1-2 mm) were cut from the surface of the samples and then investigated by SAXS.

## 6.5 Microscopic Techniques

Different microscopic techniques (atomic force microscopy AFM, transmission electron microscopy TEM, scanning electron microscopy SEM, high voltage electron microscopy HVEM) were used to investigate morphology and deformation behavior of the samples.

Morphology of the samples was studied by transmission electron microscopy (JEM 2010). For the TEM studies, ultra-thin sections ( $\sim 80$  nm thickness) were cut from the bulk sample at room temperature and were stained with  $\text{RuO}_4$  vapor in order to make the EVA phase detectable by the microscope.

Scanning electron microscopy was used to study the fracture surfaces of the failed samples after the Bell-telephone ESCR test in Igepal at  $50^\circ\text{C}$ . The fracture surfaces were covered with thin gold film prior to the SEM investigations.

To investigate the deformation behavior of a few selected samples, semi-thin sections (ca.  $0.5 - 0.8$   $\mu\text{m}$  thickness) were cut and studied using high voltage electron microscope (1000 kV Joel HVEM). The semi-thin sections were strained in a special tensile device fixed to the HVEM.

For comparable study of morphology of some samples, atomic force microscopy (Nanoscope IIIa, Digital Instruments) was used. The microscope was operated in tapping mode at room temperature. The samples were scanned using a silicon cantilever.

## 6.6 Tensile Testing and Mechanical Properties

Mechanical behavior of the samples was characterized by uniaxial tensile testing. Tensile tests were performed using Instron 4507 testing machine at speed of 50 mm/min and at temperatures of 23, 50 and 70°C in the temperature chamber of the Instron machine. At least 10 samples were measured in order to prevent preparation artifacts and to obtain a good statistics of data. Blends were compression-molded between two rigid metal plates. Dumb-bell shaped specimens were cut from the plates (ca. 4 mm thickness). The main objective of this test is to have a comparative insight into the mechanical behavior of the investigated samples. Stress-strain curves were recorded using following equations for the calculation of stress ( $\sigma$ ) and strain ( $\varepsilon$ ):

$$\sigma = \frac{F}{A_0} \quad (6.1)$$

where F is the applied force in N and  $A_0$  is the cross-sectional area of the sample in  $\text{mm}^2$ .

$$\varepsilon = \frac{(L - L_0)}{L_0} \times 100 = \frac{\Delta L}{L_0} \times 100 \% \quad (6.2)$$

where  $\Delta L$  is the change in the gauge length of the specimen relative to the initial sample length  $L_0$ .

The modulus of elasticity (Young's modulus) was determined by the slope of the initial part of the stress-strain curves.

Tensile strength at yield  $\sigma_y$  is the stress at which the sample yields, divided by its cross-sectional area:

$$\sigma_y = \frac{F_y}{A_0} \quad (6.3)$$

where  $F_y$  is the applied force at yield in N and  $A_0$  is the initial cross sectional area of the sample in  $\text{mm}^2$ .

## 6.7 Image Processing System analySIS 3.1

This software was used for determination of the average particle size of the EVA particles and the average particle-particle distance (surface-to-surface) distance. A circle was drawn around each EVA particle visible in the TEM images of PE/EVA-5.4 and PE/EVA-8.9 samples by using the computer mouse and following the edge of the particle. The surface area of the



particles was automatically calculated by the computer program. The diameter of the particle was calculated by using following well known equation:

$$d = \sqrt{\frac{4S}{\pi}}, \text{ nm} \quad (6.4)$$

where S is the surface area of the EVA particle in  $\text{nm}^2$ .

The average diameter of the EVA particles is equal to  $\frac{\sum_{i=1}^m d_i}{n}$  where  $d_i$  is the diameter of i EVA particle and n is the total number of the measured EVA particles.

## 7. Results and Discussion

### 7.1 Environmental Stress Cracking Experiments

The Bell-telephone test was carried out at temperatures of 30, 50, 60 and 70°C. The time to failure ( $t_f$ ) values of different samples are shown in Table 7.1. The time to failure is defined as the time that passes until the first out of five test specimens fails during the ESCR test.

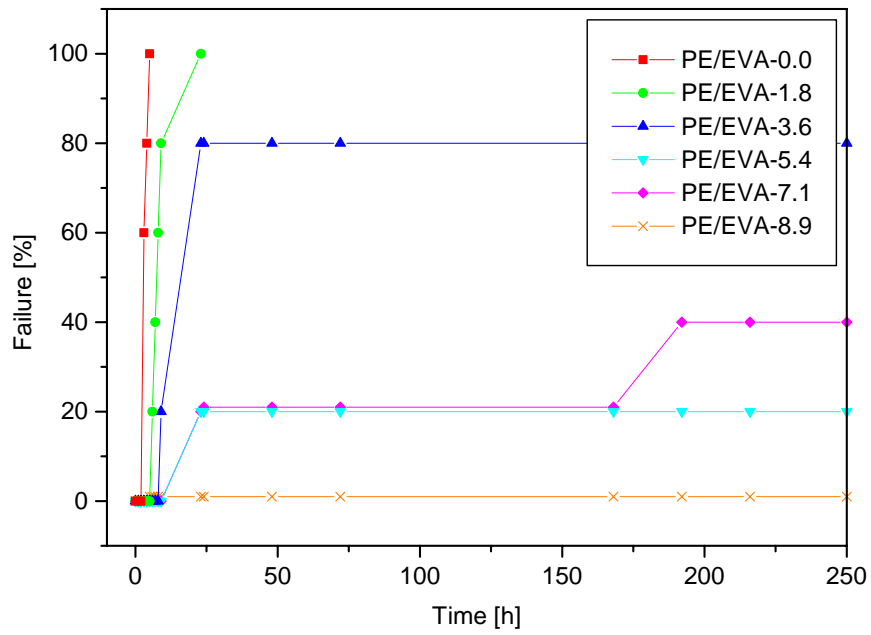
Table 7.1 Failure time  $t_f$  of PE blends with different EVA contents in Igepal at various temperatures determined by BTT. (- means that failure does not occur up to 1000 hours)

Sample	EVA content [wt.-%]	$t_f$ at 30°C [h]	$t_f$ at 50°C [h]	$t_f$ at 60°C [h]	$t_f$ at 70°C [h]
PE/EVA-0.0	0.0	3	1	6	5
PE/EVA-1.8	1.8	6	2	10	8
PE/EVA-3.6	3.6	9	3	23	-
PE/EVA-5.4	5.4	23	5	46	-
PE/EVA-7.1	7.1	23	7	-	-
PE/EVA-8.9	8.9	-	-	-	-

The percentage of failed samples is plotted in Figure 7.1 and 7.2 against time to failure in Igepal solution during the ESCR test at different temperatures. The results indicate that only the PE/EVA-8.9 did not fail at all during the ESCR test at different temperatures. The duration of the tests was 1000 h. In most of the cases, cracking starts on both sides in a direction perpendicular to the notch (see Figure 6.1), which can be explained by simple finite element calculations using the ANSYS finite element method.<sup>[97]</sup> These small cracks grow and lead to catastrophic failure. Samples that do not contain any EVA copolymer always failed during the first hours of the test.

On the basis of the finite element method, simulations were carried out to locate the areas of the highest stress on a bent test strip.<sup>[98]</sup> Figures 7.3 and 7.4 show the local stress distribution in a bent strip with a hole and a notch.

a)



b)

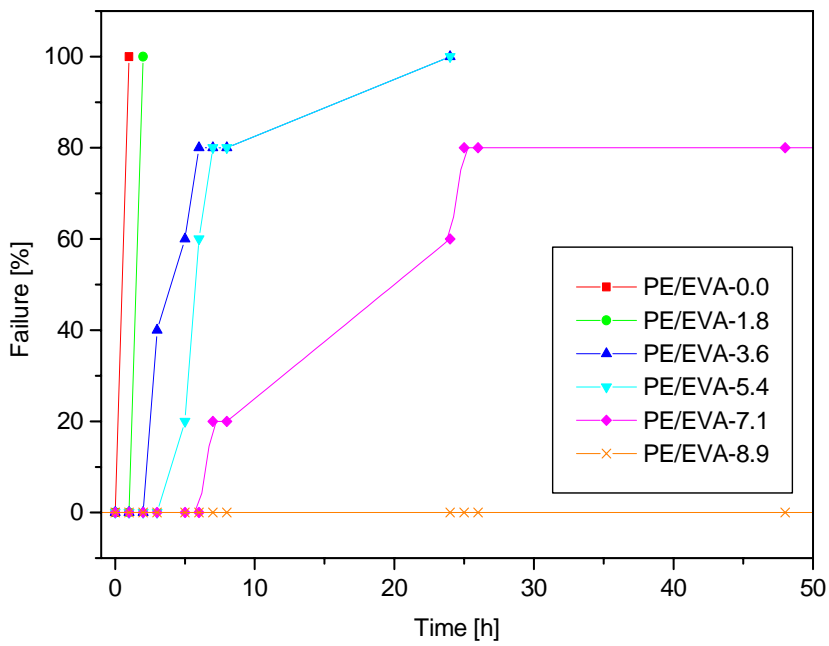
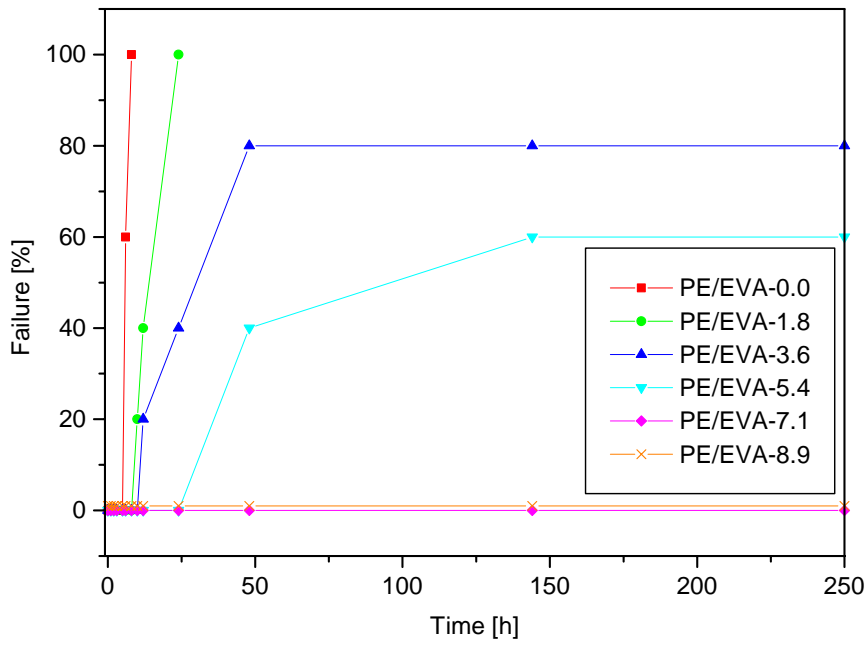


Figure 7.1 Failure as a function of time in ESCR test conditions a) at 30°C, and b) at 50°C.

a)



b)

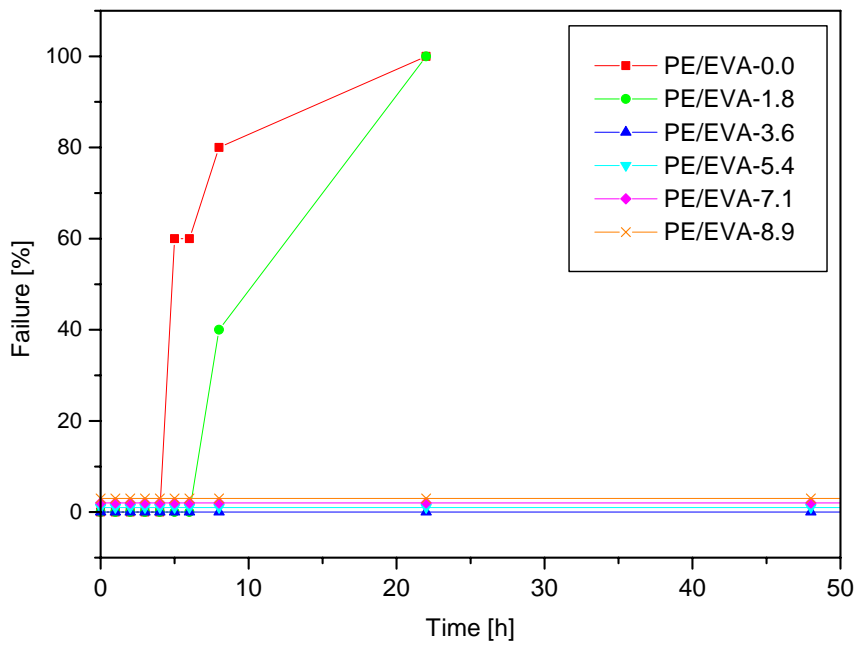


Figure 7.2 Failure as a function of time in ESCR test conditions a) at 60°C, and b) at 70°C.

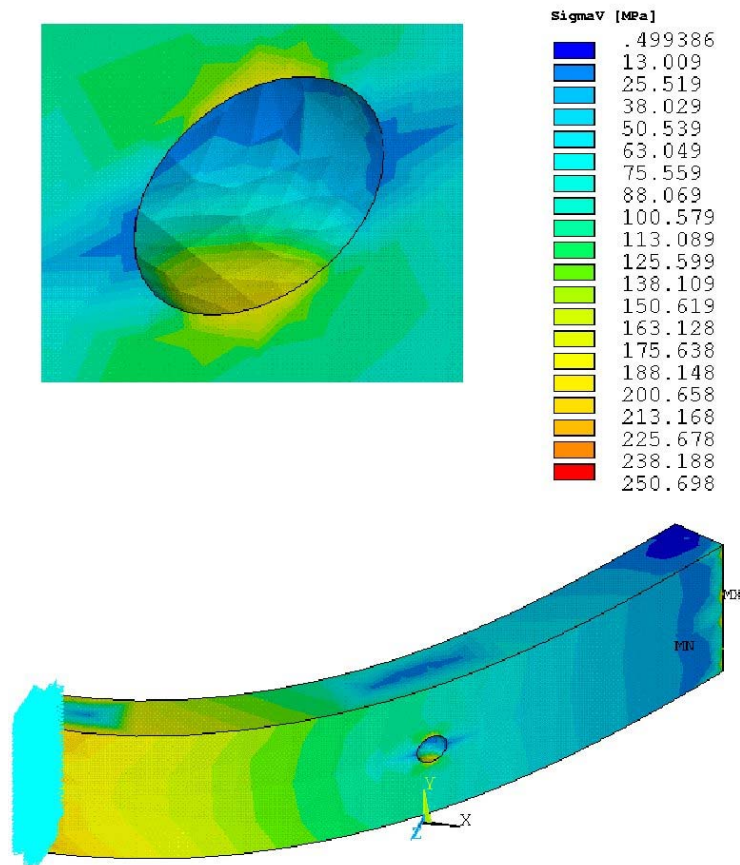


Figure 7.3 Simulation of the *von Mises* stress (SigmaV) distribution on a clamped bent test-strip with a hole.<sup>[98]</sup>

The *von Mises* stresses (SigmaV) are illustrated by color bars in the right side of Figures 7.3 and 7.4. If there is a hole in a bent strip, the stress increases at the edges of the hole which are parallel to the direction of the applied stress (Figure 7.3). The simulation with the clamped bent strip with a notch (Figure 7.4) show that the highest stress values are at the bottom of the notch. The field of increased stress propagates orthogonal to the external load.

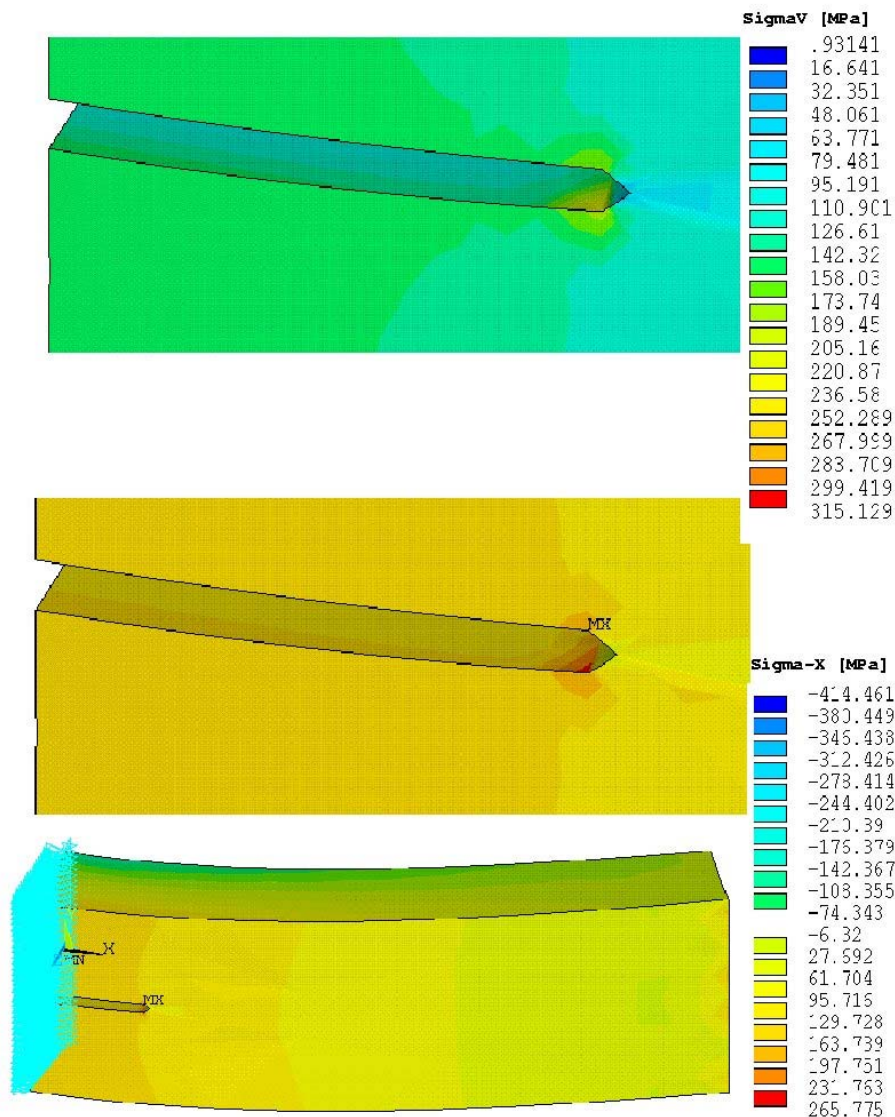


Figure 7.4 Simulation of the *von Mises* stress ( $\sigma_v$ ) and the bend stress ( $\sigma_x$ ) distribution on a clamped bent test-strip with a notch.<sup>[98]</sup>

If stress is applied to a ductile polymer such as PE in air, the material will fail eventually via a process known as static fatigue or cold drawing.<sup>[2]</sup> Polyethylene undergoes brittle fracture when broken in the presence of stress cracking agents. The transition to brittle behavior is shifted to shorter times with increasing temperature, cyclic loading, and stress concentration. Ward and Brown<sup>[14]</sup> investigated slow crack growth in an ethylene-octene copolymer in Igepal and air. The single edge notch specimens were loaded in a range of temperatures and stresses. Crissman<sup>[55]</sup> investigated the ESCR performance of commercial grade linear

polyethylene (average molar mass 98 800 g/mol) at different applied stresses and temperatures from 23 to 90°C. Typically, the specimens were unnotched strips which were bent around a metal cylinder having a specified radius of curvature. It was found that increasing of the test temperature decreases the time to brittle failure.

The times to failure of the PE/EVA samples observed at 30°C are longer than those at 50°C. Therefore, our results confirm the statement that an increase in temperature shortens the time to failure. A further reduction of the time to failure during the BTT was expected from an increase of the test temperature to 60 and 70°C according to studies of neat polyethylene and ethylene-octene copolymers.<sup>[10, 14, 55]</sup> However, different results were obtained from the test at 70°C (Table 7.1). Only PE/EVA-0.0 and PE/EVA-1.8 samples showed failure time within the first hours of the test, whereas all other samples remained intact until the end of the test (1000 h). This might be related to the melting point of long ethylene sequences in EVA at about 50°C, which was determined by DSC measurements (see Chapter 7.2). The samples are above the melting point of EVA during the test at 70°C. Then, the EVA phase is more easily deformed (see Chapter 7.4), as a consequence of which crack initiation and growth are likely to be prevented. The thermal properties of the blends and their deformation behavior will be discussed below.

## 7.2 DSC and WAXS Investigations

Figure 7.5 shows the WAXS trace of neat EVA, and the corresponding DSC trace in the inset. The EVA has a vinyl acetate content of 28 wt.-%. Although EVA is a random copolymer, it is nevertheless able to crystallize, as indicated by the melting endotherm observed between 50 and 80°C in the DSC trace and the occurrence of the (110) reflection, known for PE, in the WAXS trace at an angle of  $2\theta = 21^\circ$ . The broad crystalline melting range reveals that EVA contains different type of crystallites having different internal order which need different amount of energy for fusion. These crystals of EVA also have smaller thickness compared to PE which is evident from the broad X-ray diffraction peak for EVA in Figure 7.5.

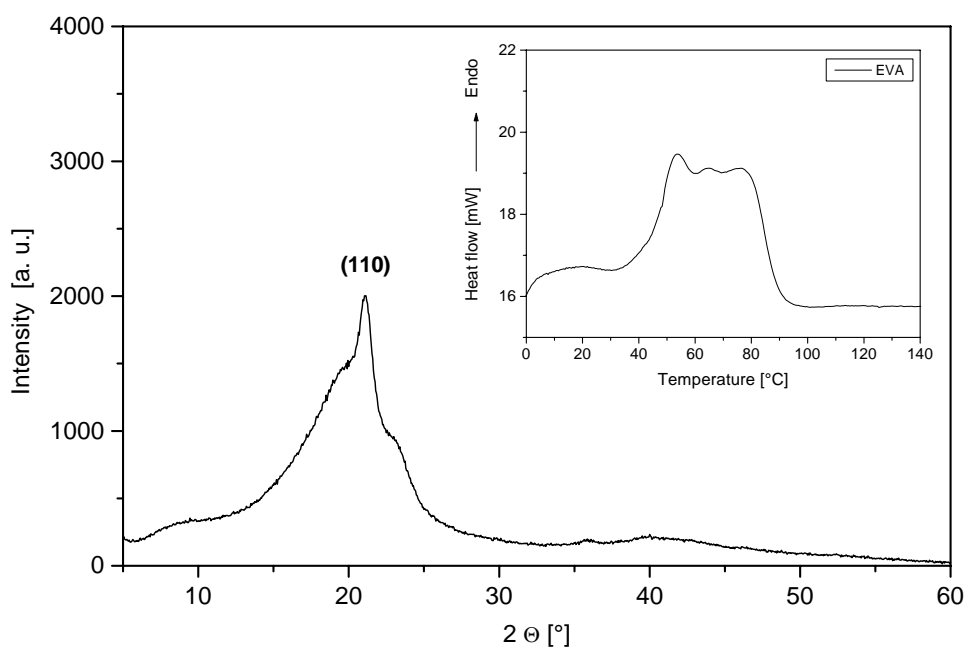


Figure 7.5 WAXS trace of neat EVA as received. The inset shows the DSC trace (first scan).

It is well established that polymers crystallize into the form of lamellae in which the molecular chains are folded. It may be anticipated, therefore, that uncrystallizable units, if introduced into a crystallizable polymer chain, might strongly prohibit the chain folding and enhance the fringed micelle type of crystallization. In the fringed micelle model, crystallites are envisaged as small bundles (“micelles”) of parallel extended linear chain segments disposed randomly in a matrix of disordered chains (Figure 7.6).

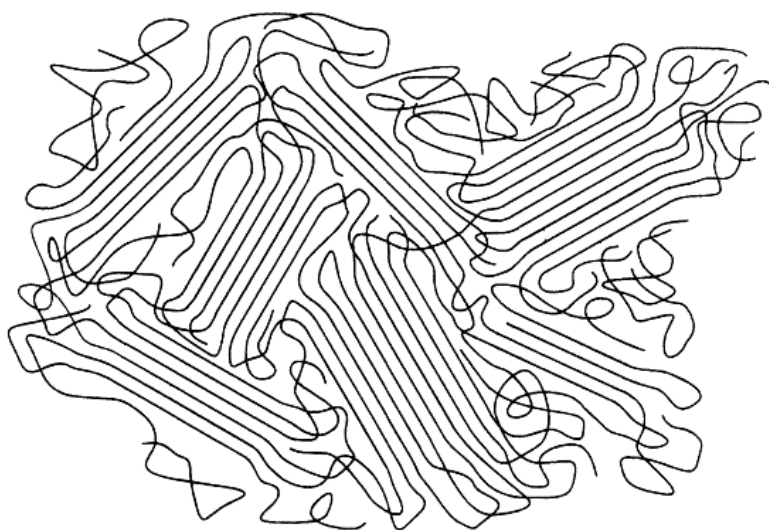


Figure 7.6 Fringed micelle model of PE.<sup>[99]</sup>



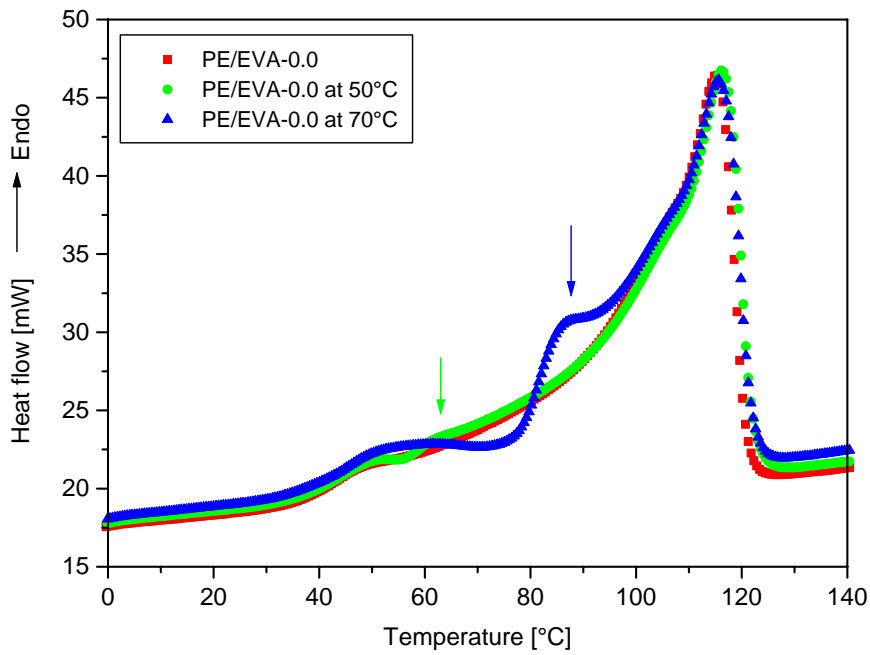
In the case of EVA copolymers, the vinyl acetate units are not crystallizable and will not enter into the crystalline lattice at all. Okui and Kawai<sup>[100]</sup> studied the crystallization and resultant texture of EVA random copolymers as functions of composition (from 2.2 to 33 wt.-% VA) and crystallization temperature by using differential thermal analysis and electron microscopy. They found that the transition from the chain folding crystallization to bundle-like crystallization of EVA did not occur sharply at a given composition as expected but the two types of crystallization coexist in a rather wide range of compositions, depending on the crystallization temperature.

The DSC trace of a neat EVA copolymer in Figure 7.5 confirms the observed melting behavior of EVA by other authors. This result is extremely important whenever the ESCR behavior of PE/EVA blends is discussed. Below the melting point, EVA is a rather hard, semicrystalline material. Above the melting point, EVA is a viscoelastic liquid that acts much more as a rubber-like phase compared to the partially crystalline material.

A problem of interest is the conditions for the co-crystallization of mixtures of homopolymers and copolymers. Mixtures of linear polyethylene and EVA copolymers with different VA content have been investigated concerning their co-crystallization.<sup>[101]</sup> DSC and selective extraction techniques were used to assess whether co-crystallization occurs. It is found that co-crystallization between a linear polyethylene and a random copolymer exists when the copolymer contains up to 2 mol.-% acetate branches. When the branching content becomes greater than about 3 mol.-%, co-crystallization does not occur. The EVA copolymer that we used in the blends has a 28 wt.-% VA content and i.e. calculated that it contains respectively 11.2 mol.-% VA. Therefore, we can conclude that in the investigated PE/EVA blends co-crystallization does not occur.

DSC measurements of different PE/EVA blend samples were carried out in order to investigate their thermal behavior. Samples were cut from the damaged area directly under the notch and investigated by DSC. Figure 7.7a and 7.7b present typical DSC traces (first scan) of PE/EVA-0.0 (neat LDPE) and PE/EVA-8.9 samples as received and after the ESCR tests at 50 and 70°C, respectively. The traces reveal that with the main endotherm a second endotherm is generated (indicated by arrows), which begins immediately above the annealing temperature  $T_a$  (the test temperature during the ESCR test), respectively 50 and 70°C.

a)



b)

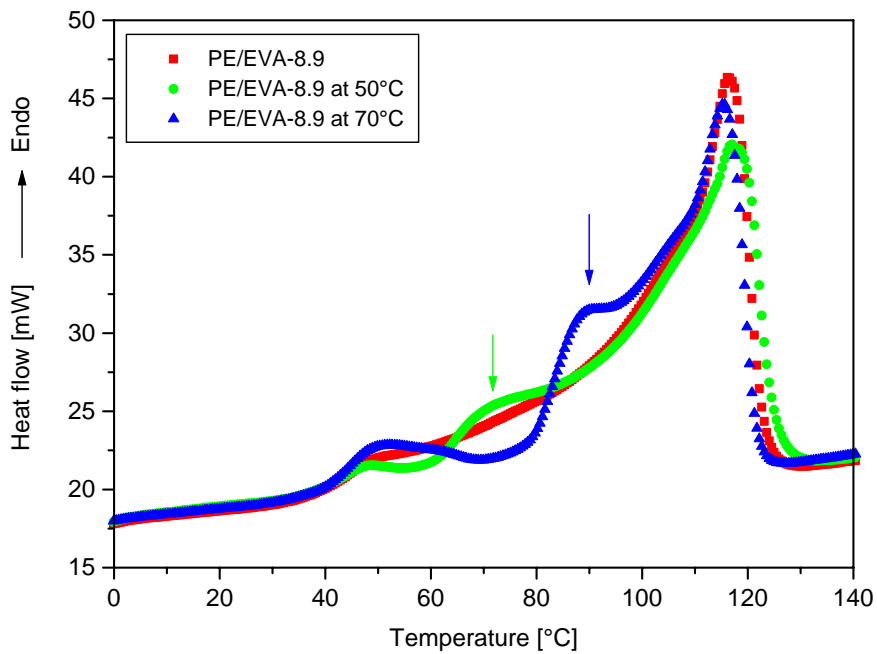


Figure 7.7 a) DSC traces of neat, as received PE (red signs), after 1000 h in ESCR test conditions at 50°C (green signs), and after 1000 h in ESCR test conditions at 70°C (blue signs). b) DSC traces of as-received PE/EVA-8.9 (red signs), after 1000 h in ESCR test conditions at 50°C (green signs), and after 1000 h in ESCR test conditions at 70°C (blue signs).

Different reorganization processes can occur when semicrystalline polymers are treated thermally. If the applied annealing temperature is lower than the crystallization temperature of the less stable fraction of PE, the following transitional phenomena can occur: nucleation and growth of new crystals directly from the amorphous state, lateral growth of the preexistent crystals, and thickening of the crystals.<sup>[86, 102]</sup> On the other hand, if the temperature is higher than that one observed during crystallization of a particular fraction, melting of that fraction can occur in addition to the above transitions. This new material can re-crystallize. The overall process is known as partial melting-re-crystallization.<sup>[102]</sup> Re-crystallization is a process in which the initial, rather imperfect, lamellae melt and re-crystallize to produce thicker and more perfect lamellae that as a consequence melt at a higher temperature.

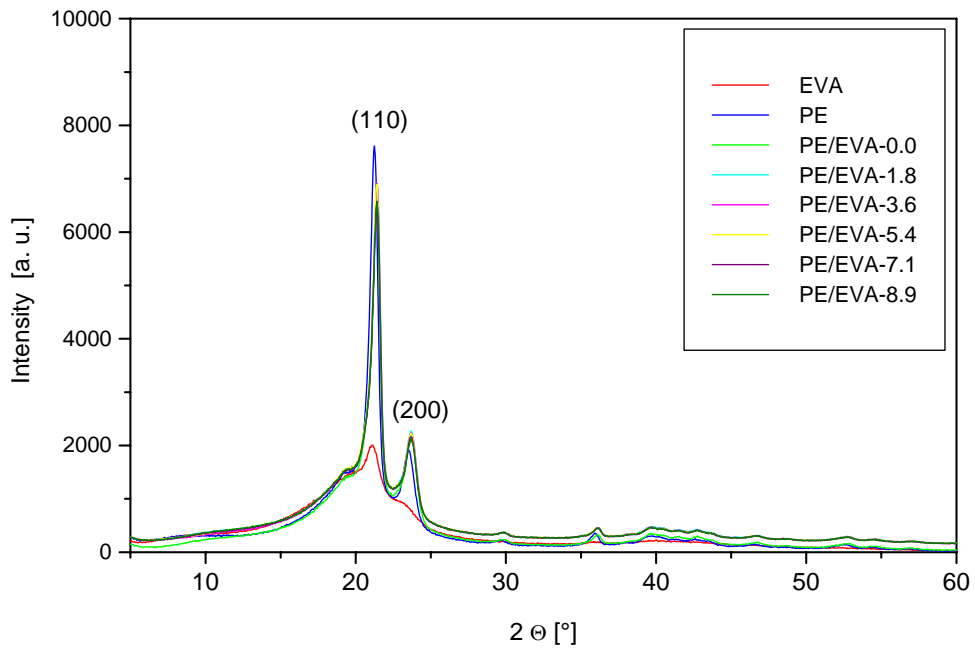
For polymers with a broad crystal size distribution such as LDPE,<sup>[103, 104]</sup> the structural changes discussed above may happen even far from the melting temperature of the largest fraction. Annealing of LDPE and ethylene copolymers (ethylene-hexene, ethylene-octene, and ethylene-vinyl acetate copolymers) usually results in more than one endothermic peak in subsequent DSC heating experiments.<sup>[86, 87, 102, 105, 106]</sup> The second endotherm usually arises from applying high annealing temperatures  $T_a$ , but the results for neat LDPE show that even at low annealing temperatures (40°C) a second endotherm is generated.<sup>[102]</sup> This endotherm reflects the melting of the population of crystallites generated by annealing at  $T_a$  by a partial melting-re-crystallization mechanism. Such fraction is formed by very thin crystallites, which can melt at  $T_a$ , generating amorphous material capable of re-crystallization at the same temperature.

The DSC traces of all PE/EVA samples after the ESCR test at 50 and 70°C correspond exactly to what was reported in the literature on the melting-re-crystallization process of neat LDPE and neat ethylene copolymers. As a result of the long thermal treatment of the samples during the ESCR tests, a second endotherm is generated in the DSC heating traces, which begins immediately above the annealing temperature. Therefore, blending of PE with EVA has a minor influence on the melting-re-crystallization process.

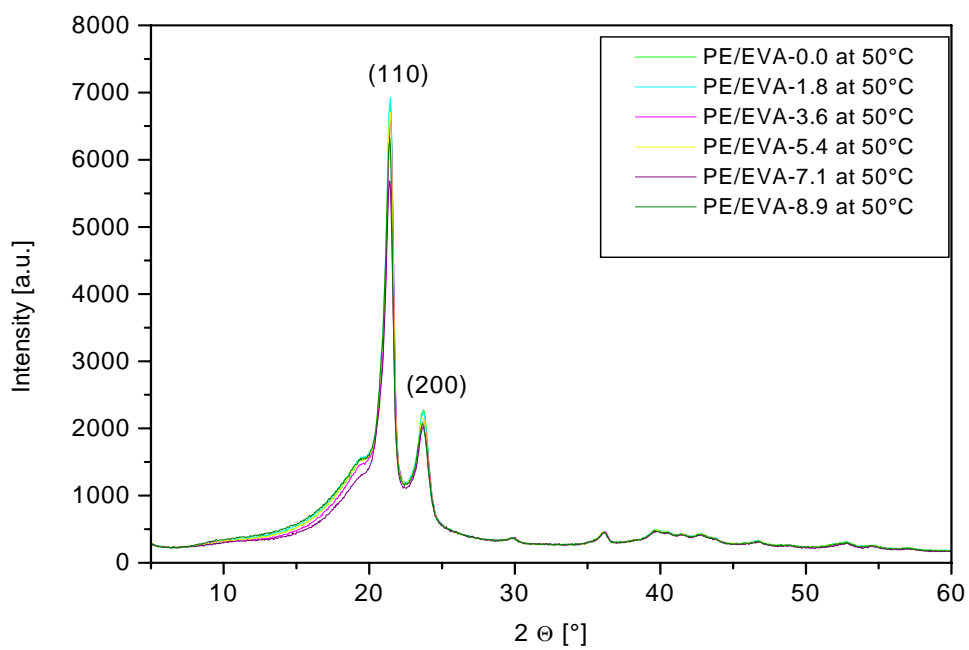
The WAXS measurements are useful to obtain information on changes of the crystalline state of the samples before and after the ESCR test. WAXS data were collected in the range  $0^\circ < 2\theta < 60^\circ$ , and only the strong (110) and (200) reflections resulting from the orthorhombic lattice were used for analysis.<sup>[33, 107]</sup> The samples for the WAXS measurements were annealed at 50 and 70°C in 10 vol.-% Igepal solution for 48 h. We assumed that any change of the crystal morphology would have happened within 48 h according to the failure times observed

during the BTT (most of the samples failed in the first hours of the test). Obtained WAXS traces are shown in Figure 7.8. On the first view, there are not any tremendous differences in the WAXS traces of the samples annealed at 50 and 70°C.

a)



b)



c)

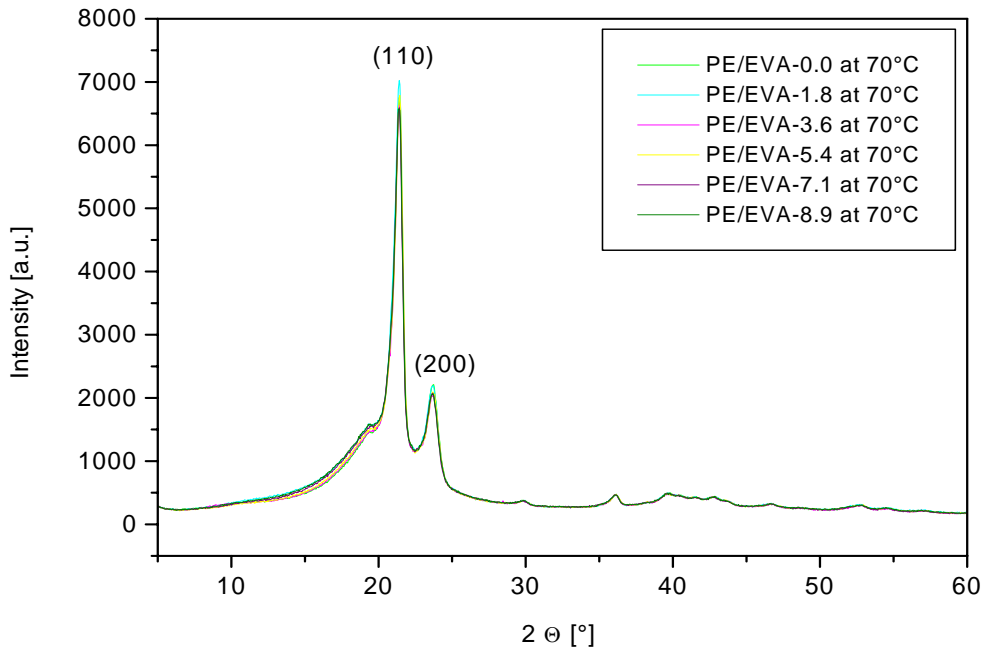


Figure 7.8 WAXS traces of a) neat PE, neat EVA and PE/EVA blends as received, b) PE/EVA samples annealed at 50°C in 10 vol.-% Igepal solution for 48 h, and c) PE/EVA samples annealed at 70°C in 10 vol.-% Igepal solution for 48 h.

There are three main causes that change the diffraction line shape from the ideal delta function. They are the small crystal size and imperfections of the first and second kind.<sup>[108]</sup> Small crystal size broadens all (hkl) diffraction lines. The imperfection of the first kind does not actually cause any line broadening, but instead simply reduces the height of the diffraction peaks. At the same time, the scattering energy that has been lost from the diffraction lines as a result of the reduced height reappears as a diffuse scattering in the region of non-Bragg angles. The imperfection of the second kind produces a line broadening in which the width of the diffraction line increases.

In the imperfections of the first kind, we imagine that an ideal lattice, or an ideal average lattice, exists throughout the crystal, and the actual positions of atoms are displaced from their ideal positions to the extent governed by some statistical law. The displacements are assumed to be small compared with the interatomic distances, and moreover the displacement of one atom from its ideal position is totally uncorrelated with that of a neighboring atom. A crystal with imperfection of the first kind may also contain a substitutional disorder, in which some of the atoms are replaced by foreign atoms.

In the imperfections of the second kind, the distance between nearest-neighbor atoms fluctuates moderately around an average value according to a statistical law, there is no longer any average lattice to which the atomic positions can be referred. Thus, although a short-range order is maintained, there is no longer a long-range order.

The difference between the two types of imperfection can be seen more easily in Figure 7.9.

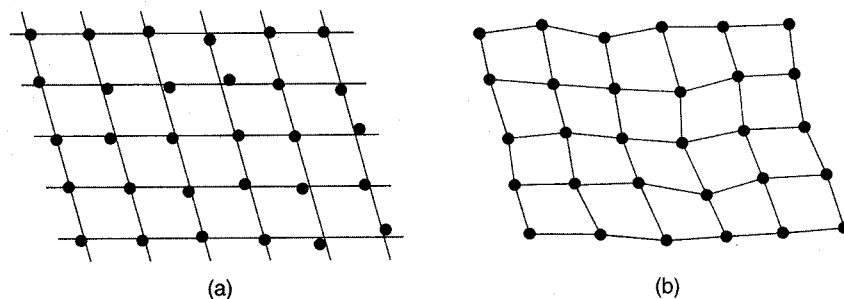


Figure 7.9 Imperfections of (a) the first and (b) the second kind in two-dimensional crystals.

The WAXS data can be used for determination of the degree of crystallinity of the investigated samples by using mathematical fitting procedures. WAXS traces were fitted by using Origin software. The degree of crystallinity was calculated by dividing the crystalline area of the WAXS trace (which is the area from the baseline, i.e. integrated intensity from the baseline) to the whole area ( which is the integrated intensity from  $y = 0$  including the amorphous halo). The baseline was drawn automatically by the computer software and afterwards it was smoothed manually. Figure 7.10 shows the degree of crystallinity of different samples annealed in 10 vol.-% Igepal solution for 48 h as a function of the EVA content. It is visible that annealing of the PE/EVA samples at 50 and 70°C causes slight differences in the degree of crystallinity. We can expect an increase of the degree of crystallinity due to the annealing procedure. But it cannot be detected by WAXS measurements for both annealing temperatures. Only the samples with more than 3 wt.-% EVA and annealed at 50°C have higher crystallinity than the untreated samples. It is not clear why the crystallinity of the samples annealed at 70°C is lower or equal to the untreated samples.

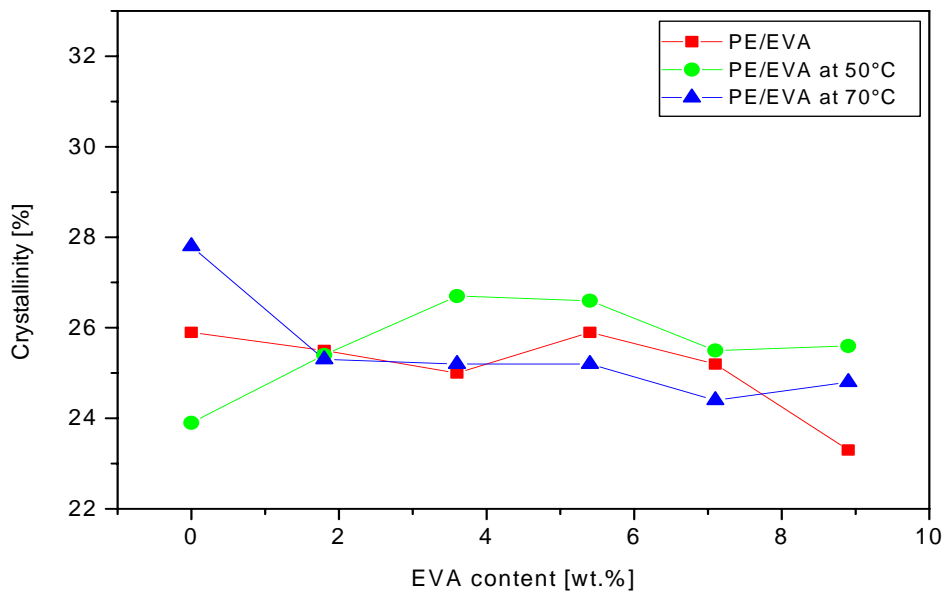


Figure 7.10 Crystallinity of PE/EVA-blends before and after annealing at 50 and 70°C in 10 vol.-% Igepal solution for 48 h.

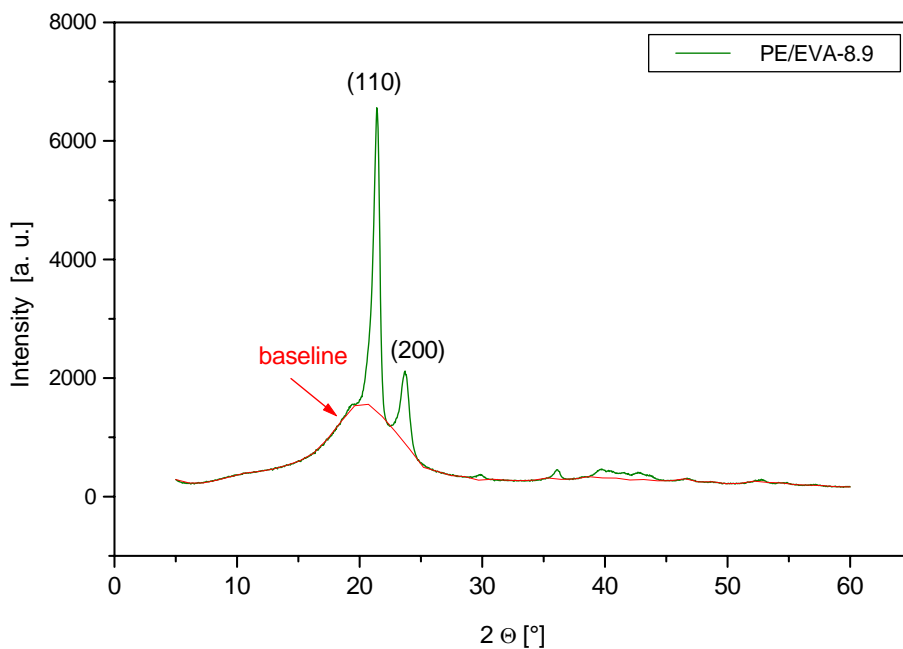


Figure 7.11 WAXS trace of a PE/EVA-8.9 sample as received and the corresponding baseline (red line).

Information on relative area of the peaks ( $A_{110}/A_{200}$ ), height of the diffraction peaks, and full width at the half-maximum (FWHM) can be derived from the obtained WAXS data. The relative area is an indication of the crystallite size, whereas the height of the peaks and FWHM are indications of the crystallite perfection.

The height and the area of the (110) and (200) diffraction peaks were determined from the baseline as it is shown in Figure 7.11 (this procedure was done for all of the investigated samples).

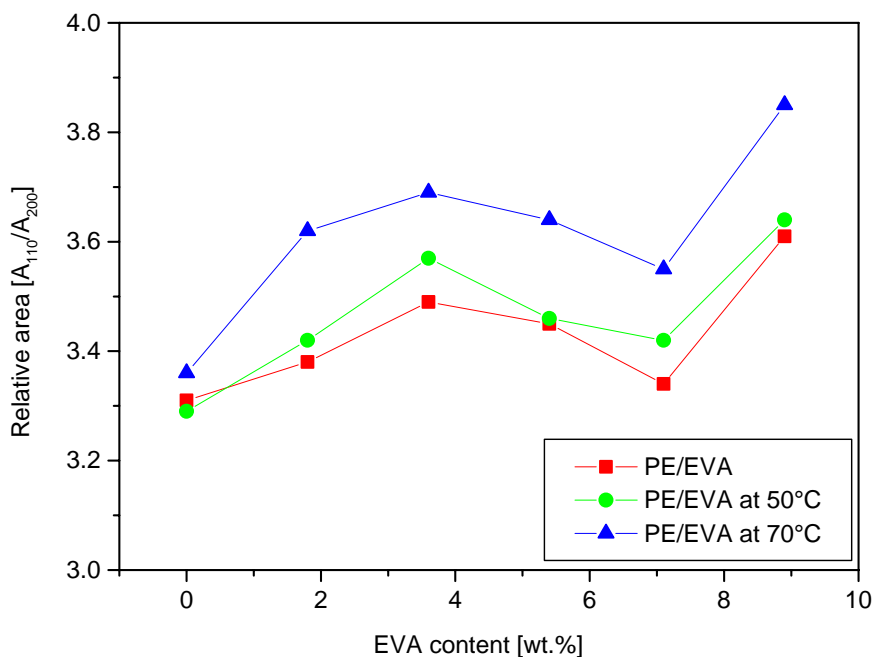


Figure 7.12 Relative area [ $A_{110}/A_{200}$ ] of the (110) and (200) reflections as a function of the EVA content (samples annealed in 10 vol.-% Igepal for 48 h).

Figure 7.12 shows that annealing of the samples at 70°C increases the relative area, therefore we might guess that the lamella thickness increases during annealing. Zhu et al.<sup>[109]</sup> carried out WAXS and infrared spectroscopy investigations to detect any morphological changes in annealed ultrahigh molecular weight polyethylene (UHMWPE) films prepared by gel-spinning technique. The X-ray diffraction results have revealed that the large deformation of the UHMWPE films annealed at high heating rates, thus causing the changes in the film morphology. According to their investigations the relations of the annealing temperatures  $T_a$  and the crystallite dimensions show that  $T_a$  has greater influence on the deformation than annealing time. The authors concluded from their experimental observations that the increase in the lamellar thickness along the c-axis to nearly twice the initial value occurs via chain sliding. The molecular chains can slide in the c-axis direction without destroying the



orthorhombic lattice structure. During thickening, the crystal dimension along the b-axis increases, while the dimension along the a-axis remains constant. The increase along the b-axis suggested that the chain sliding along the c-axis is feasible, because of the expansion along the (020) sectors of the crystal.

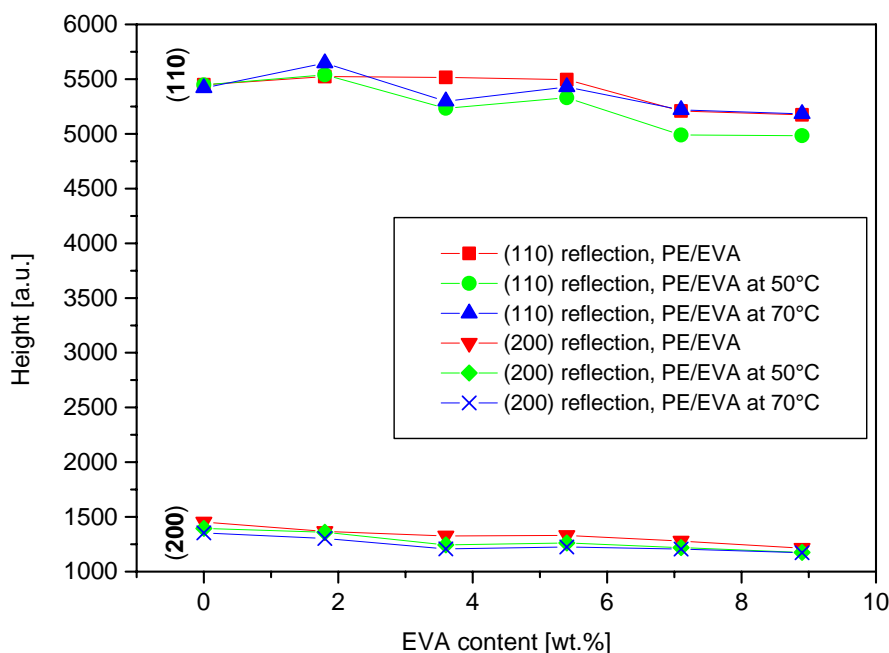


Figure 7.13 Height of (110) and (200) diffraction peak as a function of the EVA content in the blends and the annealing temperature.

Figure 7.13 shows that the height of (110) and (200) reflections continuously decreases with increasing EVA content in the blends, which is an indication of the imperfection of the first kind. But the height of the peaks is not influenced significantly by the different annealing temperatures, respectively 50 and 70°C.

The imperfection of the second kind increases the full width at the half-maximum (FWHM). As smaller the FWHM, as more perfect the crystals are. FWHM of (110) and (200) reflections are shown in Figure 7.14. It is visible that there is an increase of the FWHM of (200) reflection with increasing EVA content of the samples, which is an indication of the imperfection of the second kind.

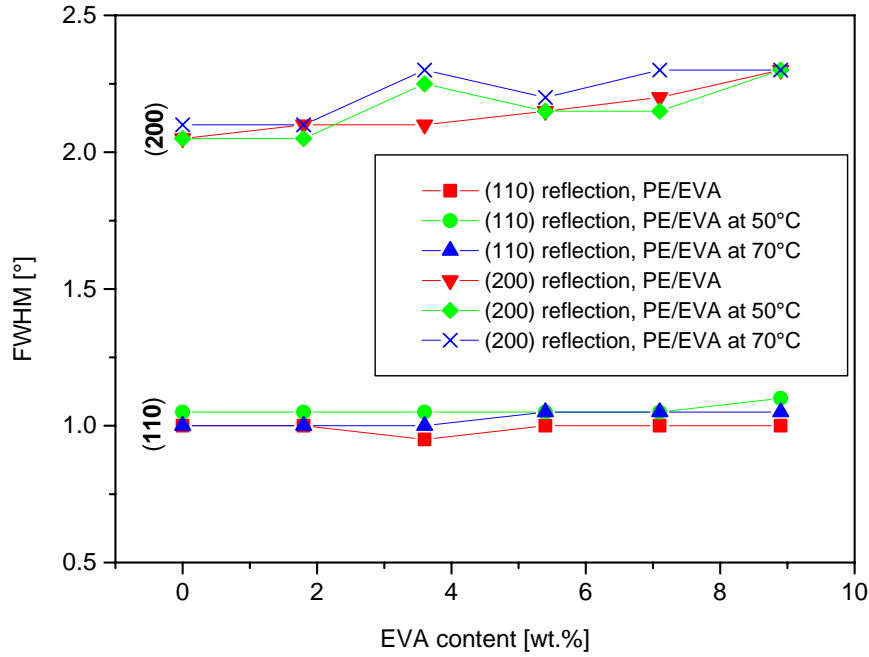


Figure 7.14 Full width at the half-maximum (FWHM) of (110) and (200) reflections as a function of the EVA content in the blends and the annealing temperature.

### 7.3 SAXS Investigations

SAXS is a well-established method for the structural investigation of semicrystalline polymers. SAXS measurements are useful to determine the influence of the ESCR test on lamellae thickness and interfacial region between amorphous and crystalline parts which might influence the failure behavior of the samples.<sup>[110]</sup>

In a simple case, SAXS profiles for semicrystalline polymers having a lamellar morphology in an unoriented state are generally characterized by one or more diffuse maximums, and the first maximum at the lowest scattering angle corresponds to the “long period”  $d=2\pi/q^*$  by applying Bragg’s law, where  $q^*$  is the scattering vector.

If the scattering angle is  $2\theta$  (the angle between the incident wave and the scattered wave), and the wavelength is  $\lambda$ , then the scattering vector is<sup>[111]</sup>:

$$q = |q| = \frac{4\pi}{\lambda} \sin \theta \quad (7.1)$$

If there is a lamella thickening due to the annealing of the samples at 50 and 70°C during the ESCR test, this would lead to a sharper peak at the first maximum in the SAXS trace as in the thickness distribution of the crystallites the smaller ones are missing.

The SAXS data for PE/EVA-8.9 before and after 1000 h ESCR test conditions at 50 and 70°C, and in the melt at 140°C are shown in Figure 7.15, where the Lorentz and background corrected intensities after the desmearing procedure are plotted against the scattering vector  $q$ .

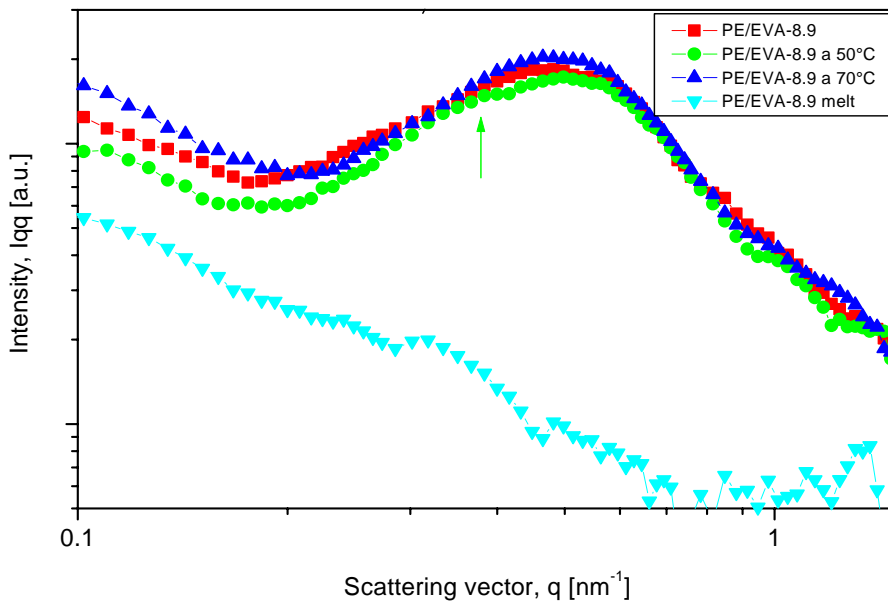


Figure 7.15 SAXS profiles of PE/EVA-8.9 samples before, after 1000 h ESCR test conditions at 50 and 70°C, and in melt at 140°C.

The peak for the long period of LDPE is at about  $0.5 \text{ nm}^{-1}$ . But even in the melt, in a  $q$ -range between  $0.1$  and  $0.7 \text{ nm}^{-1}$  some structures can be detected. It might be due to some filler particles or the EVA phase dispersed in the matrix. These structures are located at the left side of the dominant peak for the long period of PE crystallites. Therefore, a fitting of the PE peak by a Gaussian function to get the width and the height, could not be done properly.

For particles with a simple well-defined shape, dispersed in a matrix so that there is no interaction between them, the angular dependence of the scattered intensity can be calculated. For instance, for a homogeneous sphere of radius  $r$ ,

$$I(q) = I_0 \left[ 3 \frac{\sin(qr) - (qr) \cos(qr)}{(qr)^3} \right]^2 \quad (7.2)$$

where  $I_0$  contains the geometry independent terms,  $q$  is the scattering vector, and  $r$  is the radius of a spherical particle.

The SAXS trace of a PE/EVA-8.9 sample in the melt at 140°C was fitted according to Equation 7.2. It was found that there are two kinds of spherical scattering (Figure 7.16). Investigated PE/EVA compounds contain 2.5 wt.-% carbon black. The average size of a single carbon black particle is maximum 20 nm. But actually, carbon black agglomerates are present in the blends which is proved by the TEM investigations and the TEM images can be seen in Chapter 7.4.1. Therefore, the scattering at about  $0.33 \text{ nm}^{-1}$  is due to the carbon black particles. The scattering at about  $0.79 \text{ nm}^{-1}$  might be due to the EVA phase.

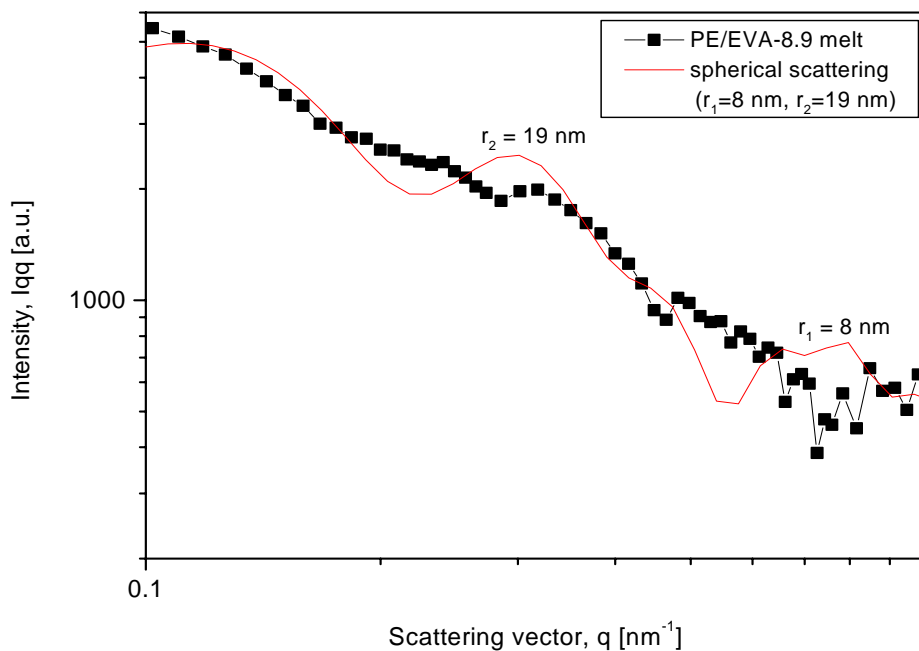


Figure 7.16 SAXS profile of a PE/EVA-8.9 sample in the melt at 140°C (black signs) and corresponding fitting (red line) for spherical particles.

From all measurements the main peak and some higher orders could be detected in the SAXS traces. The described structure appears more significant for the samples after the ESCR test, especially for the samples annealed at 50°C, when a proper shoulder or peaks could be detected.

The SAXS data for PE/EVA-5.4 samples before and after the ESCR test at 50 and 70°C are shown in Figure 7.17, where the Lorentz and background corrected intensities after the desmearing procedure are plotted against the scattering vector  $q$ . In Figures 7.15 and 7.17 it can be seen clearly that the peak for the long period of PE broadens and a shoulder appears in the case of annealing at 50°C during the ESCR test. The lack of such a shoulder for the samples annealed at 70°C might be due to the fact, that in the case of a 70°C annealing followed by a cooling to room temperature, more amorphous parts crystallize at lower temperature, which leads to a broadening of the peak for the long period of PE. This recrystallization can be seen in the DSC traces as a peak below 70°C. But this peak is very low and should not lead to a significant effect. Probably, other effects (e.g. statistics) may play a role.

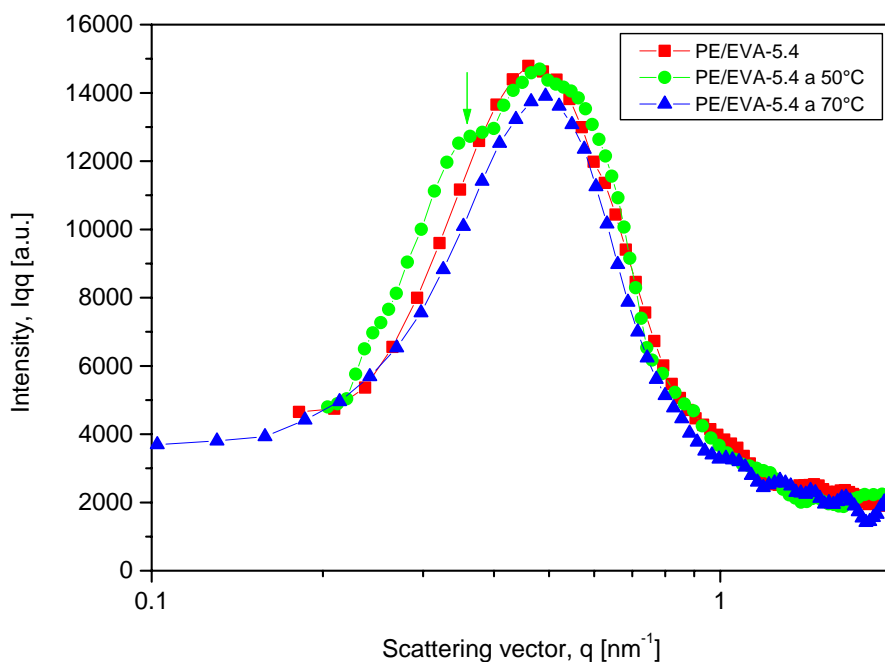


Figure 7.17 SAXS profiles of PE/EVA-5.4 samples before and 1000 h ESCR test conditions at 50 and 70°C.

## 7.4 Morphology Analysis

### 7.4.1 AFM and TEM Investigations

AFM and TEM were applied in order to study the morphology of the PE/EVA samples before and after the ESCR test at 50 and 70°C. A typical AFM image of PE/EVA-5.4 taken in height and in phase mode is shown in Figure 7.18. The darker area in the phase mode (right side) is due to the soft EVA phase, and the bright area represents the semi-crystalline LDPE matrix. The EVA particles are homogeneously distributed in the LDPE matrix. The carbon black particles are observed as the small bright dots (carbon black agglomerates) located mainly within the EVA phase.

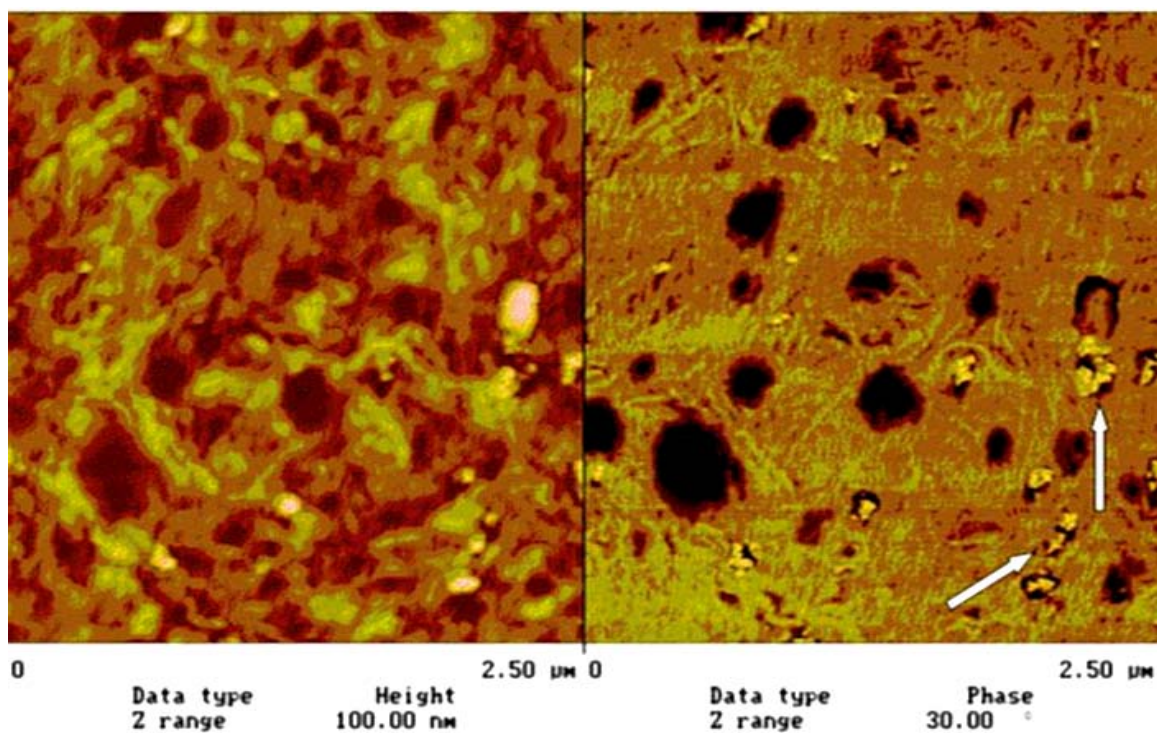
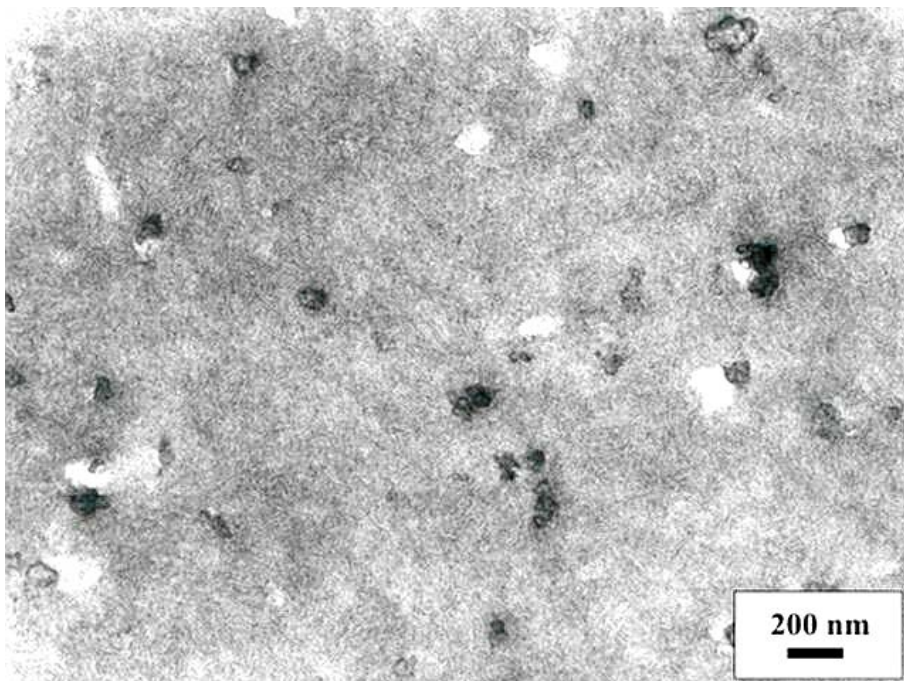


Figure 7.18 AFM image of as-received PE/EVA-5.4 in height (left) and in phase mode (right). The dark areas correspond to the EVA phase. The bright (yellow) spots in the EVA phase are carbon black particle agglomerates (indicated by arrows).

Morphology of PE/EVA-0.0, PE/EVA-5.4 and PE/EVA-8.9 samples as received from the supplier was investigated by TEM. In the case of PE/EVA-0.0 sample shown in Figure 7.19 the bright area is the PE matrix and the small dark spots correspond to the carbon black

agglomerates. As already mentioned (Chapter 7.3), the carbon black filler used for preparation of the blends has an average single-particle size of 20 nm.

a)



b)

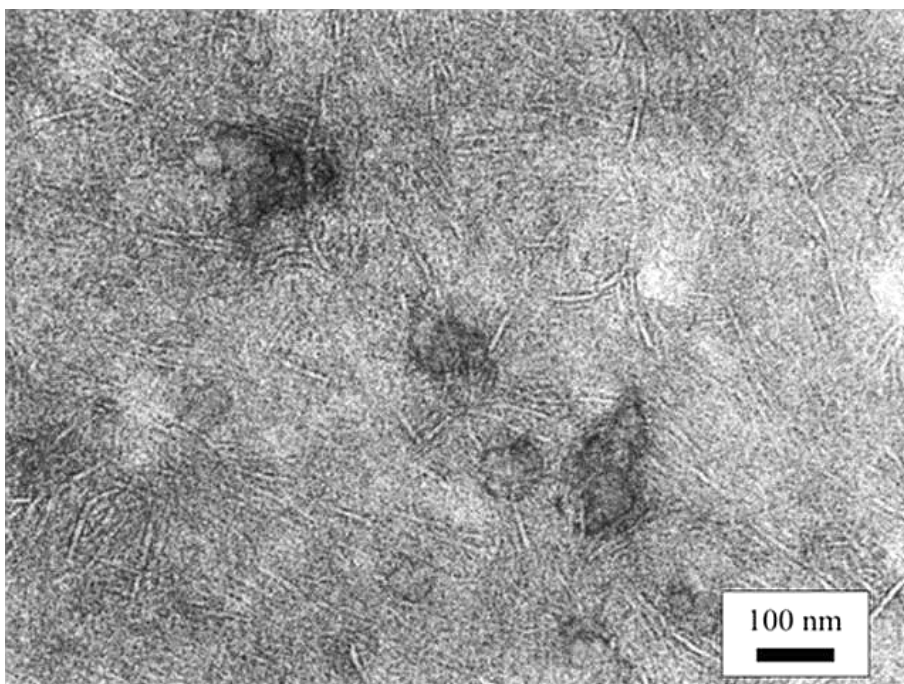


Figure 7.19 TEM image of PE/EVA-0.0 sample as received (before the ESCR test).

a) lower magnification and b) higher magnification. Dark spots correspond to carbon black particles.

Some cavitation mainly in the boundary area between the PE matrix and the filler particles can be seen, maybe obtained during cutting of the samples for the TEM studies or due to the crystallization phenomenon called “negative pressure effect”.<sup>[112, 113]</sup> This effect describes the formation of “holes” at the impingement lines of spherulites during the crystallization process (Figure 7.20 and 7.21).

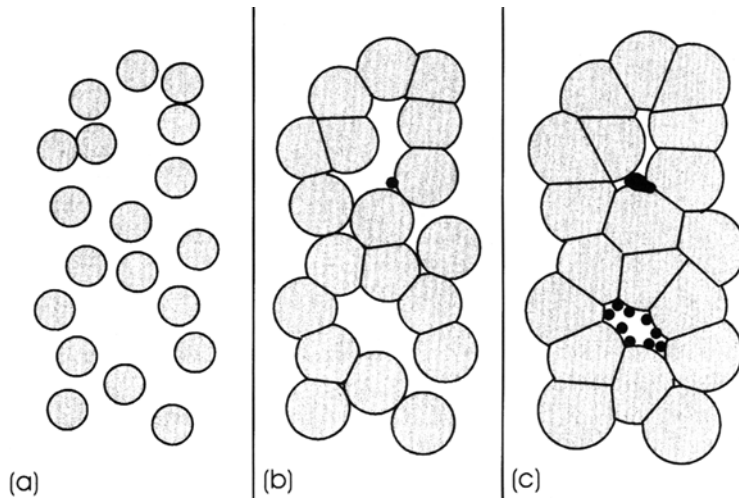


Figure 7.20 Scheme of different stages of spherulite growth: a) nucleation and growth in all radial directions, b) first impingement of spherulites and c) formation of geometries where parts of the liquid are completely confined by spherulites followed by a hole formation at the growth front.<sup>[112]</sup>

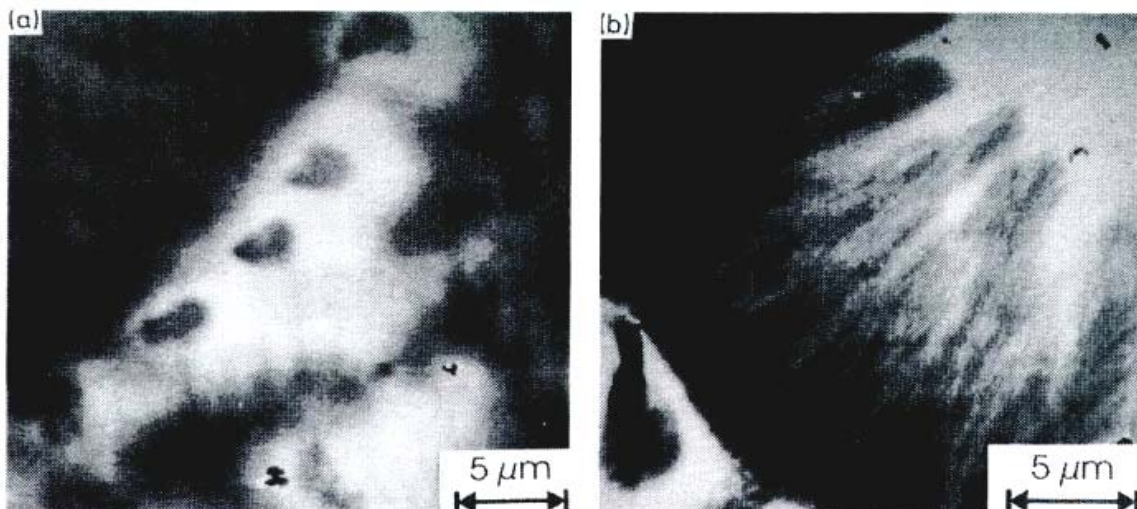
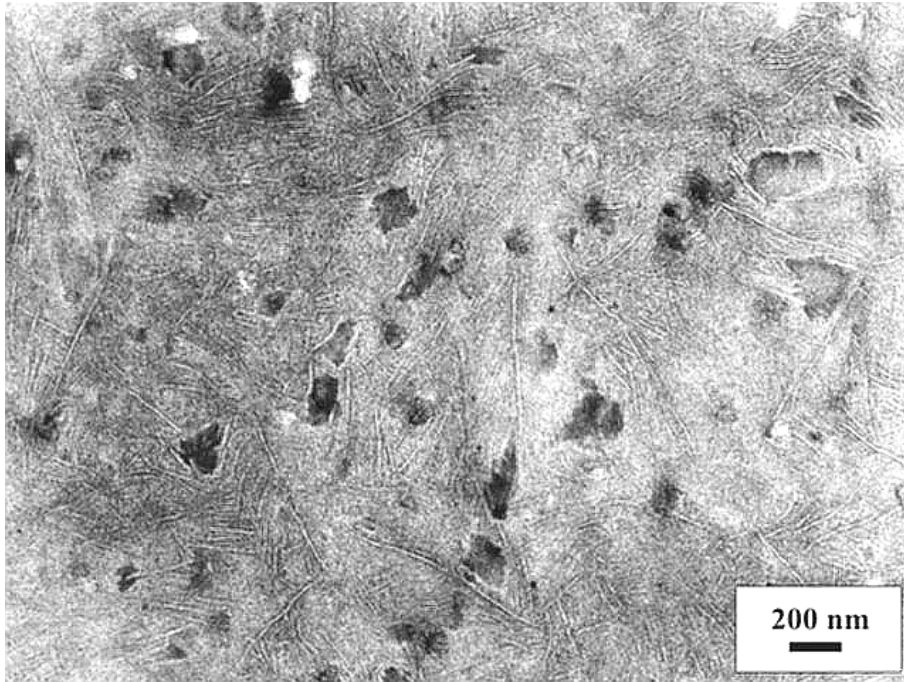


Figure 7.21 AFM image taken near to the growth front of the spherulites of PP: a) several holes at the growth front, and b) a single hole.<sup>[112]</sup>



Impingements of spherulites in the course of crystallization lead to the formation of pockets of the melt between spherulites where the confinement of the melt and lower specific volume of the solid result in a buildup of negative pressure. The negative pressure in the melt can grow only up to a certain limit. Beyond that limit, fracture of the melt occurs and cavities are formed inside weak spots.<sup>[113]</sup>

a)



b)

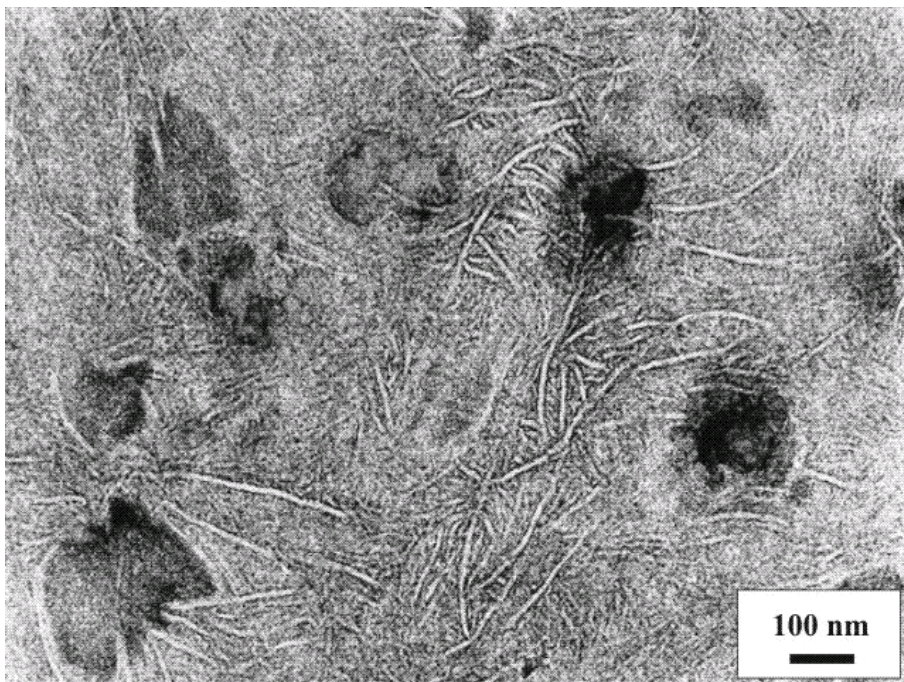


Figure 7.22 TEM image of PE/EVA-5.4 sample as received (before the ESCR test).

a) lower magnification and b) higher magnification. Dark spots correspond to EVA phase.

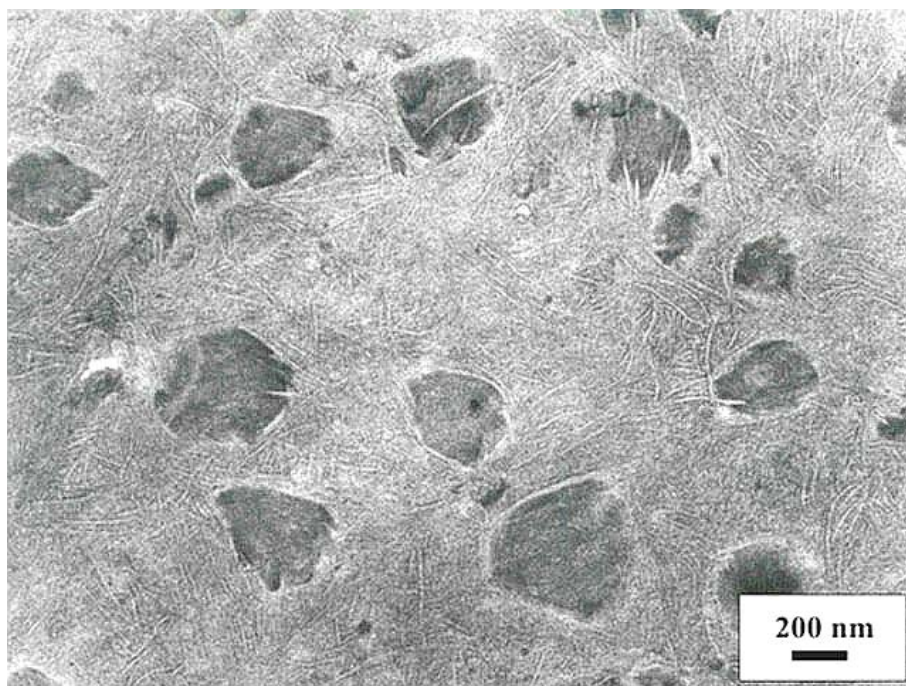


Figure 7.23 TEM image of PE/EVA-8.9 sample as received (before the ESCR test).

Figures 7.22 and 7.23 show the morphology of PE/EVA-5.4 and PE/EVA-8.9 samples as received from the supplier. The dark spots of various size and shape are due to the EVA copolymer distributed into the semi-crystalline PE matrix. The crystalline lamellae of PE can be easily seen. Some thick crystalline lamellae, which appear as bright lines, penetrate into the EVA particles.

As it was discussed in chapter 7.2, it was found that PE and EVA copolymer do not co-crystallize into lamellae if the content of VA branches is higher than 3 mol.-%. The growth of PE lamellae into the EVA phase is may be due to the partial solubility of the PE into the EVA phase. The two polymers in the system under investigation here, namely the blends of EVA (with 28 wt.-% VA) copolymer and LDPE, have a structural similarity in the sense that the former is a copolymer of a non-polar methylenic chain  $(-\text{CH}_2-)_n$  with the polar acetate group, and the later is a completely non-polar methylenic chain. It is well known that decreasing of the VA content in the EVA macromolecules increases miscibility of the components (PE and EVA). When the critical content of VA is reached the homo- and the copolymer become completely miscible.<sup>[114]</sup> Figure 7.24 shows the phase diagram of PE/EVA blend on dependence of blend composition at isothermal conditions (see also Appendix A and B). The inner part of the curve corresponds to the immiscible PE/EVA systems. The phase diagram shows that at very low contents of EVA copolymer in the blend (right open blue circle) there

is a small amount of PE dissolved in the EVA phase. We assume that there is a partial miscibility between PE and EVA in the blends we investigated, which allows growth of PE lamellae into the EVA phase.

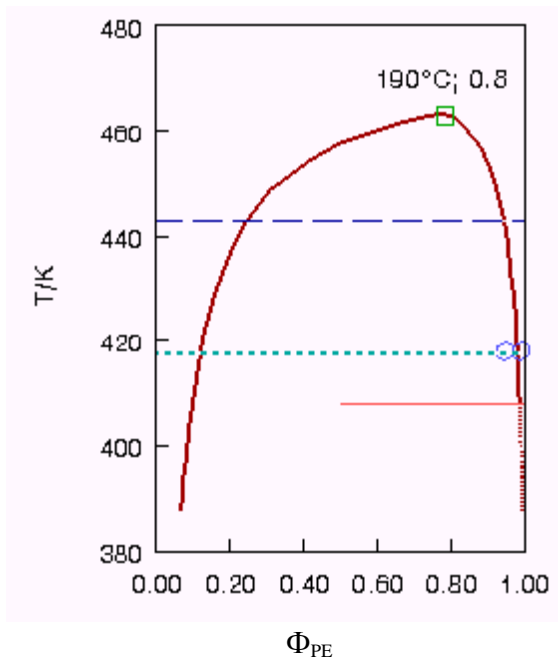


Figure 7.24 Phase diagram of PE/EVA blends on dependence of composition and temperature ( $M_{PE} = 100\ 000\ \text{g/mol}$ ,  $M_{EVA} = 15\ 500\ \text{g/mol}$ ). Dotted line:  $T = 145^\circ\text{C}$ , dashed line:  $T = 170^\circ\text{C}$ , straight rose line indicates melting temperature of PE at about  $130^\circ\text{C}$ .

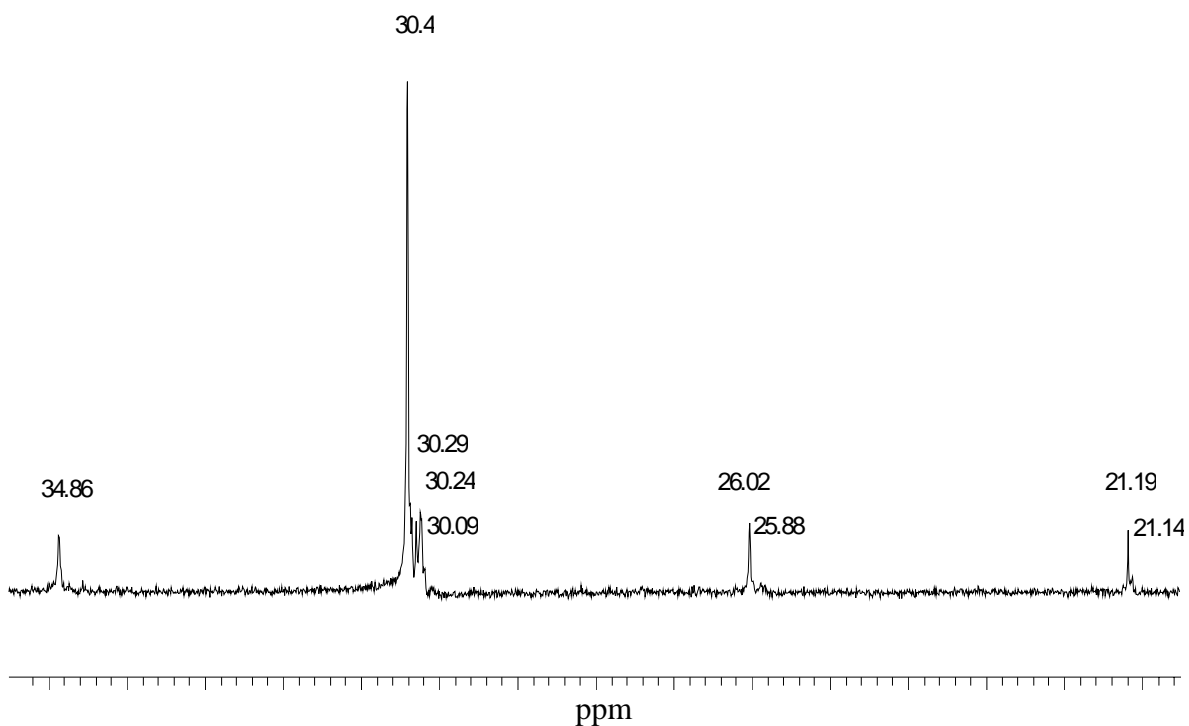
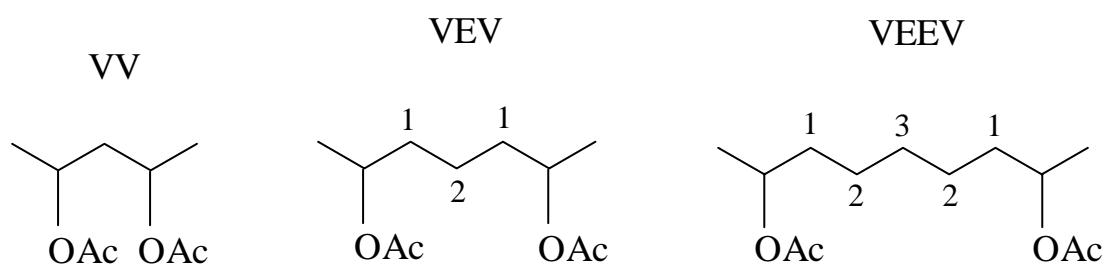


Figure 7.25  $^{13}\text{C}$  NMR spectrum of 20 wt.-% EVA solution in 1,2,4-trichlorobenzene and deuterium benzene as a lock solvent.

These results are extremely important for the interpretation of the TEM images. We may assume that the growth of lamellae in the EVA phase is fed by PE dissolved in the EVA phase due to the partial miscibility of the LDPE and the EVA copolymer.

The EVA copolymer was studied by  $^{13}\text{C}$  nuclear magnetic resonance (NMR) employing solution technique for determination of the comonomer sequence length. 20 wt.-% solution of EVA in 1,2,4-trichlorobenzene and deuterium benzene as a lock solvent was prepared and analyzed by NMR. Figure 7.25 shows the NMR spectrum in the range 20 to 36 ppm.

The assignments of the microstructures in the copolymer (Table 7.2) were done by Tavares<sup>[115, 116]</sup> and Beshah.<sup>[117]</sup> The  $\text{CH}_2$  and  $\text{CH}$  groups of vinyl acetate were assigned as  $\text{C}_\beta$  and  $\text{C}_\alpha$  respectively. The  $\text{CH}_2$  units of ethylene were marked in accordance with the position that they are located in relation to the acetate neighbor groups (Scheme 7.1).



Scheme 7.1 Assignment of the groups in EVA copolymer.<sup>[116]</sup>

Table 7.2 Assignment of the peaks in the NMR spectrum of EVA copolymer. (E – ethylene comonomer, V – vinyl acetate comonomer)

$\delta$ (ppm)	Assignment
34.86	$\text{C}_1$ (VEEV)
30.4	$\text{C}_3$ (VEEV)
30.09	EEEE
26.02 and 25.88	$\text{C}_2$ (VEEV)
21.19 and 21.14	$\text{CH}_3$ (V)

The aim of the NMR analysis was to detect any long ethylene sequences in the EVA copolymer which would be an indication that they will be able to crystallize. A very low intensity peak was found at 30.09 ppm which belongs to the EEEE segments. On the other hand, the minimum segmental sequence length of  $\text{CH}_2$  entities that can participate in

crystalline lamellae is found equal to 18.2.<sup>[118]</sup> This value is fully consistent with the statistical sequence length of seventeen CH<sub>2</sub> entities between two vinyl branches for a EVA copolymer containing 28 wt.-% VA. The NMR spectrum shows the presence of ethylene sequences in the EVA copolymer and this result is in a complete agreement with the DSA and WAXS data about the EVA copolymer. But the thick lamellae (visible in Figure 7.22 and 7.23) which penetrate into the EVA particles are due to PE dissolved into the EVA phase as a result of the partial solubility of the components.

It was observed that the size of the EVA particles increases with increasing EVA content in the blends (Figures 7.22 and 7.23). But it is known that the diameter of modifier particles and the interparticle distance play an important role in toughening of plastics.<sup>[119, 120, 130]</sup> Maybe these two parameters govern the ESC process and therefore influence the ESCR of the investigated PE/EVA blends. The size of the EVA particles and particle-particle distance were determined by using Image Processing System analySIS 3.1. It was established that the average diameter of the EVA particles in PE/EVA-5.4 and PE/EVA-8.9 samples is 160 (average out of 111 particles) and 212 nm (average out of 50 particles) respectively, and the average particle-particle (surface-to-surface) distance is 352 and 306 nm respectively. Figure 7.26 shows the size of the EVA particles in the investigated samples.

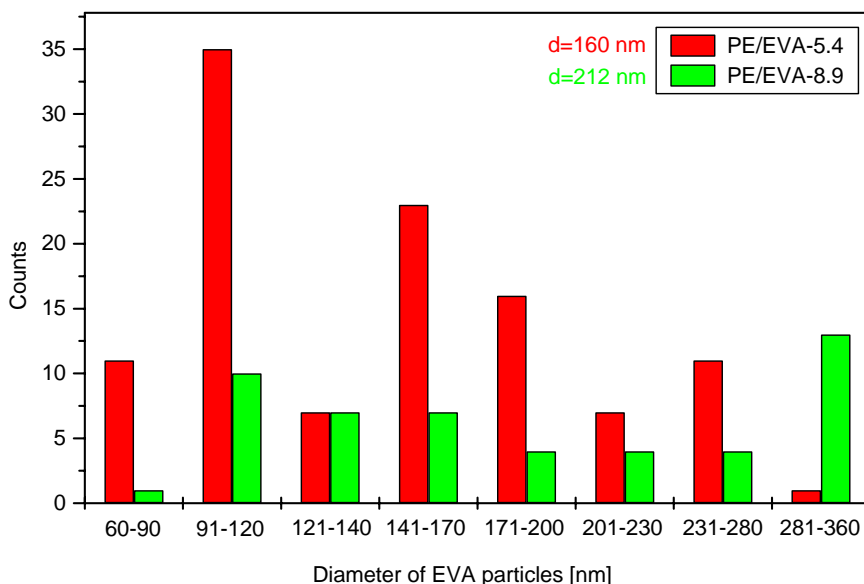


Figure 7.26 Size of EVA particles in PE/EVA-5.4 and PE/EVA-8.9 samples as received.

Therefore, in the case of PE/EVA-8.9 sample more larger EVA particles are present and the particle-particle distance is smaller than in the PE/EVA-5.4 sample. In general, rubber content, rubber particle size, and the interparticle distance are important factors in the

deformation and fracture of all toughened plastics.<sup>[120]</sup> It is frequently observed that the critical rubber content required to obtain a given level of toughness increases with increasing strain rate. Rubber particle size can effect the deformation behavior of rubber modified plastics in three ways, through its effect on (1) the critical volume strain to cavitate the rubber, (2) the critical tensile strain to initiate a craze, and (3) the volume strain to de-bond the particles and the matrix. Michler<sup>[119]</sup> studied the role of the particle size and the interparticle distance in maximizing the toughness of HIPS, ABS polymers and high-impact polyamides. It was found that there is an optimum particle diameter and a critical interparticle distance. Particles of diameter larger than the optimum diameter are less effective for craze initiation and toughening. The decisive role of the interparticle distance in contrast to the particle diameter has been explored first by Wu<sup>[121, 122]</sup> and later by Borggreve and co-workers.<sup>[123, 124]</sup> Wu found that blends of modified polyamide with higher values of interparticle distance are brittle, whereas blends with smaller values of the interparticle distance are tough. This means that a critical interparticle distance exists, which describes the brittle-tough transition of the material.

Blends with 8.9 wt.-% EVA never failed during the ESCR tests in 10 vol.-% Igepal solution, which can be referred to the higher EVA content and the smaller particle-particle distance compared to the rest of the blends. It seems that the 8.9 wt.-% EVA content is enough for prevention of crack initiation and growth in the samples. The higher crack resistance attained through the addition of 8.9 wt.-% EVA is related probably to greater tendency of the blends to relax under stress.

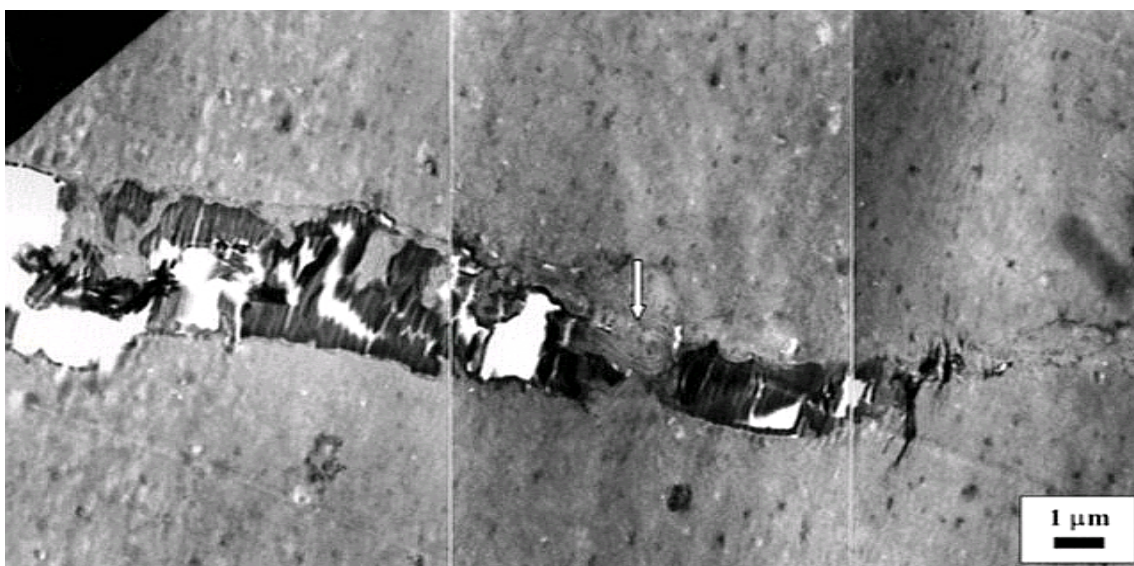


Figure 7.27 TEM image of the crack and craze tip in PE/EVA-0.0 sample that failed after 1 h the ESCR test at 50°C.

Information about the fracture process and the crack growth mechanism was obtained through TEM investigations of PE/EVA-0.0 samples that failed the BTT at 50°C within 1 h (Figure 7.27). A growing crack with its craze leading the way is visible in that micrograph. The crack grows in a direction perpendicular to the notch. The primary craze ahead of the crack is dark. It is evident that the damaged zone has fibrillar structure (indicated by the dark, highly stained regions). The higher magnification image (Figure 7.28) shows a large area of highly deformed and oriented PE matrix in the damaged zone.

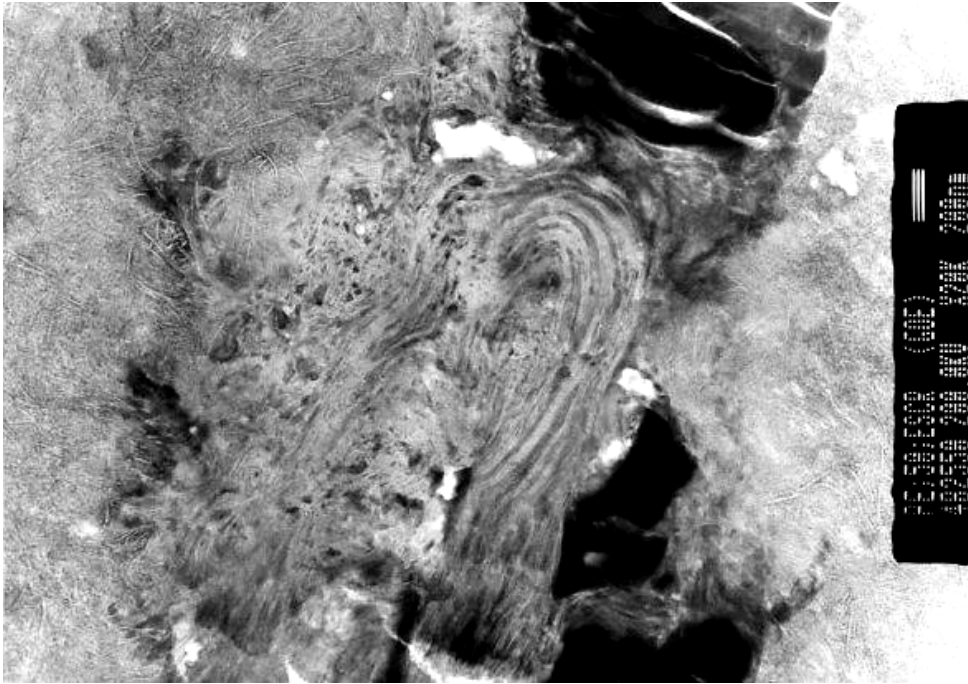


Figure 7.28 TEM image (higher magnification image) of the area indicated by an arrow in Fig. 7.27.

TEM was applied to detect morphological changes of PE/EVA-5.4 and PE/EVA-8.9 samples after the ESCR test at 50 and 70°C. PE/EVA-5.4 samples failed within 24 h during the ESCR test at 50°C in Igepal solution. The cracking starts in most cases on both sides in a direction perpendicular to the notch. TEM investigations were carried out of the damaged area under the notch. The process of crack propagation is demonstrated by the TEM image in Figure 7.29a. The tip of the crack (indicated by an arrow) is shown in Figure 7.29b where broken PE lamellae and cavitation inside and around the EVA particles can be seen. The cavities appear as bright areas surrounding the EVA particles. This de-bonding of the EVA phase from the PE matrix is probably due to the bending of the samples into the U-shaped specimen holder during the ESCR test and maybe due to the influence of the environmental stress cracking (ESC) agent. The ESC agent does not cause chemical degradation of the polymer, it only

accelerates the process of macroscopic brittle-crack formation.<sup>[1, 2]</sup> The ESC agent enhances craze growth by plasticizing amorphous regions; and it enhances fracture by interacting with the crystalline region of the fibrils at the base of the craze.<sup>[14]</sup> Diffusion of detergent molecules into the polymer due to stress might result in increased chain mobility and therefore in a reduction of the activation energy of the deformation process.<sup>[7]</sup>

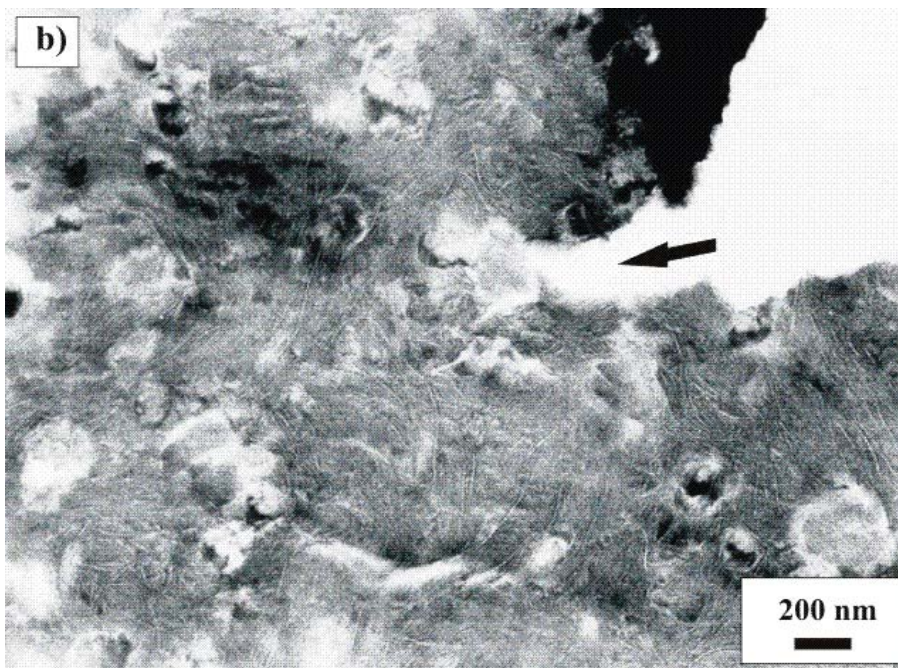
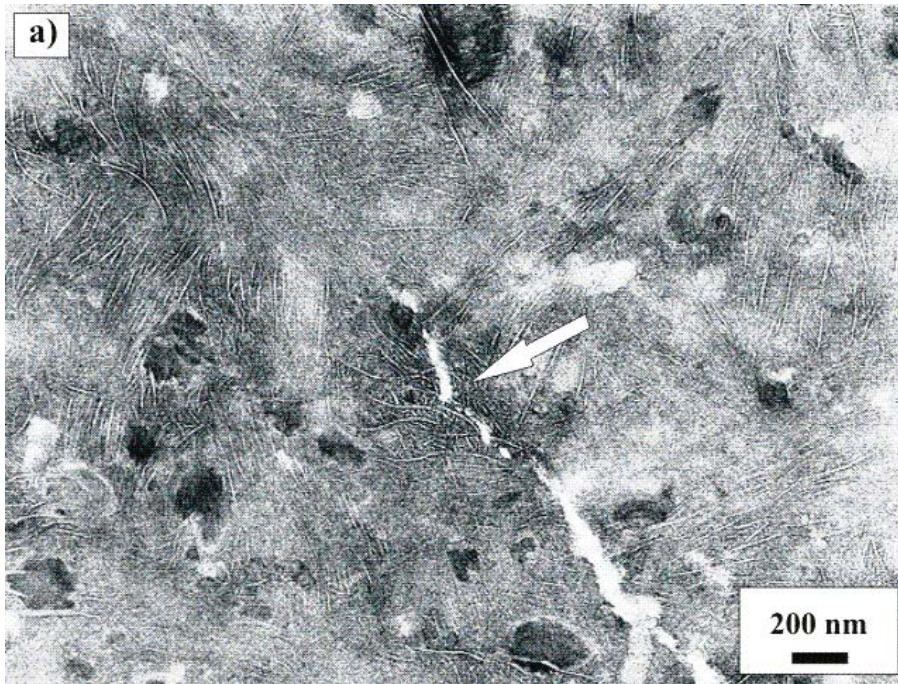


Figure 7.29 TEM image of PE/EVA-5.4 sample which cracked within 24 h during the ESCR test at 50°C in Igepal. a) crack propagation and b) crack tip.



Under an external stress, stress concentration or stress that is increased additionally by superposition of local stress fields is built up between the rubber-like particles.<sup>[119, 125-127]</sup> Owing to stress concentration and formation of shear bands, higher hydrostatic stress is generated inside the particles, giving rise to cracking and formation of micro-voids inside the blend. The result is a higher local stress concentration between the elastomeric particles. There is an effect influencing the crack propagation. Cracks, which enter the elongated micro-voids, are rounded at their tips. These cracks are prevented from further propagation (Figure 7.29b).

PE/EVA-5.4 samples surprisingly did not show failure during the ESCR test at 70°C. The TEM image in Figure 7.30 shows the morphology of a sample that passed the ESCR test at 70°C.

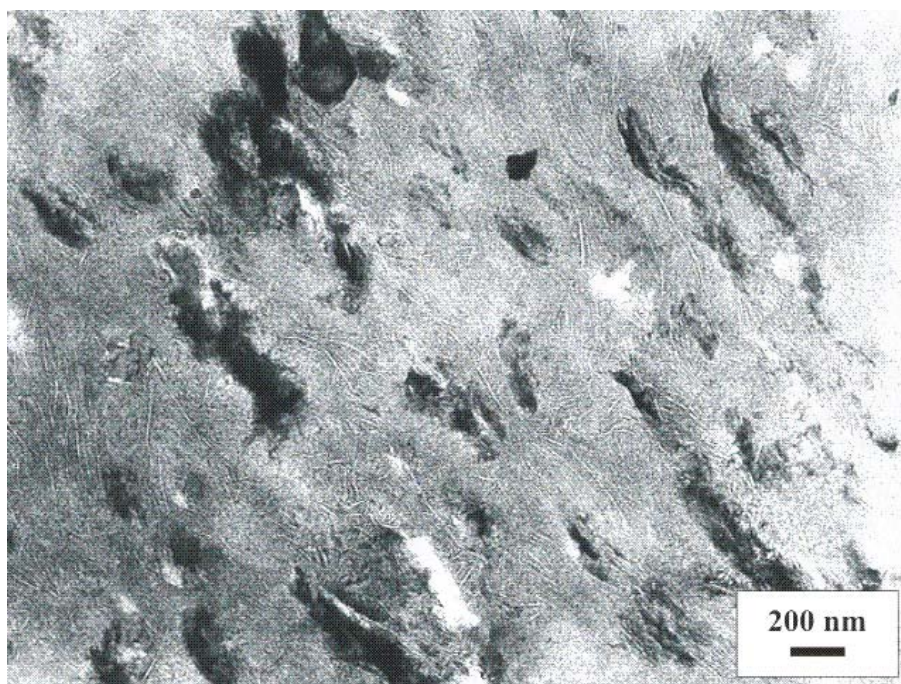


Figure 7.30 TEM image of PE/EVA-5.4 sample after 1000 h ESCR test conditions at 70°C. Dark elongated spots correspond to EVA particles.

As the test temperature was above the melting temperature of EVA, EVA particles are melted. In contrast to the previous samples annealed at lower temperature, they are deformed and aligned in bending direction which somehow prevents crack initiation and growth.

The TEM image in Figure 7.31 reveals the morphology of PE/EVA-8.9 sample that passed the ESCR test at 50°C. Duration of the test was 1000 h. It is clearly seen that the EVA

particles are deformed and oriented in direction of bending of the samples. They appear as dark elongated entities.

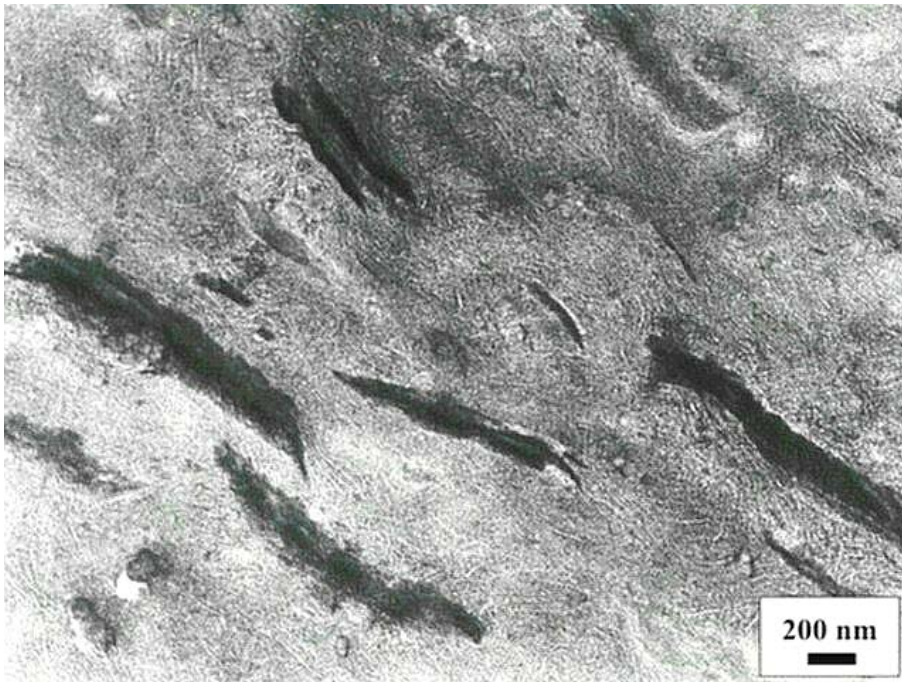


Figure 7.31 TEM image of PE/EVA-8.9 sample after 1000 h ESCR test conditions at 50°C. Dark elongated spots correspond to EVA particles.

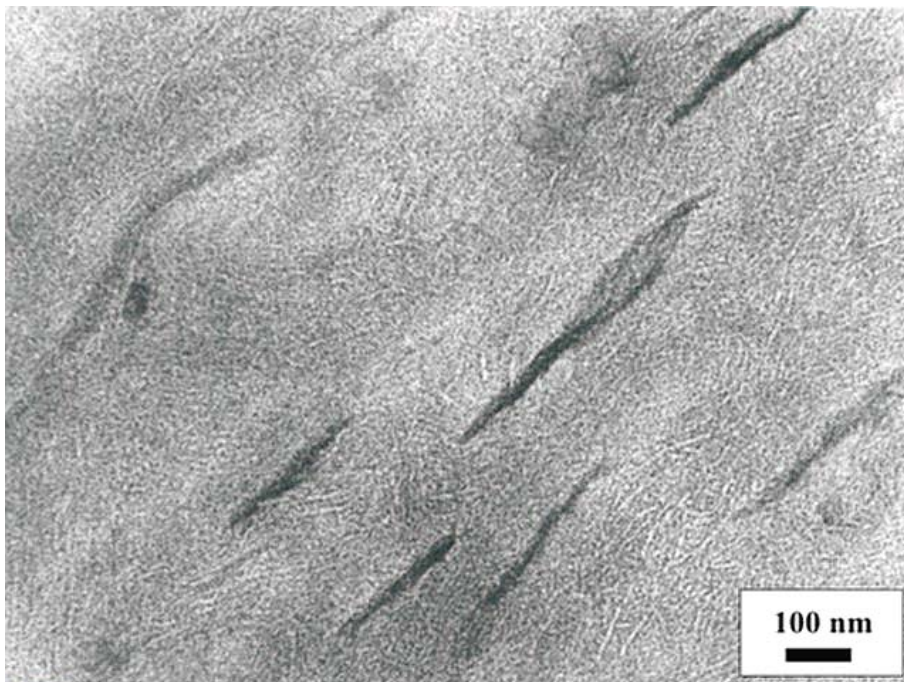


Figure 7.32 TEM image of PE/EVA-5.4 sample after 1000 h ESCR test conditions in air at 50°C. Dark elongated spots correspond to EVA particles.

In order to check how the ESC agent affects morphology of the blends, ESCR test was carried out in air instead of Igepal as ESC agent. Samples were bent and kept in air at 50°C for 1000 h. Then ultra-thin sections were cut and investigated by TEM. Figure 7.32 reveals the morphology of a PE/EVA-5.4 sample prepared in that way. The EVA particles are deformed and oriented in direction of bending of the samples. They appear as dark elongated entities. But compared to the TEM image in Figure 7.29 cavitation inside and around the EVA particles cannot be detected. Therefore, in the case of ESCR test in Igepal the semi-crystalline PE matrix is very quickly attacked by the Igepal solution (which provokes crack initiation and growth) and this process is faster than the creep deformation of the EVA particles.

Increasing the EVA content in the blends makes the samples more flexible, and therefore they can deform and relax better under stress. By increasing the VA content in the EVA copolymer the product becomes soft and flexible, having predominant rubber-like properties. It is observed that when the VA content is increased, the relative quantity of polyethylene amorphous phase increases and the degree of crystallinity decreases.<sup>[118]</sup> ESCR of polymers increases with decreasing crystallinity. Side-chain branches suppress crystallization and they increase the resistance to disentanglement and ESC.

#### **7.4.2 SEM Investigations**

Fracture surfaces of the samples that failed the BTT at 50°C were investigated by SEM. Images were taken from the damaged area close to the notch. The SEM micrograph of PE/EVA-0.0 sample (Figure 7.33) shows that the fracture surface is flat and visually smooth. In contrast, with addition of EVA in the system, the fracture surfaces display fibrous texture. Deformed strands coming out from the surface can be seen in Figures 7.34 and 7.35, indicating that the EVA phase makes the material tougher and with increasing the EVA content the failure mechanism tends to be rather ductile than brittle.

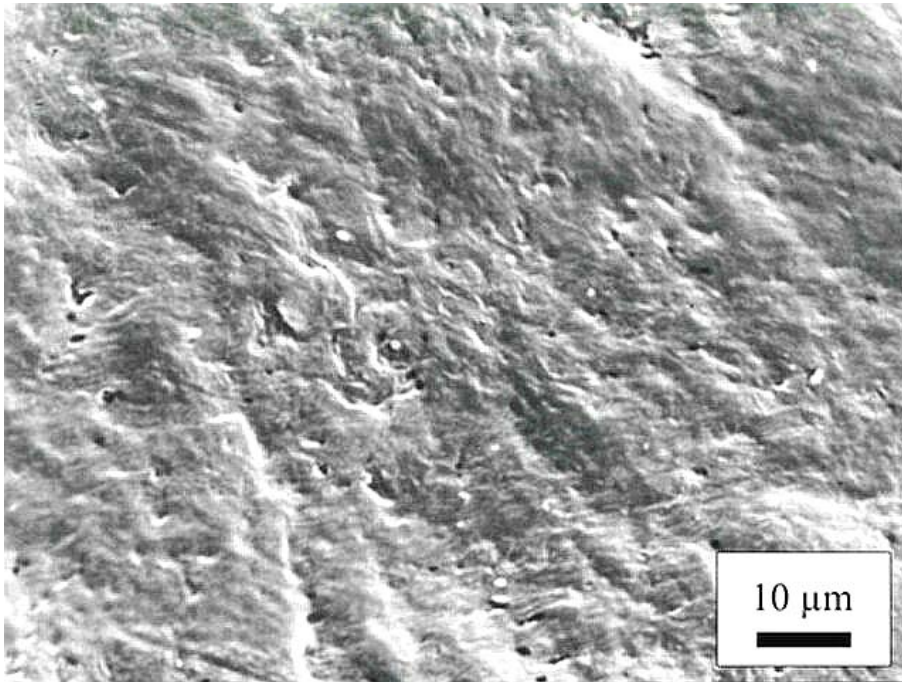


Figure 7.33 SEM image of the fracture surface of PE/EVA-0.0 sample that failed the ESCR test in Igepal at 50°C within 1 h.

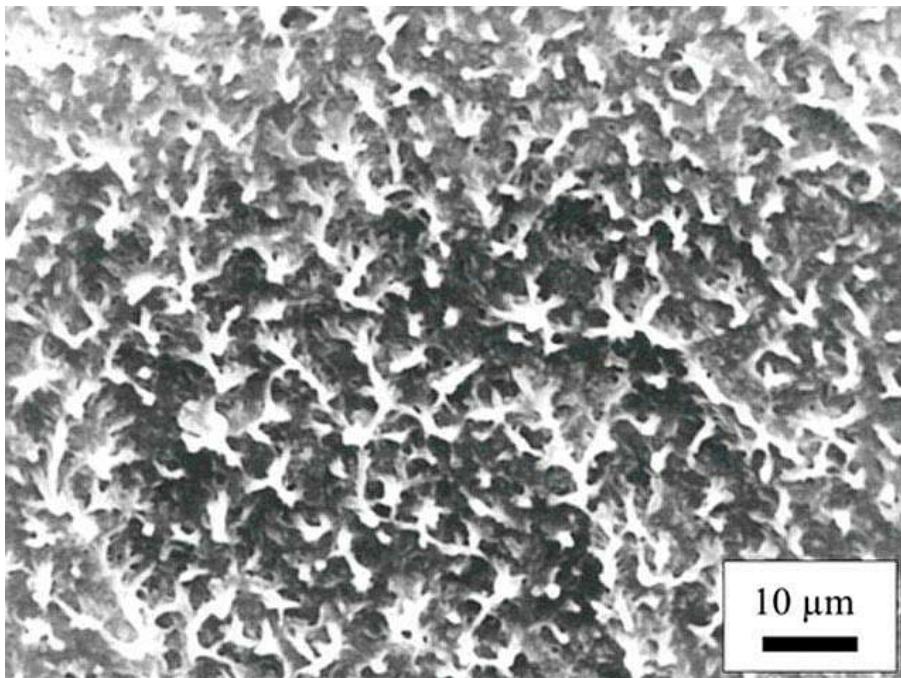


Figure 7.34 SEM image of the fracture surface of PE/EVA-5.4 sample that failed the ESCR test in Igepal at 50°C within 24 h.

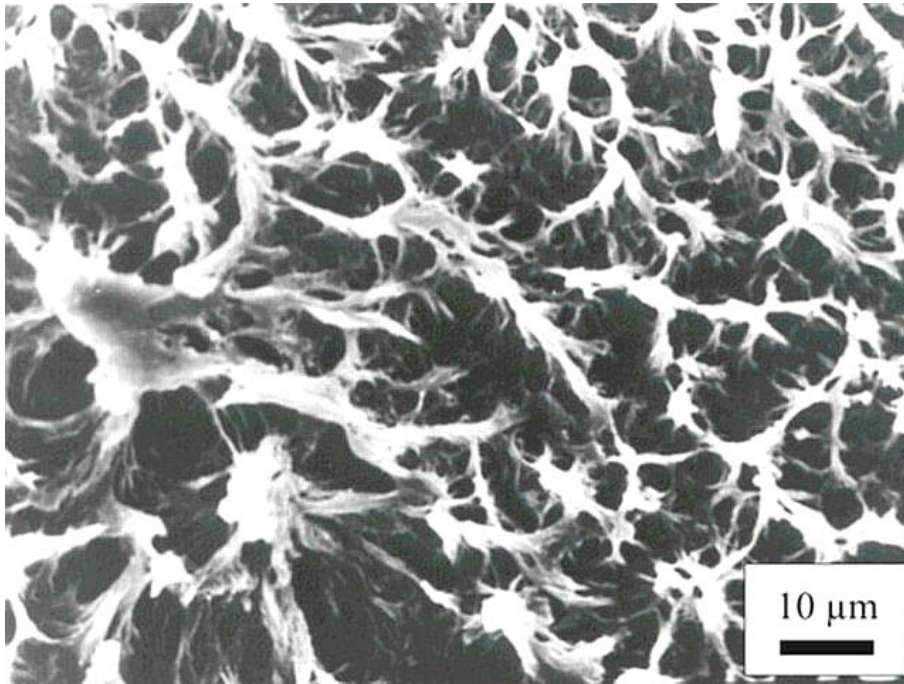


Figure 7.35 SEM image of the fracture surface of PE/EVA-7.1 sample that failed the ESCR test in Igepal at 50°C within 24 h.

### 7.4.3 HVEM Investigations

HVEM was applied to study phase structures and the micromechanical deformation processes in some of the blends. Although the stress-strain state in semi-thin sections is different from that in bulk materials even under the same external loading condition, the deformation mode cannot be changed, because the semi-thin sections are representative of the morphology. Only the degree of plastic deformation, i.e. the degree of elongation should be changed. Therefore, it is difficult to compare the degree of elongation between semi-thin sections and bulk material, but the character and type of deformation, i.e. the micromechanical deformation mechanisms are comparable in both cases.<sup>[14, 126]</sup>

In the literature it is generally assumed that the deformation of PE is a continuous change into the *c*-texture (i.e. a continuous orientation of the chain segments parallel to the deformation direction).<sup>[125]</sup> This conclusion is based mainly on X-ray scattering measurements, which show a steadily increased draw ratio. Direct electron microscopic investigations have shown that the improvement of the *c*-axis orientation results from a superposition of several local deformation processes.

Figure 7.36 shows typical deformation structures of PE/EVA-5.4 sample during the *in situ* deformation in HVEM.

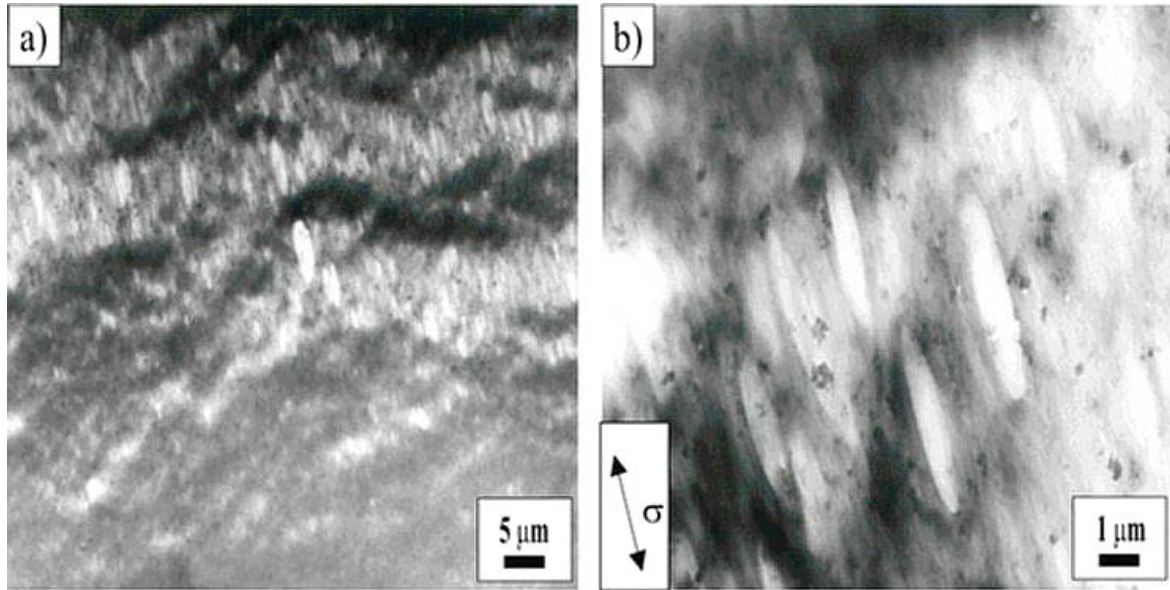


Figure 7.36 Strained semi-thin sections of PE/EVA-5.4 sample (as received) in the HVEM. a) shear bands deformation structures, and b) micro-voids formation.

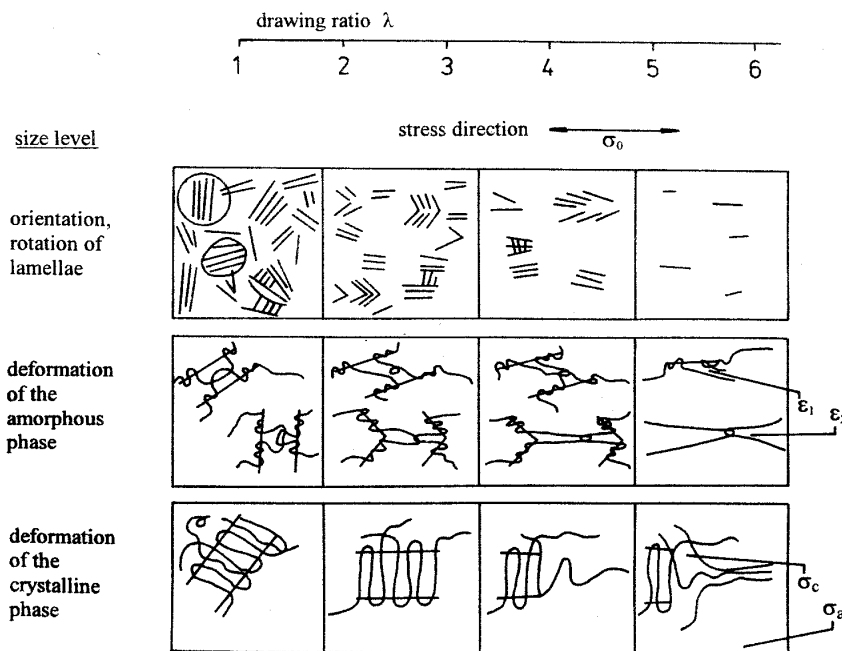


Figure 7.37 Scheme of the micromechanical processes of orientation with increasing draw ratio.<sup>[125]</sup>

Figure 7.37 shows schematically the deformation process in these three stages occurring on the supermolecular level and the molecular level of the amorphous and of the crystalline phase. In the first stage of deformation, large lamellae break into shorter pieces, and the lamellae tend to twist with their length directions ( $b$ -axes) toward the deformation direction.<sup>[125]</sup> In the second stage, the lamellae no longer appear as customary in TEM. The final stage of deformation is the improvement of the  $c$ -axis orientation.

The plastically deformed specimen in lower magnification (Figure 7.36a) reveals band-like structures. When the stress concentration reaches a critical value, void formation takes place through cavitation inside plastically elongated EVA particles or de-bonding at the particle matrix interface<sup>[127]</sup> (Figure 7.36b). As the strain is increased, the voids are elongated gradually in the direction of the applied stress. As a result shear yielding in the matrix will be induced. Because of the rigidity of the carbon black filler particles, they cannot be deformed by external stress in the specimen. So, they appear in the images as small dark spots (carbon black agglomerates).

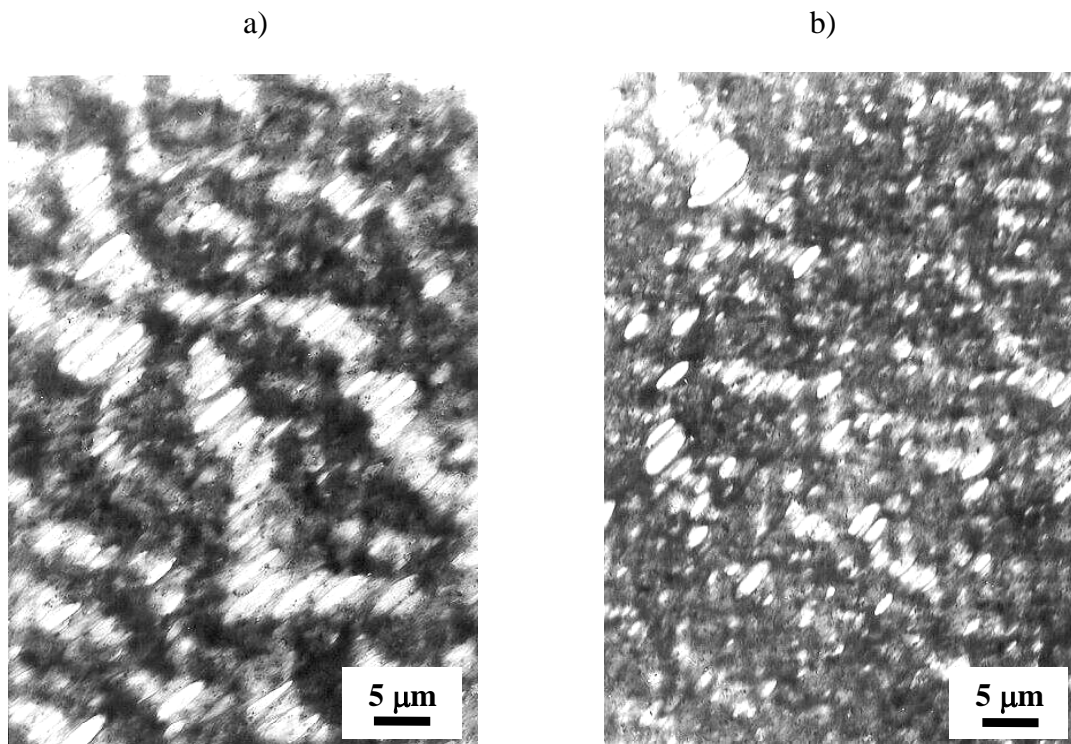


Figure 7.38 Strained semi-thin sections of a) PE/EVA-5.4 sample that failed the ESCR test in Igepal at 50°C for 24 h, and b) PE/EVA-5.4 sample taken after 1000 h ESCR test conditions in Igepal at 70°C.

Figure 7.38 shows typical deformation structures of PE/EVA-5.4 samples after the ESCR test in Igepal at 50 and 70°C during the *in situ* deformation in HVEM. Necking was observed

during the deformation of PE/EVA-5.4 sample annealed a 50°C. It is visible that the sample deformed through shear yielding. Shear bands and highly elongated voids are visible in Figure 7.38a. In the case of PE/EVA-5.4 sample annealed at 70°C (Figure 7.38b), the sample deformed without necking. Material was very stiff as a result of the long thermal treatment at 70°C during the ESCR test and therefore the voids are not so well deformed and elongated. It can be concluded that the different annealing temperatures during the BTT do not influence the deformation mechanism in the samples and they deform through shear yielding.

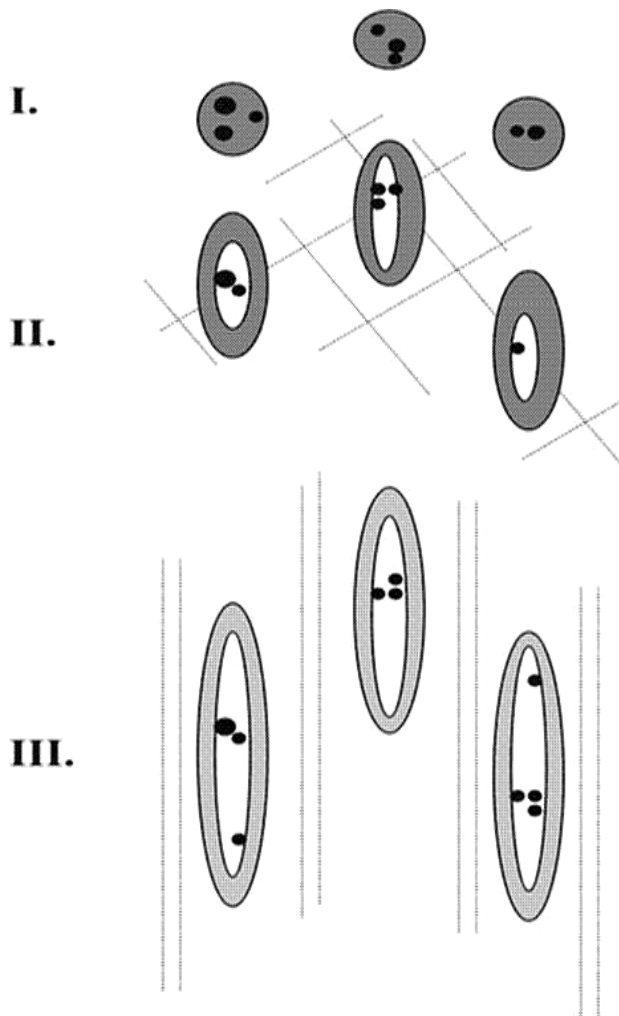


Figure 7.39 Model representation for micromechanical deformation process in PE/EVA/carbon black blends. Carbon black particles (dark dots) are located in the EVA phase.

- I. Stress concentration around the EVA particles
- II. Void formation
- III. Shear yielding



The results of the *in situ* microscopic observations of micromechanical deformation processes in various toughened and particle filled semicrystalline polymers have been described as three-stage mechanism.<sup>[126, 127]</sup>

*Stage 1: stress concentration.* The modifier particles act as stress concentrators, because they have different elastic properties from the matrix. The stress concentration leads to stretching of the rubber-like particles in the direction of the applied stress.

*Stage 2: void formation.* Due to the stress concentration, void formation occurs through cavitation inside particles or de-bonding at the particle matrix interface.

*Stage 3: shear yielding.* With further increase of the strain, the voids gradually elongate and the yield strength is lowered. As a consequence, shear yielding is induced in the matrix.

Figure 7.39 shows a model representation for the above mentioned three-stage mechanism applied for the investigated PE/EVA/carbon black blends.

## 7.5 Mechanical Properties

The mechanical properties of a polyethylene specimen can be defined as those attributes that involve the physical rearrangement of its component molecules or distortion of its initial morphology in response to an applied force. The nature of a specimen's response to applied stress can be correlated with its morphological and molecular characteristics.

The mechanical properties of polyethylene may be divided into two broad categories: (1) low strain properties such as yield stress and initial modulus and (2) high strain properties such as ultimate tensile strength and draw ratio at break.<sup>[99]</sup> Tensile properties of polymers are measured on instruments that record the force required to elongate a sample as a function of elongation. The applied force can be plotted as stress, i.e. force per cross-sectional area of the specimen. The elongation of the specimen can be plotted as strain which is increased in sample length compared to the original gauge length.

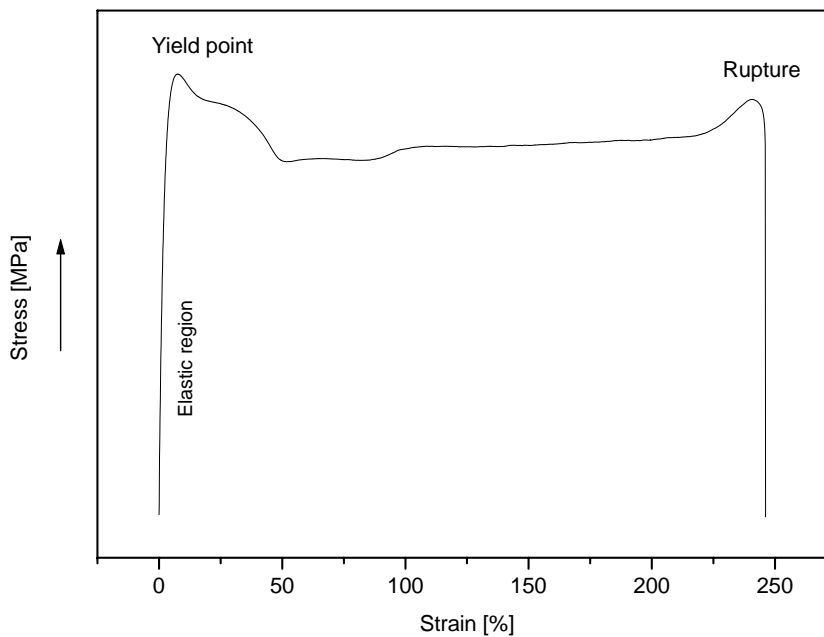


Figure 7.40 Stress-strain behavior over the entire strain range for as-received PE/EVA-5.4 sample.

A schematic stress-strain curve illustrating the major tensile phenomena of PE/EVA blends is shown in Figure 7.40. The initial part of the stress-strain curve corresponds to the *elastic region* (where the stress and strain values are small). The material begins to deform plastically when all of the strain will not be recovered. This point is marked as *yield point*. The yield point is important because it marks the upper limit of applied stress from which full recovery of shape occurs when the stress is removed. Beyond the yield point, the material is permanently deformed. Even when the stress is removed, the material will not recover to its original shape. The region beyond the yield point is called the *plastic region*.<sup>[128]</sup>

The molecular interpretation of the elastic and plastic behavior is that in the elastic region the strain is due to the stretching of the macromolecules in the amorphous phase and minor deformations in the crystalline regions. At the yield point non-recoverable movements begin that result in permanent deformation. Some of the most common deformation processes are: disentanglement of the molecules and crack formation. Further increase of the applied stress leads to break of the sample.

Obtained stress-strain curves for the PE/EVA blends reveal a well-defined yield point, a region of stress-softening and strain hardening effect. In the stress hardening region the stress increases at fast rate with the increase of strain till the ultimate failure. At this stage, molecular segments of both amorphous and crystalline components get oriented in a more

orderly manner along drawing direction. These orientations during drawing lead to close packing of chains and thereby cause appreciable increase in the intermolecular forces of attraction which accounts for high stress at rupture.<sup>[129]</sup>

The elastic deformation which is due to intermolecular force of attraction can be estimated in terms of Young's modulus. The elastic modulus of a sample is a measure of its stiffness. The higher the modulus, the stiffer the material. The value of elastic modulus is normally derived from the initial slope of the stress-strain curve.

Tensile strength at yield is the force at which the sample yields, divided by its cross-sectional area. The yield stress of a specimen is of great interest from a practical point of view. In many cases it represents the maximum permissible load that a sample can withstand while still performing its assigned role.

The tensile properties of PE samples are strongly influenced by temperature, especially between room temperature and their melting temperatures. Elastic modulus and yield stress fall monotonically with increasing temperature.<sup>[99]</sup>

Mechanical properties of PE samples containing different amounts of EVA copolymer were investigated at room temperature, 50 and 70°C by Instron test machine. Figure 7.41 shows the dependence of Young's modulus on the EVA content in the blends and the test temperature. It is visible that the Young's modulus slowly decreases with increasing the EVA content. The increased temperature reduces the stiffness of the polymer as observed from the decreased Young's modulus with increasing the measurement temperature. Increased temperature also reduces the yield stress for all blends (Figure 7.42).

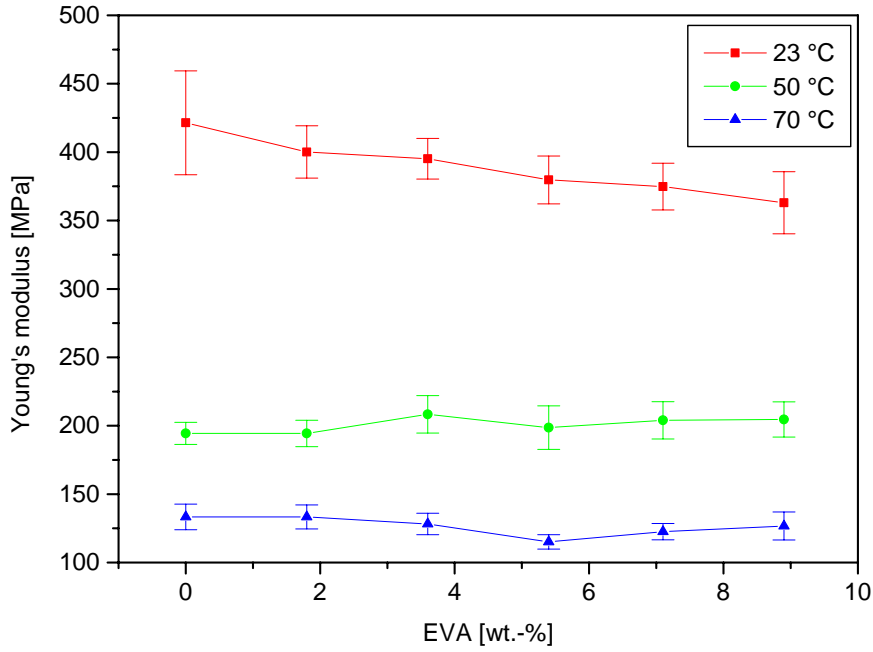


Figure 7.41 Young's modulus of PE/EVA blends as a function of the EVA content and the test temperature during the Instron measurements.

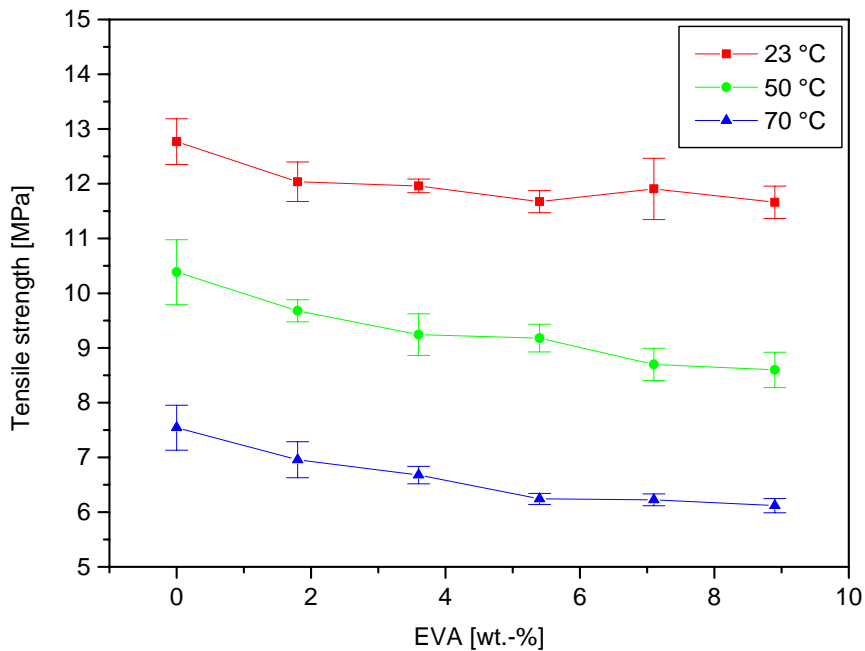


Figure 7.42 Tensile strength of PE/EVA blends as a function of the EVA content and the test temperature during the Instron measurements.

## 8. Summary and Conclusions

This work deals with ESCR of LDPE/EVA compounds in dependence on the test temperature and the EVA content in the blends, their thermal and mechanical properties, morphology, failure behavior and deformation mechanism of selected samples as a function of the EVA content. ESCR experiments were carried out with the final goal to find a solution for the acceleration of the test and to predict the ESC behavior of the blends much faster. The investigations carried out in this work can be employed for a better understanding of the fundamentals of the phenomenon of ESC in the special case of LDPE/EVA compounds. All these results can be taken to develop a criterion for the long-term ESC behavior of the materials used and finally it would be possible to develop a theoretical model for their ESC behavior.

It can be concluded that a strong interplay exists between composition, morphological features and the ESCR behavior of PE/EVA blends. Obtained results demonstrate that EVA containing 28 wt.-% VA is a very effective copolymer for the retardation of ESC in LDPE. Samples containing 8.9 wt.-% EVA always pass the ESCR test at all temperatures up to 1000 h. When the EVA content is 7.1 wt.-% and less, the affinity of polyethylene to ESC can be clearly seen. In most of the cases, cracking starts on both sides in a direction perpendicular to the notch as expected from the finite element calculations. TEM images of PE/EVA-5.4 and PE/EVA-8.9 samples, as received (before the ESCR test), reveal that the size of the EVA particles increases with increasing the EVA content in the blends. It seems that the size of the EVA particles and the interparticle distance govern the ESC process and therefore influence the ESCR behavior of the investigated LDPE/EVA compounds. Blends with 8.9 wt.-% EVA never failed during the ESCR tests in 10 vol.-% Igepal, which can be referred to the higher EVA content and the smaller particle-particle distance compared to the rest of the blends. It is obvious that the 8.9 wt.-% EVA content is enough for prevention of crack initiation and growth in the samples. The higher crack resistance attained through the addition of 8.9 wt.-% EVA is related probably to greater tendency of the blends to relax under stress.

TEM images of PE/EVA-5.4 and PE/EVA-8.9 samples as received show that a few thick crystalline lamellae penetrate into the EVA phase. The growth of lamellae in the EVA phase is probably fed by PE dissolved in the EVA phase due to the partial miscibility of the polymers or by long ethylene sequences in the EVA copolymer capable of crystallization.

For all samples, the time to failure was shorter during the ESCR test at 50°C than at 30, 60 and 70°C. The increase of the time to failure of the samples at 60 and 70°C as compared with that at 50°C might be as a result of melting of the semicrystalline material of

EVA. During the test at 60 and 70°C the system is in the range of the melting temperature of EVA copolymer, and thus the EVA particles are deformed more easily under the influence of stress. TEM images of PE/EVA-5.4 and PE/EVA-8.9 samples annealed at 70°C during the ESCR test show that the EVA particles are deformed and stretched in direction of bending of the samples which prevents crack initiation and growth.

Different reorganization processes can occur as a result of the long thermal treatment of the samples during the ESCR test. DSC measurements were carried out for investigation of the thermal properties of the samples before and after the ESCR test. DSC traces of the samples taken after the BTT show that a second endothermic peak is generated alongside the main one. The onset of this new peak was observed immediately above the annealing temperature  $T_a$  (the test temperature during the BTT). This second peak reflects the melting of the population of crystallites generated by annealing at  $T_a$  by a partial melting-re-crystallization mechanism.

WAXS investigations were performed for determination of the degree of crystallinity of the samples as received and after 48 h annealing at 50 and 70°C in 10 vol.-% Igepal solution. It was found that the degree of crystallinity does not change significantly after annealing of the PE/EVA samples at 50 and 70°C. We can expect increasing of the degree of crystallinity due to the annealing procedure. But it cannot be detected by WAXS measurements for both annealing temperatures.

SAXS measurements were carried out in order to determine any changes in the crystal structure and lamellae arrangement after the long thermal treatment of PE/EVA-5.4 and PE/EVA-8.9 samples during the BTT at 50 and 70°C. The peak for the long period of LDPE is at about  $0.5 \text{ nm}^{-1}$ . This peak broadens and shoulders appear in the case of annealing at 50°C. Even in the melt, in a  $q$ -range between  $0.1$  and  $0.7 \text{ nm}^{-1}$  some structures could be detected. The scattering at about  $0.33 \text{ nm}^{-1}$  is due to the carbon black particles, whereas the scattering at  $0.79 \text{ nm}^{-1}$  might be due to the EVA phase.

Broken PE lamellae and cavitation inside and around the EVA particles were observed in the case of PE/EVA-5.4 samples which failed the BTT in Igepal at 50°C within 24 h. BTT test was carried out in air at 50°C with PE/EVA-5.4 samples in order to check how the ESC agent influences the morphology. TEM images show that cavities around the EVA particles do not appear in the case of a sample thermally treated in air. Therefore, in the case of ESCR test in Igepal the semicrystalline PE matrix is very quickly attacked by the Igepal solution and this process is faster than the creep deformation of the EVA particles and crack initiation cannot be prevented.

Fracture surfaces of the samples which failed the BTT at 50°C, investigated by SEM, display a transition from flat and visually smooth to fibrous texture with addition of EVA in the blends. Deformed strands coming out from the surface were observed, indicating that the EVA phase makes the material tougher and the failure mechanism tends to be rather ductile than brittle with increasing the EVA content.

Phase structures and micromechanical deformation process were investigated by HVEM. It was established that PE/EVA/carbon black blends deform through shear yielding and a model was suggested representing the deformation mechanism in the blends. It can be concluded that the different annealing temperatures during the BTT do not influence the deformation mechanism in the samples and they deform through shear yielding.

Mechanical properties of PE/EVA samples were investigated at room temperature, 50 and 70°C by using Instron test machine. The results show that the increased temperature reduces the stiffness of the polymer as observed from the decreased Young's modulus. Both Young's modulus and yield stress fell monotonically with increasing temperature.

## 9. Outlook

In order to fully clarify the issues raised in the course of this study, the future works should be concentrated on the following points.

1. In order to determine the critical size of the EVA particles and the critical particle-particle distance, a systematic study on blends containing more than 8.9 wt.-% EVA would be necessary.
2. Fracture mechanics investigations could be helpful for evaluating the material resistance against unstable and stable crack propagation and afterwards to develop a model for the long-term ESC behavior of the blends.
3. Additional WAXS and SAXS investigations are necessary for determination of any changes in lamellae arrangement as a result of the long thermal treatment during the ESCR test.
4. It would be helpful to investigate the ESCR of the blends by applying a constant load test, to compare the failure times and the resulting deformation and failure mechanisms of the samples tested at both constant stress and constant strain. Afterwards, to select a test method which gives more reliable results and a shorter test-time procedure, that would be applied in industrial conditions for routine investigations of the ESCR of PE/EVA blends.



## 10. Zusammenfassung

Gegenstand der Arbeit ist die Spannungsrißbeständigkeit von LDPE/EVA Compounds. An ausgewählten Proben wurden die Abhängigkeiten der Spannungsrißbeständigkeit (ESCR) von der Temperatur und dem EVA-Gehalt sowie die thermischen und mechanischen Eigenschaften, die Morphologie, das Bruchverhalten sowie die Deformationsmechanismen untersucht. Die Ergebnisse sind ein Beitrag zu einem besseren Verständnis der Grundlagen des Spannungsrißphänomens, speziell für LDPE/EVA-Compounds. Damit sind Grundlagen für die Entwicklung von Langzeitkriterien bezüglich des Spannungsrißverhaltens erarbeitet worden, die letztendlich die Entwicklung eines theoretischen Modells für das Spannungsrißverhalten ermöglichen.

Das Spannungsrißverhalten von LDPE/EVA-Blends ist in komplexer Weise sowohl von der Zusammensetzung als auch von der Morphologie abhängig. Die Ergebnisse belegen, dass insbesondere die Zusammensetzung des EVA-Copolymeren von entscheidender Bedeutung ist. So verursacht ein Vinylacetat-Massegehalt von 28 Gew.-% in dem EVA-Copolymeren eine starke Verzögerung der Ausbildung von Spannungsrisen. Proben, die 8,9 Gew.-% EVA enthalten, bestehen generell den Test. Wenn der EVA-Gehalt kleiner ist als 7,1 Gew.-%, neigt das Polyethylen deutlich zu ESC (Spannungsrisen). In den meisten Fällen wird der Riss beidseitig, senkrecht zur Kerbe eingeleitet. Transmissionselektronenmikroskopische Bilder von PE/EVA-5.4 und PE/EVA-8.9 Proben vor dem ESCR-Test belegen, dass die Größe der EVA-Partikel in den Blends mit steigendem EVA-Gehalt zunimmt. Wahrscheinlich bestimmen die Größe der Partikel als auch ihr Abstand zueinander das Spannungsrißverhalten. Blends mit einem EVA-Gehalt von 8,9 Gew.-% versagten in keinem Fall. Diese Blends hoben sich von den anderen Proben dadurch ab, dass sie sowohl den höchsten EVA-Gehalt hatten und sich ausserdem durch den geringsten Partikelabstand auszeichneten. Folglich erweist sich ein EVA-Gehalt von 8,9 Gew.-% als ausreichend, um Rißbildung zu verhindern. Es wird angenommen, dass das in einer besseren Stressrelaxation dieser Proben begründet liegt.

Die elektronenmikroskopischen Aufnahmen von PE/EVA-5.4 und PE/EVA-8.9 zeigen, dass einige Lamellen relativ hoher Dicke in die EVA-Phase eindringen. Das ist bedingt durch die partielle Löslichkeit von PE in Bereichen langer Ethylensequenzen in dem EVA-Copolymeren, die ebenfalls zur Kristallisation fähig sind.

Im Falle des ESCR-Tests war die Versagenszeit bei 50°C für alle Proben die kürzeste. Sowohl bei 30 als auch bei 60 und 70°C widerstanden die Proben den Spannungsriß-Testbedingungen besser. Die höhere Spannungsrißbeständigkeit bei 60°C und 70°C könnte

durch ein bei diesen Temperaturen bereits auftretendes partielles Schmelzen der teilkristallinen EVA-Phase bedingt sein, wodurch die Partikel leichter deformierbar werden. Das ist mit elektronenmikroskopischen Aufnahmen an PE/EVA-5.4 und PE/EVA-8.9 nach dem Spannungsrißtest bei 70°C belegt. Diese zeigen deformierte und in Deformationsrichtung orientierte EVA-Partikel, die offensichtlich die Rißbildung verhindern. In Folge der Langzeitbeanspruchung im Spannungsrißtest können verschiedene morphologische Reorganisationsprozesse auftreten. DSC Untersuchungen gaben hierüber Aufschluß. Es zeigte sich, dass durch den ESCR-Test neben dem Hauptschmelzpeak ein zweiter endothermer Peak generiert wurde, dessen Onset-Temperatur leicht oberhalb der Temperatur des ESCR-Tests liegt. Dieser zusätzlich auftretende, zweite endotherme Peak wird als das Schmelzen einer Kristallitpopulation interpretiert, die durch partielle Schmelz-Rekristallisations-Vorgänge unter der Testtemperatur während des ESC-Tests entstanden sein kann.

Zur Bestimmung des Kristallinitätsgrades wurden Röntgen-Weitwinkeluntersuchungen (WAXS) durchgeführt. Die Proben wurden vor und nach einer 48-stündigen Temperung in 10 Vol.-% Igepallösung gemessen. Die Temperungen erfolgten sowohl bei 50°C als auch bei 70°C. Die erwartete Zunahme der Kristallinität aufgrund der Temperung konnte experimentell nicht bestätigt werden.

Um nähere Aufschlüsse über die Kristallstruktur und Lamellenanordnung zu bekommen, wurden Röntgen-Kleinwinkeluntersuchungen durchgeführt (SAXS). Der die Langperiode beschreibende Peak liegt bei  $0,5 \text{ nm}^{-1}$ . Dieser erfährt infolge der Temperung bei 50°C eine Verbreiterung und zusätzlich tritt eine Schulter auf. Sogar in der Schmelze konnten einige Strukturen detektiert werden, die im Streufaktor-Bereich von  $0,1$  bis  $0,7 \text{ nm}^{-1}$  liegen. Der Streueffekt bei  $0,33 \text{ nm}^{-1}$  wurde dem Füllstoff Ruß und der bei  $0,79 \text{ nm}^{-1}$  der EVA-Phase zugeordnet.

Parallele Untersuchungen wurden durchgeführt, um den Einfluß des Mediums, in dem die Spannungsrißuntersuchungen durchgeführt wurden, auf die morphologischen Änderungen zu untersuchen. Hierfür wurde die Probe PE/EVA-5.4 und der ESCR-Test bei 50°C ausgewählt. Unter Igepal durchgeführte Messungen zeigten in transmissionselektronenmikroskopischen Aufnahmen sowohl gebrochene Lamellen als auch Kavitäten innerhalb der EVA-Phase wie auch in den angrenzenden Bereichen. Der unter Normalatmosphäre bei 50°C durchgeführte ESCR-Test verursachte hingegen keinerlei Kavitäten. Das heißt, dass die teilkristalline PE-Matrix vom Igepal angegriffen wird. Dieser Prozeß läuft schneller ab als sich die EVA-Partikel deformieren können, so dass die Rißinitiierung nicht verhindert werden kann.

Die Untersuchung der Bruchflächen erfolgte mittels Rasterelektronenmikroskopie. Untersucht wurden die Bruchflächen der dem ESCR-Test bei 50°C unterzogenen Proben. Die Strukturen der Bruchoberflächen reichen von glatt bis fasrig. Aus der Bruchoberfläche ragende, deformierte Stränge sind ein Beleg dafür, dass die Zähigkeit der Blends mit steigendem EVA-Anteil erhöht wird. Dies bedeutet weiterhin, dass der Bruchmechanismus mit höherem EVA-Gehalt durch zähes Verhalten bestimmt ist.

Darüberhinaus wurden Phasenstrukturen und mikromechanische Deformationsprozesse mittels Hochspannungs-Elektronenmikroskopie untersucht. Es wird ein Modell vorgeschlagen, das den Mechanismus der Scherdeformation der rußgefüllten PE/EVA-Blends beschreibt und durch die experimentellen Ergebnissen bestätigt wird. Der Deformationsmechanismus ist unabhängig von der Temperatur, bei der der ESCR-Test durchgeführt wurde.

Die mechanischen Eigenschaften der PE/EVA-Blends wurden bei Raumtemperatur, bei 50°C und bei 70°C untersucht. Wie zu erwarten, sinkt die Steifigkeit, ermittelt aus dem E-Modul, mit steigender Temperatur. Sowohl der E-Modul als auch die Spannung an der Streckgrenze fallen monoton mit steigender Temperatur.

## **Ausblick**

Zur vollständigen Klärung, der in dieser Arbeit gefunden Aussagen, sollten in zukünftigen Arbeiten folgende Punkte untersucht werden:

1. Systematische Untersuchungen an PE/EVA-Blends mit mehr als 8,9 Gew.-% EVA hinsichtlich der kritischen Teilchgröße der dispersen Phase sowie des kritischen Partikelabstandes.
2. Die Materialbeständigkeit gegen stabile und instabile Rißausbreitung sollten mit den Methoden der Bruchmechanik im Detail untersucht werden um letztendlich ein Modell für das Langzeit-Spannungsrißverhalten dieser Blends entwickeln zu können.
3. Weiterführende WAXS- und SAXS-Untersuchungen zur Analyse veränderter Kristallmorphologien und Lamellenanordnungen in Korrelation zu Langzeit-Spannungsrißuntersuchungen.
4. Untersuchungen zu Versagensdauer, Deformation und Versagensmechanismen unter konstanter Spannung im Vergleich zu den unter konstanter Dehnung durchgeführten ESCR-

Testklassen Ergebnisse erwarten, die aussagekräftigere Ergebnisse hinsichtlich Voraussagen zum Spannungsrißverhalten von PE/EVA-Blends liefern. Darüber hinaus dürfte das die Basis sein, um Methoden zu entwickeln, die diese Aussagen in kürzeren Testzeiten ermöglichen.

## 11. References

- [1]. J. Scheirs, “*Compositional and Failure Analysis of Polymers*”, J. Wiley & Sons, Chichester 2000.
- [2]. D. Wright, “*Environmental Stress Cracking of Plastics*”, RAPRA Technology Ltd., Shawbury 1996.
- [3]. M. C. Hough, D. C. Wright, *Polymer Testing* **1996**, 15, 407-421.
- [4]. A. Lustiger, “Understanding Environmental Stress Cracking in Polyethylene” in “*Medical Plastics: Degradation, Resistance & Failure Analysis*”, R. C. Portnoy, SPE, Plastic Design Library 1998, p. 66-71.
- [5]. J. Pinsky, *Plast. Tech.* **1959**, 1, 159.
- [6]. J. Lagaron, N. M. Dixon, B. J. Kip, *Macromolecules* **1998**, 31, 5845-5852.
- [7]. J. Lagaron, J. Pastor, B. Kip, *Polymer* **1999**, 40, 1629-1636.
- [8]. H. Schmiedel, “*Handbuch der Kunststoffprüfung*”, Carl Hanser Verlag, München 1992.
- [9]. D. Felbeck, A. Atkins, “*Strength and Fracture of Engineering Solids*”, 2<sup>nd</sup> edition, Prentice Hall, NJ 1996, p. 447.
- [10]. P. Hittmair, R. Ullman, *J. Appl. Polym. Sci.* **1962**, 6, 1-14.
- [11]. A. Lustiger, R. D. Corneliussen, *J. Mater. Sci.* **1987**, 22, 2470-2476.
- [12]. R. Deanin, D. Hauser, *Polym. Plast. Technol. Eng.* **1981**, 17, 123-137.
- [13]. S. Bandyopadhyay, H. R. Brown, *J. Mater. Sci. Letters* **1977**, 12, 2131-2134.
- [14]. A. L. Ward, X. Lu, Y. Huang, N. Brown, *Polymer* **1991**, 32, 2172-2178.
- [15]. C. Plummer, A. Goldberg, A. Ghanem, *Polymer* **2001**, 42, 9551-9564.
- [16]. J. Lagaron, G. Capaccio, L. J. Rose, B. J. Kip, *J. Appl. Polym. Sci.* **2000**, 77, 283-296.
- [17]. A. Lustiger, N. J. Ishikawa, *J. Polym. Sci., Polym. Phys.* **1991**, 29, 1047.
- [18]. N. Brown, X. Lu, *Polymer* **1995**, 36, 453.
- [19]. A. L. Volynskii, A. G. Aleskerov, N. F. Bakeev, *Vysokomol. Soedin.* **1982**, A24, 1855.
- [20]. C. Hansen, L. Just, *Ind. Eng. Chem. Res.* **2001**, 40, 21-25.
- [21]. R. P. Kambour, C. L. Gruner, E. E. Ramagosa, *J. Polym. Sci., Polym. Phys.* **1973**, 11, 1879.
- [22]. R. P. Kambour, A. F. Yee, *Polym. Eng. Sci.* **1981**, 21, 218.
- [23]. K. Friedrich, “Crazes and Shear Bands in Semi-Crystalline Thermoplastics” in “*Advances in Polymer Science*”, Vol. 52-53, Springer-Verlag Berlin 1983, p. 225-274.
- [24]. X. Lu, N. Brown, *J. Mater. Sci.* **1990**, 25, 29-34.
- [25]. R. Hiss, S. Hobeika, C. Lynn, G. Strobl, *Macromolecules* **1999**, 32, 4390-4403.
- [26]. S. Hobeika, Y. Men, G. Strobl, *Macromolecules* **2000**, 33, 1827.

- [27]. M. Al-Hussein, G. Strobl, *Macromolecules* **2002**, 35, 8515-8520.
- [28]. C. P. Lafrance, P. Chabot, M. Pigeon, M. Prud'homme, M. Pezolet, *Polymer* **1993**, 34, 5029.
- [29]. J. C. Rodriguez-Cabelo; J. C. Merino, J. M. Pastor, *Polymer* **1995**, 36, 4233-4238.
- [30]. C. P. Lafrance, P. Chabot, M. Pigeon, R. Prud'homme, M. Pezolet, *Polymer* **1993**, 34, 5029-5037.
- [31]. M. Pigeon, R. Prud'homme, M. Pezolet, *Macromolecules* **1991**, 24, 5687-5694.
- [32]. N. W. Brooks, A. P. Unwin, R. A. Duckett, I. M. Ward, *J. Macromol. Sci. Phys.* **1995**, B34, 29.
- [33]. J. M. Lagaron, N. M. Dixon, W. Reed, J. M: Pastor, B. J. Kip, *Polymer* 1999, 40, 2569-2586.
- [34]. A. Opdahl, G. A. Somorjai, *J. Polym. Sci., Polym. Phys.* **2001**, 39, 2263-2274.
- [35]. X. Lu, R. Qian, N. Brown, *Polymer* **1995**, 36, 4239-4244.
- [36]. J. M. G. Cowie, I. J. McEwen, R. McIntyre, "Aging and Degradation of Polymer Blends" in "*Polymer Blends Handbook*" Vol. 2, L. A. Utracki, Kluwer Academic Publishers, Dordrecht 2002, p. 977-1021.
- [37]. Y. Huang, N. Brown, *J. Mater. Sci.* **1988**, 23, 3648-3655.
- [38]. J. Soares, R. Abbott, J. Kim, *J. Polym. Sci., Polym. Phys.* **2000**, 38, 1267-1275.
- [39]. A. Lustiger, "Environmental Stress Cracking: The Phenomenon and Its Utility" in "*Failure of Plastics*" W. Brostow, R. Corneliussen, Hanser, Munich 1986, p. 305-329.
- [40]. K. Kendall, F. R. Sherliker, *The British Polymer Journal* **1980**, 12, 111-113.
- [41]. I. Narisawa, M. Ishikawa, "Crazing in Semicrystalline Thermoplastics" in "*Polymer Science*" 91-92, p. 353-391.
- [42]. N. Brown, I. M. Ward, *J. Mater. Sci.* **1983**, 18, 1405-1420.
- [43]. X. Lu, N. Brown, *Polymer* **1987**, 28, 1505-1511.
- [44]. R. J. Roe, C. Gieniewski, *Polym. Eng. Sci.* **1975**, 15, 421-427.
- [45]. H. T. Wang, B. R. Pan, Q. G. Du, Y. Q. LI, *Polymer Testing* **2003**, 22, 125-128.
- [46]. J. C. Arnold, *Polym. Eng. Sci.* **1994**, 34, 665-670.
- [47]. *International Standard CEI/IEC 811-4-1*, 1985.
- [48]. S. Saeda, Y. Suzaka, *Polym. Adv. Technol.* **1995**, 6, 593-601.
- [49]. X. Lu, N. Brown, *Polymer Testing* **1992**, 11, 309-319.
- [50]. Z. Zhou, N. Brown, *Polymer Testing* **1996**, 15, 549-558.
- [51]. J. T. Yeh, J.-H. Chen, H.-S. Hong, *J. Appl. Polym. Sci.* **1994**, 54, 2171-2186.
- [52]. A. L. Ward. X. Lu, N. Brown, *Polym. Eng. Sci.* **1990**, 30, 1175-1179.
- [53]. X. Lu, Z. Zhou, N. Brown, *Polym. Eng. Sci.* **1997**, 37, 1896-1900.

- [54]. J. N. Hay, D. J. Kemmish, *Polymer* **1988**, 29, 613.
- [55]. J. Crissman, *J. of Testing and Evaluation* **1983**, 11, 273-278.
- [56]. L. A. Utracki, "Introduction to Polymer Blends" in "*Polymer Blends Handbook*" Vol. 1, Kluwer Academic Publishers, Dordrecht 2002, p. 12-24.
- [57]. L.H. Sperling, "*Introduction to Physical Polymer Science*", 2<sup>nd</sup> Edition, chapter 4,, Wiley-Interscience Publ., New York 1992, p. 122-150.
- [58]. U. Eisele, "*Introduction to Polymer Physics*", Springer Verlag, Heidelberg 1990.
- [59]. L. Utracki, "Thermodynamics of Polymer Blends" in "*Polymer Blends Handbook*", Vol. 1, L. A. Utracki Ed., Kluwer Academic Publishers, Dordrecht 2002, p.123-201.
- [60]. P.J. Flory, *J. Chem. Phys.* **1941**, 9, 660.
- [61]. M. L. Huggins, *J. Chem. Phys.* **1941**, 9, 440.
- [62]. G. D. Merfeld, D. R. Paul, "Polymer-Polymer Interactions Based on Mean Field Approximations" in "*Polymer Blends: Formulation*", Vol. 1, D. R. Paul, C. B. Bucknall Ed., Wiley-Interscience Publ., New York 2000, p. 55-91.
- [63]. D. J. Lohse, W. W. Graessley, "Thermodynamics of Polyolefin Blends" in "*Polymer Blends: Formulation*", Vol. 1, D. R. Paul, C. B. Bucknall Ed., Wiley-Interscience Publ., New York 2000, p. 219.237.
- [64]. *Concise Encyclopedia of Polymer Science and Engineering*, John Wiley & Sons, New York 1990, p. 350-357.
- [65]. *Polymeric Materials Encyclopedia*, Vol. 8, J. Salamone, CRC Press, London 1996.
- [66]. C. Harper, "*Handbook of Plastics, Elastomers, and Composites*", 4<sup>th</sup> Edition, McGraw-Hill, New York 2002, p. 38-43.
- [67]. H. Domininghaus, "*Plastics for Engineers: Materials, Properties, Applications*", Hanser, Munich 1993, p. 23-72.
- [68]. O. A. Serenko, V. S. Avinkin, *Polym. Sci., Ser. A* **2001**, 43, 129-133.
- [69]. X. Yi, G. Wu, D. Ma, *J. Appl. Polym. Sci.* **1998**, 67, 131-138.
- [70]. V. Kurnosov, R. Deberdeev, *J. Polym. Eng.* **1997**, 17, 281-294.
- [71]. I. Ray, D. Khastgir, *Polymer* **1993**, 34, 2030-2037.
- [72]. I. Ray, D. Khastgir, *Plastics, Rubber & Composites* **1994**, 22, 37-45.
- [73]. I. Ray, D. Khastgir, *J. Polym. Eng.* **1994**, 13, 29-47.
- [74]. M. Rodriguez-Perez, A. Duijsens, *J. Appl. Polym. Sci.* **1998**, 68, 1237-1244.
- [75]. R. Mcevoy, S. Krause, *J. Appl. Polym. Sci.* **1997**, 64, 2221-2235.
- [76]. N. Brown, X. Lu, *Polymer* **1995**, 36, 542-548.
- [77]. N. Brown, X. Lu, Y. Huang, R. Qian, *Macromol. Chem, Macromol. Symp.* **1991**, 41, 55-67.

- [78]. X. Lu, N. Brown, *J. Mater. Sci.* **1986**, 21, 2423-2429.
- [79]. X. Lu, R. Qian, N. Brown, *J. Mater. Sci.* **1991**, 26, 917-924.
- [80]. X. Lu, N. Brown, *J. Mater. Sci.* **1986**, 21, 4081-4088.
- [81]. X. Lu, R. Qian, N. Brown, *Polymer* **1995**, 36, 4293-4244.
- [82]. Y. Huang, N. Brown, *J. Polym. Sci., Polym. Phys.* **1990**, 28, 2007-2021.
- [83]. Y. Huang, N. Brown, *J. Polym. Sci., Polym. Phys.* **1991**, 29, 129-137.
- [84]. Z. Zhou, N. Brown, B. Crist, *J. Polym. Sci., Polym. Phys.* **1995**, 33, 1047-1051.
- [85]. N. Brown, Z. Zhou, *Macromolecules* **1995**, 28, 1807-1811.
- [86]. X. Lu, A. McGhie, N. Brown, *J. Polym. Sci., Polym. Phys.* **1993**, 31, 767-772.
- [87]. X. Lu, A. McGhie, N. Brown, *J. Polym. Sci., Polym. Phys.* **1992**, 30, 1207-1214.
- [88]. A. Lustiger, R. Corneliusen, *J. Polym. Sci., Polym. Phys.* **1986**, 24, 1625-1629.
- [89]. K. Tonyali, C. Rogers, *Polymer* **1987**, 28, 1472-1477.
- [90]. K. Tonyali, C. Rogers, *Polym. Eng. Sci.* **1987**, 27, 82-85.
- [91]. M. Schick, “*Nonionic Surfactants*”, Marcel Dekker, Inc., New York 1967.
- [92]. A. Ray, *Nature* **1971**, 231, 313.
- [93]. K. Tonyali, H. Brown, *J. Mater. Sci.* **1987**, 22, 3287-3292.
- [94]. P. Chang, J. A. Donovan, *Polym. Eng. Sci.* **1990**, 30, 1431-1441.
- [95]. R. Qian, X. Lu, N. Brown, *Polymer* **1993**, 34, 4727-4731.
- [96]. G. R. Strobl, *Acta Cystallogr.* **1970**, A26, 367.
- [97]. ANSYS User’s Manual, Vol. I-IV, Swanson Analysis Systems Inc. 1994.
- [98]. S. Holweg, never published, internal script, 2000.
- [99]. A. Peacock, “*Handbook of Polyethylene: Structures, Properties, and Applications*”, Marcel Dekker, New York 2000.
- [100]. N. Okui, T. Kawai, *Die Makromolekulare Chemie* **1972**, 154, 161-176.
- [101]. R. G. Alamo, R. H. Glaser, L. Mandelkern, *J. Polym. Sci., Polym. Phys.* **1988**, 26, 2169-2195.
- [102]. S. G. Moyses, *Polymer Journal* **2000**, 32, 486-491.
- [103]. L. Mandelkern, M. Glotin, R. A. Benson, *Macromolecules* **1981**, 14, 22-34.
- [104]. G. R. Strobl, W. Hagedorn, *J. Polym. Sci., Polym. Phys.* **1978**, 16, 1181-1193.
- [105]. M. Huskic, *J. Appl. Polym. Sci.* **1996**, 60, 1741-1745.
- [106]. X. Lu, R. Qian, N. Brown, *J. Polym. Sci., Polym. Phys.* **1992**, 30, 899-906.
- [107]. B. Goderis, H. Reynaers, R. Scherrenberg, *Macromolecules* **2001**, 34, 1779-1787.
- [108]. Ryong-Joon Roe, “*Methods of X-ray and Neutron Scattering in Polymer Science*”, Oxford University Press, New York 2000, p. 104-113.
- [109]. Q. R. Zhu, K. L. Hong, L. Q. Ji, *J. Polym. Sci., Polym. Phys.* **1995**, 33, 739-744.



- [110]. H. Zhou, G. L. Wilkes, *Polymer* **1997**, 38, 5735-5747.
- [111]. C. Williams, R. May, A. Gunier, "Small-Angle Scattering of X-Rays and Neutrons" in "*X-ray Characterization of Materials*", Eric Lifshin Ed., Wiley-VCH, Weinheim 1999, p. 211-251.
- [112]. R. Thomann, C. Wang, J. Kressler, R. Mülhaupt, *Macromol. Chem. Phys.* **1996**, 197, 1085-1091.
- [113]. E. Piorkowska, A. Galeski, *J. Polym. Sci., Polym. Phys.* **1993**, 31, 1285-1291.
- [114]. I. Druz, A. D. Aliev, *Vysokomol. Soed., Ser. B* **1987**, 29, 2, 101-104.
- [115]. G. Stael, M. Tavares, *Polymer Testing* **1997**, 16, 193-198.
- [116]. C. Souza, M. Tavares, *Polymer Testing* **1998**, 17, 533-541.
- [117]. K. Beshah, *Macromolecules* **1992**, 25, 5597-5600.
- [118]. M. Brogly, M. Nardin, J. Schultz, *J. Appl. Polym. Sci.* **1997**, 64, 1903-1912.
- [119]. G. H. Michler, *Acta Polymerica* **1993**, 44, 113-124.
- [120]. C. B. Bucknall, "Rubber Toughening" in "*The physics of Glassy Polymers*", R. N. Haward, R. J. Young, Chapman & Hall, London 1997, p. 363-412.
- [121]. S. Wu, *Polymer* **1985**, 26, 1855.
- [122]. A. Margolina, S. Wu, *Polymer* **1988**, 29, 2170.
- [123]. R. Borggreve, R. G. Gaymans, *Polymer* **1988**, 29, 1441.
- [124]. R. Borggreve, R. Gaymans, A. Luttmer, *Macromol. Chem., Macromol. Symp.* **1988**, 16, 195.
- [125]. G. H. Michler, "Deformation and Fracture" in: *Polymeric Materials Encyclopedia*, Vol. 3, J. Salamone, CRC Press, London 1996, p. 1771-1780.
- [126]. G.-M. Kim, G. H. Michler, *Polymer* **1998**, 39, 5689-5697.
- [127]. G.-M. Kim, G. H. Michler, *Polymer* **1998**, 39, 5699-5703.
- [128]. A. Brent Strong, "*Plastics: Materials and Processing*", Prentice-Hall, Englewood Cliffs, New Jersey 1996, p. 104-107.
- [129]. I. Ray, D. Khastgir, P. G. Mukunda, *Die Angew. Makromol. Chemie* **1993**, 205, 59-74.
- [130]. I. Walker, A. A. Collyer, "Rubber Toughening Mechanisms in Polymeric Materials" in "*Rubber Toughened Engineering Plastics*", A. A. Collyer, Chapman & Hall, London 1994, p. 29-56.

## Appendix A

The phase diagram was estimated using the data given by Druz et. al.<sup>[114]</sup> in Table 2 of their publication about the miscibility of PE/EVA blends.

$$M_{PE} = 100\,000 \text{ g/mol}, M_{0PE} = 28, N_1 \sim 3571$$

$$M_{EVA} = 15\,500 \text{ g/mol}, M_{0EVA} = 42, N_2 \sim 370$$

$N_1$  and  $N_2$  are the degree of polymerization.

The dependence of the existent phases in the PE/EVA blends on molar mass of PE ( $M_{PE}$ ) is given by the following equations<sup>[114]</sup>:

$$\Phi_1' = \Phi_{1\infty}' + \frac{k'}{M} \quad \text{and} \quad \Phi_1'' = \Phi_{1\infty}'' + \frac{k''}{M} \quad (\text{A-1})$$

where  $\Phi_1'$  and  $\Phi_1''$  are the volume fractions at equilibrium.

The extrapolation allows to determine the phases at the temperature of the experiment and the solubility of the components (PE and EVA) at  $M \rightarrow \infty$ .

We assume that the interaction parameter  $\chi$  is:  $\chi = A + \frac{B}{T}$

Therefore, (in rough approximation) according to Ref. 114:

$$\chi = -0.03 + \frac{14.25}{T} \quad (\text{A-2})$$

$\chi_{393} = 6.3 \times 10^{-3}$  and  $\chi_{433} = 2.9 \times 10^{-3}$  are the binary interaction parameters at temperatures of 393 and 433 K respectively.

After Flory-Huggins approximation (see Appendix B):  $\Phi_{1\infty}' \propto \frac{1}{\chi}$  and  $\Phi_{1\infty}'' \propto \frac{1}{\chi}$ . Hence, we

assume temperature dependence of these quantities and the coefficients  $k'$  and  $k''$ :

$$\Phi_{1\infty}' = \frac{\alpha' + \beta'T}{\chi} \quad \text{and} \quad k' = a' + \frac{b'}{T}$$

which results in:

$$\Phi_{1\infty}' = \frac{-3.55 + 0.02T}{10^4 \chi} \quad \Phi_{1\infty}'' = \frac{-6.14 + 0.0166T}{10^4 \chi} \quad (\text{A-3})$$

$$k' = 0.0288 + \frac{212.7}{T} \quad k'' = -0.805 + \frac{251.0}{T}$$

where  $\chi$  is given by Equation (A-2). The phase compositions can be calculated by using Equations (A-1) – (A-3).

## Appendix B

Flory-Huggins (FH) approximation:

$$\frac{\Delta\mu_1}{RT} = \frac{\ln \Phi}{N_1} + (1 - \Phi) \left( \frac{1}{N_1} - \frac{1}{N_2} \right) + \chi(1 - \Phi)^2 \quad (\text{B-1})$$

$$\frac{\Delta\mu_2}{RT} = \frac{\ln(1 - \Phi)}{N_2} - \Phi \left( \frac{1}{N_1} - \frac{1}{N_2} \right) + \chi\Phi^2 \quad (\text{B-2})$$

where  $\Delta\mu_1$  and  $\Delta\mu_2$  are the chemical potential of PE and EVA.

There is phase equilibrium when:

$$\Delta\mu_1' = \Delta\mu_1'' \quad \text{and} \quad \Delta\mu_2' = \Delta\mu_2'' \quad (\text{B-3})$$

Using (B-1) and (B-2), the first equation of (B-3) refers to  $N_1 \rightarrow \infty$

$-(1 - \Phi') + N_2\chi(1 - \Phi')^2 = -(1 - \Phi'') + N_2\chi(1 - \Phi'')^2$  and the solution of this equation is:

$$1 - \Phi' = \frac{1}{N_2\chi} - (1 - \Phi'') \quad (\text{B-4})$$

By using (B-4) we obtain the second equation of (B-3):

$$\ln \left[ \frac{1 - \chi N_2(1 - \Phi'')}{\chi N_2(1 - \Phi'')} \right] = 2[1 - 2\chi N_2(1 - \Phi'')] \quad (\text{B-5})$$

which leads to:  $\chi N_2(1 - \Phi'') = 0.5$

$N_1$  and  $N_2$  are degree of polymerization of PE and EVA respectively.

## **Erklärung**

Ich erkläre, daß ich die vorliegende Dissertation selbständig und nur unter Verwendung der angegebenen Literatur und Hilfsmittel angefertigt habe. Diese Dissertation wurde bisher an keiner Universität oder Hochschule vorgelegt. Frühere Bewerbungen um den akademischen Grad eines Dr.-Ing. wurden von mir nicht vorgenommen.

Kaiserslautern, den 25.06.2004

Bistra Andersen

# CURRICULUM VITAE

**Name:** Bistra Andersen  
**Date and Place of Birth:** 09 January 1973, Ruse, Bulgaria  
**Marital Status:** Married  
**Address:** Mannheimer Str. 106  
D-67655 Kaiserslautern, Germany

**Education:**  
01.2001-05.2004 Scientific co-worker (**wissenschaftliche Mitarbeiterin, Promotion Student**) at Martin-Luther-Universität Halle-Wittenberg, Germany  
FB Ingenieurwissenschaften  
Research topic: Environmental Stress Cracking Resistance of LDPE/EVA Blends, Their Morphology, Thermal, Mechanical Properties, and Deformation Behavior  
Supervisor: Prof. Dr. J. Kreßler

09.1992-10.1997 University of Chemical Technology and Metallurgy, Sofia, Bulgaria  
Subjects: Chemical Technologies, Technology of Plastics  
**Masters degree in Chemical Technologies and professional qualification “Chemical Engineer”**  
Diploma thesis work done at Martin-Luther-Universität Halle-Wittenberg, supervisor: Prof. Dr. S. Marinow  
Graduation in October 1997 and both elaboration and defence of the diploma work got excellent mark

09.1988-06.1992 Secondary Technical School of Industrial Chemistry, Ruse, Bulgaria

**Practical Experience:**  
05.1998-12.2000 Regional manager in the “Import-Export Department” of the chemical trade company “CHIMSNAB 7004” AD, Ruse. My responsibilities included (i) establishing contacts with new suppliers for import of various chemical substances, contract negotiations, (ii) regular contacts with local authorities, customs offices, and the “Directory of Quality Control”.

11.1997-04.1998 Scientific co-worker in a research team at the University of Chemical Technology and Metallurgy, Sofia

**Languages:** English – fluent, basic German and Russian, Bulgarian as mother tongue

Kaiserslautern, June 2004